NASA CONTRACTOR REPORT

NASA CR-2737

THE EFFECT OF HELICOPTER MAIN ROTOR BLADE PHASING AND SPACING ON PERFORMANCE, BLADE LOADS, AND ACOUSTICS

Santu T. Gangwani

Prepared by
ROCHESTER APPLIED SCIENCE ASSOCIATES
Newport News, Va. 23602
for Langley Research Center

NATIONAL AERONAUTICS AND SPACE ADMINISTRATION • WASHINGTON, D. C. • SEPTEMBER 1976

1. Report No.	2. Government Accession No.	3. Recipient's Catalog No.
NASA CR-2737		

4. Title and Subtitle	5. Report Date
THE EFFECT OF HELICOPTER MAIN ROTOR BLADE PHASING AND SPACING ON PERFORMANCE, BLADE LOADS, AND ACOUSTICS	September 1976
	6. Performing Organization Code

7. Author(s)	8. Performing Organization Report No.
Santu T. Gangwani	RASA SRL 3169 -0014
	10. Work Unit No.

9. Performing Organization Name and Address	11. Contract or Grant No.
RASA Division Systems Research Laboratories, Inc. 1055 J. Clyde Morris Boulevard Newport News, Virginia 23602	NAS1-13705
	13. Type of Report and Period Covered
12. Sponsoring Agency Name and Address National Aeronautics and Space Administration Washington, D.C. 20546	Contractor Report
	14. Sponsoring Agency Code

15. Supplementary Notes

Langley Technical Monitor W. R. Mantay
Final Report

16. Abstract

The performance, blade loads and acoustic characteristics of a variable geometry rotor (VGR) system in forward flight and in a pullup maneuver were determined by the use of existing analytical programs. The investigation considered the independent effects of vertical separation of two three-bladed rotor systems as well as the effects of azimuthal spacing between the blades of the two rotors. The computations were done to determine the effects of these parameters on the performance, blade loads and acoustic characteristics at two advance ratios in steady-state level flight and for two different "g" pullups at one advance ratio. To evaluate the potential benefits of the VGR concept in forward flight and pullup maneuvers, the results were compared as to performance, oscillatory blade loadings, vibratory forces transmitted to the fixed fuselage and the rotor noise characteristics of the various VGR configurations with those of the conventional six-bladed rotor system.

17. Key Words (Suggested by Author(s))	18. Distribution Statement
Variable Geometry Rotor (VGR), Rotor Wake Blade Loads, Transmitted Loads, Helicopter Performance, Acoustics, Pullup maneuver	Unclassified - Unlimited Subject Category 01

19. Security Classif. (of this report)	20. Security Classif. (of this page)	21. No. of Pages	22. Price*
Unclassified	Unclassified	99	$4.75

* For sale by the National Technical Information Service, Springfield, Virginia 22161

CONTENTS

THE EFFECT OF HELICOPTER MAIN ROTOR BLADE PHASING AND SPACING ON PERFORMANCE, BLADE LOADS, AND ACOUSTICS

By Santu T. Gangwani

Rochester Applied Science Associates*

SUMMARY

The performance, blade loads and acoustic characteristics of a variable geometry rotor (VGR) system in forward flight and in a pullup maneuver were determined by the use of existing analytical programs. The investigation considered the independent effects of vertical separation of two three-bladed rotor systems as well as the effects of azimuthal spacing between the blades of the two rotors. The computations were done to determine the effects of these parameters on the performance, blade loads and acoustic characteristics at two advance ratios in steady-state level flight and for two different "g" pullups at one advance ratio. To evaluate the potential benefits of the VGR concept in forward flight and pullup maneuvers, the results were compared as to performance, oscillatory blade loadings, vibratory forces transmitted to the fixed fuselage and the rotor noise characteristics of the various VGR configurations with those of the conventional six-bladed rotor system.

Tne results indicated some benefits in performance and blade loadings for the VGR configurations, but these benefits were accompanied with some significant amount of 3 per rev vibratory forces transmitted to the fuselage from the rotor system. These transmitted forces, nowever, depend very strongly on the azimuth spacing between the blades of the two rotors. The noise characteristics also were observed to vary significantly with the variation in the geometry of the VGR configuration.

INTRODUCTION

The concentrated tip vortex field generated by helicopter rotors has been of concern for many years as it has a significant effect on performance, dynamic blade loadings and the acoustic output of the rotor system. The first approach of understanding the importance of the concentrated vortex energy to these problem areas was the development of suitable models of the concentrated wake of the helicopter. The initial analyses treated in Reference 1 and Reference 2, have been expanded and refined over the

*Division of Systems Research Laboratories, Inc. of Dayton, Ohio

years so that realistic predictions of the characteristics of the helicopter deformed wake position and strength can be made by techniques such as that developed by Rochester Applied Science Associates, Inc. (RASA) under NASA sponsorship, Reference 3. The use of these techniques have been valuable in analyzing the dynamic problem areas associated with helicopter rotors and in investigating the effectiveness of harmonic pitch control in relieving the dynamic loads transmitted to the fuselage. Approaches are currently being investigated for the modification of the induced effects of the concentrated vortex wake. One of these approaches, called the variable geometry rotor, is to change the relative position of the concentrated wake and the blades in order to create a more favorable induced velocity field and thus enhance the performance and dynamic load characteristics of the rotor system. This approach, has shown some positive results as regards performance, particularly in hover. In Reference 3, a deformed wake analysis to investigate the effect of variable blade radius, cutout, relative azimuthal phasing and separation on the wake position and induced velocity distributions at an advance ratio of $\mu = 0.20$ has been used. In References 4 and 5, an experimental investigation of the concept for a six-bladed rotor system in hover was conducted. The rotor model, tested at two different tip speeds over a range of pitch angles, consisted of nontapered-nontwisted blades for which the rotor separation and phasing characteristics on performance of two three-bladed rotors could be evaluated. Some of the basic results of this program showed that axial spacing of alternate blades offers a significant hover performance advantage relative to a conventional rotor configuration at thrust levels near stall and varying the azimuth spacing independently from the 60 deg. spacing of the conventional coplanar rotor does not improve hover performance but combining the proper azimuth spacing with axial spacing offers an additional hover performance improvement.

In forward flight it was concluded that variations of rotor axial and azimuth spacing generally had a negligible effect on performance, and that differences in blade flapping amplitudes of variable geometry rotor configurations in forward flight implied differences in aerodynamic interference effects which may be attributable to variations in wake geometry.

In addition it was noted that the tip vortex patterns of variable geometry rotor configurations were much more complex than those of conventional rotors. The relation between these complex vortex patterns and the measured hover performance trends were difficult to interpret without an extensive analytical study of the entire rotor-wake system. However, from consideration of the tip vortex geometry and the associated blade-vortex interference effects for rotors with axial spacing, it appeared that the measured performance gain of such rotors might be due to a net improvement in the vortex orientation relative to the individual blades.

In particular, the improved performance at high thrust levels might be associated with induced stall relief on the upper blades provided by the tip vortex reorientation.

While the results that were presented in Reference 4 concentrated on the hover performance, the limited results obtained in forward flight generally indicated that the performance and dynamic load characteristics were not adversely affected. It is noted that these results were obtained for the optimum hover parameters and it was not determined if the parameters not particularly beneficial in hover might be beneficial as regards dynamic loads and the acoustic signature in forward flight.

The purpose of the program reported on herein was to conduct a series of calculations using existing deformed wake and dynamic loads prediction programs to provide a better understanding of the aerodynamic and dynamic and acoustic characteristics of variable geometry rotors in forward flight and pullup maneuvers, and to provide guidance and direction toward a possible experimental program using a model of a realistic helicopter.

SYMBOLS

A_c	longitudinal cyclic pitch, deg
a_n	sine part of $n^{\underline{th}}$ harmonic of sound pressure
B_c	lateral cyclic pitch, deg
b_n	cosine part of $n^{\underline{th}}$ harmonic of sound pressure
dB	decibel
$d\psi$	azimuthal step size, rad
EIX,EIY,EIZ	torsional rigidity, chordwise bending stiffness and flatwise bending stiffness respectively, $N\text{-}m^2$
F_x,F_z	aerodynamic forces per unit span acting tangential and normal to the rotor plane, respectively, N/m
g	gravity factor
Hz	cycle/sec

I	blade section number
IX	section torsional mass moment of inertia of the lumped parameter blade model, m-N sec^2
IY	section flatwise mass moment of inertia, m-N/sec^2
M_y,M_z	flapwise and chordwise moments, respectively, m-N
n	n^{th} harmonic
N	number of revolution of wake retained for wake induced flow computations
p_n	n^{th} harmonic of sound pressure
R	radius of rotor blade, m
r	radial position of blade station, m
SPL	sound pressure level in dB referenced to .0002 dyne/cm^2
T	torsional moment, m-N
t	time, sec
v	mode shape quantity representing linear flap deflection at the tip of blade
V_f	forward velocity of helicopter, m/sec
VGR	abbreviation for variable geometry rotor
V_y,V_z	flatwise and chordwise shears, respectively, N
w	inflow velocity, m/sec or mode shape quantity representing linear edgewise deflection at the tip of blade
ZA	chordwise length between midchord and neutral axis, m
α_s	shaft tilt angle, positive aft, rad
$\dot{\alpha}$	pitching rate of helicopter during symmetrical pullup, rad/sec

$\beta_o, \beta_1, \beta_2$	steady and first harmonic lateral and longitudinal blade flapping components, deg
Γ	vortex element circulation, m^2/sec
δ_3	pitch-flap coupling, rad
Δt	$d\psi/\Omega$, sec
$\Delta\phi$	incremental twist, deg
ΔLZ	neutral axis chordwise incremental offset, m
$\Delta\psi$	azimuthal spacing between the blades of two rotors of VGR system, deg
$\Delta\bar{z}$	axial spacing between the two rotors of VGR system, nondimensionalized with respect to chord of the rotor blade.
ϵ	chordwise separation of the elastic axis and center of mass, positive forward, m
θ_o	collective at the root of the blade, deg
μ	advance ratio, $V_f/\Omega R$
ρ	air mass density, $N\text{-}sec^2/m^4$
ϕ	mode shape quantity representing angular torsional deflection at the tip of blade, rad
ψ	azimuthal coordinate, positive counter-clockwise, zero aft, rad
ω	base frequency, rad/sec, for harmonic analysis of sound pressure
Ω	rotor speed, rad/sec

Subscripts and Mathematical Terminology:

$\log_{10}( )$	logarithm to base 10
n	$n^{\underline{th}}$ harmonic
x	indicates component parallel to x-axis
y	indicates component parallel to y-axis
Z	indicates component parallel to Z-axis

Δ indicates an increment, e.g. Δt is an increment in time

indicates time derivative, e.g. $\dot{\alpha}=\frac{d\alpha}{dt}$

DISCUSSION OF THE ANALYSES UTILIZED

The overall flow chart of the manner in which the various computer programs were utilized is illustrated in Figure 1. The preliminary calculations correspond to obtaining trim control settings and other operating conditions needed for both the wake and the blade loads and response program and also obtaining the coupled blade vibration modes to be used in the blade loads and response program. The performance program, Reference 6, was utilized to determine the trim settings of the rotor for the various flight conditions. This program determines numerically the helicopter rotor performance by considering the aerodynamic characteristics of lifting rotors. The characteristics considered include the thrust, profile drag power, total power, flapping, rolling, and pitching moments, direction of the resultant force vector, and the harmonic contribution of each blade of the rotor to the shear-force input to the hub. The equations account for stall and compressibility effects and geometric parameters such as hinge offset, etc. are included. The blade is assumed to be rigid with pitch and flap freedoms but no lag motion is provided. The different hinge conditions include teetering, articulated, and a δ_3 hinge. The specified airfoil characteristics can vary with both angle of attack and Mach number. For the present computations the option of the program utilized involved the prediction of the control settings to produce the specified performance characteristics.

The natural frequencies and corresponding mode shape quantities required for the calculation of the response of the flexible blades to aerodynamic and inertia loads were obtained by utilizing the rotor vibration analysis program developed by Rochester Applied Science Associates, Inc. (RASA), Reference 7. Briefly, the model used for the real blade is a lumped parameter approximation consisting of uniform massless elastic beam sections under tension due to centrifugal loads, with point masses and inertias located at the ends of the massless lengths. A modified transfer matrix approach is used in determining the natural frequencies and mode shapes. The mode shapes and natural frequencies used for the present calculations were fully coupled edgewise, flapwise, torsion modes.

For the specified operating conditions and rotor configuration, the deformed wake analysis program, Reference 8, was utilized to carry out the deformed wake analysis to determine the wake geometry and wake influence coefficients and load estimates. The blade loads and response program, Reference 8, uses these wake influence coefficients and load estimates as inputs and determines the harmonic loads and blade motions, shears and moments, etc. The induced flow and aerodynamic forces predicted by means of loads program were used in conjunction with the noise prediction program (Reference 9) to determine the noise spectrum at one observer location. The combined analyses and programs were directed toward prediction of blade periodic air loads and response, the shears and moments transmitted from the rotating blade system to the stationary fuselage system, and the noise spectrum at an observers location. As presently implemented, the computer program could model two arbitrarily located rotors, blade-wake and wake-wake interactions are allowed. All blades on a rotor are assumed to be identical, and all blades' motions, loads, etc., are also assumed to be the same.

While the details of deformed wake analysis are given in Reference 3 and 8, a brief description of the program will be presented in order to acquaint the reader with the overall features of the program. The model for the wake is one which has a mesh of shed and trailed vortices immediately behind each blade for a limited number of azimuthal steps, followed by a set of one or more trailings vortices for the remainder of the wake. The vortex elements have finite cores of rigidly rotating fluid, are straight, and have uniform strength and core radii along each vortex element length. Vorticity is conserved in the mesh of shed and trailed vortices, but not in the trailed-vortex-only portion of the wake.

The generation of the wake geometry is done by a process similar to start-up of a rotor in a free stream. Blade positions are determined by input or preliminary calculations, and are not influenced by the wake or by blade loads. At first there is no wake, then a set of shed and trailed vortices are generated behind each blade as the blades move through an azimuthal increment $d\psi$. Bound circulations are then computed, with the newly generated trailing and shed vortex elements having strengths corresponding to the bound circulations. The bound circulations are stepwise uniform radially and have values corresponding to the midpoints between trailing vortices. Once all vortex element strengths are known, induced and free stream velocities are computed at all vortex element end points. The blades are then advanced by $d\psi$ to new specified positions, and the vortex element end points are transported to new positions, by travelling at their determined velocities for the time $\Delta t = d\psi/\Omega$. A new set of bound circulations is then computed which includes the effects of existing wake. The wake element end point velocities are again computed, the blades advance and the wake elements transported. This process is

continued until a specified number of azimuthal steps has been taken, after which the model of trailed vortices only is used to continue the wake model representation. For practical use, the number of revolutions of wake retained for actual computational purposes is given by N >1/$\mu\pi$. The spanwise locations of trailing vortices in the mesh behind the blades are specified so as to conserve the impulse of vorticity for each spanwise section by using a set of spanwise sections with approximately equal total load.

The wake computer program has logic structure such that it is able to perform deformed wake calculations for more than one rotor. The rotors may have arbitrary relative locations, with any number of identical blades spaced uniformly around the rotor. Different rotors may have blades with different physical properties. The wakes from all blades interact in determining the wake geometry, but no mechanical blade motion interaction is allowed.

Blade Loads and Response Model and Formulation

The blade loads program used for the computations of blade aerodynamic loads and harmonic shears and moments needs as input the appropriate aerodynamic quantities, blade physical properties and coupled mode natural frequencies and corresponding mode shapes, wake geometry influence coefficients which when multiplied by appropriate blade circulation values give wake-induced velocities at the rotor blades, and initial estimates of blade circulations for use in the first iteration of blade loads and blade dynamic response.

The mathematical formulation of the blade loads and response program is described in detail in References 3 and 8, and only a brief description will be presented herein. The right-handed coordinate system used in the calculation of blade circulations and blade response is located such that the Z-axis is fixed to the shaft, directed upward, the x-axis is downstream, blade azimuth angle, ψ, is measured with respect to the x-axis, and the distance radially outward from the axis of rotation on a given blade is denoted by r, as shown in Figure 2.

The aerodynamic loading at a given radial and azimuthal station is derived from the total flow experienced by the blade section. That is the velocity component in the rotor plane and that normal to the rotor plane as seen by the blade section are expressed in terms of pitch angle, blade twist, the torsional deflection of the blade section, rotational speed, plunging velocity of the blade section due to response, the wake induced downwash, climb rate and other maneuver and rotor parameters.

Wake influence coefficients and initial estimates of blade circulations from the wake program are used for the initial trial value of wake-induced downwash for aerodynamic load determination. Ultimately the blade circulations are computed in an iterative manner that is discussed fully in Reference 8. The lift, drag, and moment per unit span are readily computed once blade circulations have been obtained. The aerodynamic coefficients required for these computations are obtained from empirical approximations to experimental data. These empirical approximations are given in Reference 3 for an NACA 0012 airfoil and those for an NACA 0015 are given in Reference 8. The aerodynamic coefficients are, in general, nonlinear functions of Mach number and angle of attack.

The aerodynamic forces and moments, as computed, are put in a more convenient form for calculation of blade response. A coordinate transformation and integration of the aerodynamic loads is performed so that generalized forces acting on previously determined normal mode shapes may be computed. The total forces and moments at each radial position corresponding to a blade mass point and to each azimuth position are computed. The generalized force associated with each mode is then computed for each azimuth position of the blade. The governing second-order differential equation for the generalized coordinate is solved next, utilizing the computed generalized force for the mode, along with the frequency and damping coefficient of the mode.

Upon convergence of the iteration procedure between blade circulation and blade response, shear and moment quantities are computed from the mode shape quantities. Also the aerodynamic information which includes aerodynamic angle of attack, wake inflow angle and the resultant airflow velocity at each blade station and azimuth position is punched out by the blade loads and response program during the final iteration of the computations. This information along with the flight conditions, helicopter blade control settings, etc. is used as input to the noise prediction program.

Helicopter Rotor Noise Model and Prediction

A detailed discussion of the theory of the computer program utilized to obtain noise spectrum at one observer location is given in Reference 9. Briefly, the program calculates the rotational and vortex noise of the helicopter systems in steady state flights. The program assumes that rotor noise originates from the normal aerodynamic forces and vortex shedding at the Strouhal frequency. The program sums up the noise contribution from stations distributed along each of the blades on each of the two rotors at arbitrary locations. Each station is treated as moving lift, drag and vortex force dipole. Because of retarded time effects the noise generated by each of the rotor stations at

uniform intervals of time arrives at the microphone at random, non-uniform intervals. The program uses an interpolation procedure to calculate the pressure at the microphone (observer location) at a uniform time interval. The input of the program consists of the helicopter parameters, the helicopter altitude, helicopter flight condition, the rotor wake induced velocity, the helicopter position and the microphone position. The output of the program consists of the pressure time history at the microphone position. This pressure-time history data is subsequently spectrum analyzed by a program utilizing a fast Fourier transform analysis for the range of approximately 1 to 500 Hz. The spectrum analysis program also provided plots of pressure versus time and SPL(dB) versus frequency.

RESULTS AND DISCUSSION

This section presents and analyzes the results obtained from the blade loads and response program for the variable geometry-rotor system in forward flight and pullup maneuvers. The results of the preliminary calculations, which include those obtained from the deformed wake analysis, the blade trim settings and operating conditions determination and blade normal modes and corresponding natural frequencies estimation, are also presented. In addition, the results of the prediction of the noise spectrum at one observer location for various rotor configurations are presented and discussed.

Preliminary Calculations

Preliminary calculations comprise the determination of the helicopter flight conditions and performance type parameters, description of the blade dynamic properties in terms of normal modes and natural frequencies and prediction of the wake geometry and induced velocity field.

Flight conditions and performance parameters.- Based on the rotor blades and fuselage characteristics described in Tables I and II, the blade trim settings for all configurations and operating conditions were determined using a force balance on the rotor. The program utilized for this purpose is described in details in Reference 6. The control parameters were obtained for both the six-bladed and the three-bladed rotor systems in level steady-state trim flight at two advance ratios 0.2 and 0.3 and also in a steady pullup maneuver at two different "g" levels 1.4 and 1.8 for 0.2 advance ratio. The results of the preliminary performance calculations are presented in Table III. The airfoil characteristics used for these computations were those of a modified NACA-0012 airfoil and included compressibility effects. The computations included a tip-loss factor of 0.97 and were based on blade

rigid-body flapping motions, which were assumed to be forced by aerodynamic loads determined by assuming uniform wake induced inflow. For one flight condition, that is steady level-flight at $\mu = 0.2$, listed last in Table III, an additional set of control settings were obtained for the ship carrying approximately ten percent higher load.

Various configurations and corresponding control settings for which the blade loads and responses were to be computed are listed in Table IV. In this table cases 1 thru 7 correspond to various rotor configurations in level flight at an advance ratio of 0.2. Case number 2 represents the standard six-bladed rotor carrying a full load, case number 1 corresponds to a single three-bladed rotor carrying half the load and case number 3 is also a six-bladed rotor operating at approximately 110 percent load. The rotor configurations corresponding to case numbers 4 thru 6 represent two three-bladed rotors separated axially by 1 chord length and also azimuthally spaced. The definitions of $\Delta\bar{z}$ and $\Delta\psi$ are illustrated in Figure 3. For comparison purposes, the control settings determined from the performance analysis were utilized for all the rotor configurations operating at the same load at a given advance ratio. The cases listed as numbers 8 thru 17 in Table IV are various rotor configurations in level steady state flight at an advance ratio of 0.3, the case number 8 corresponding to standard six-bladed rotor and cases 9 thru 17 being various VGR configurations. Case number 18 represents the standard six-bladed rotor in steady pullup maneuver at 1.4 "g" factor while the case numbers 19 and 20 show the separated rotors in the same maneuver and at the same control settings. Case number 21 represents the standard six-bladed rotor in steady pullup maneuver at 1.8 "g" factor. Because insufficient steady thrust value was obtained from the blade loads and response program due to static stall for case number 21, it was decided not to study any other VGR configuration at this pullup rate.

It should be noted that for all the above noted cases, the same pitch controls settings were used as input for both the wake geometry program and for the blade loads and response program. Moreover, for the same flight condition, the control settings of both the rotor systems were assumed to be the same (that is no differential collective, etc. was used) even when the two rotors of the variable geometry-rotor (VGR) system were vertically separated and azimuthally spaced at different angles.

Normal modes and natural frequencies.- Using the blade mass, elastic and geometric characteristics of the rotor blade, the first six fully coupled blade vibration modes for the operational RPM were obtained by utilizing an independent program, Reference 7, and resulting normal mode and natural frequency data was used as input for the blade loads and response program. Blade natural frequencies and tip mode shape quantities and mode

identifications are given in Tables V and VI for the blade under consideration. Comparing the results listed in Tables V and VI, a very small change in the natural frequencies ω of the blade is noticed when the collective angle of the blade is increased from 11.75° to 13.25°. Moreover the coupling between the flatwise v and chordwise w deflection components of the mode shapes is increased slightly when the collective of the blade is increased.

All six modes were used in the blade loads and response calculations for all the bases. It should be noted that the model of the blade used for calculating the normal modes and natural frequencies included control system flexibility effect, the value used being 7,561,600 N/in spring stiffness at push rod and control link being 20.3 cm long.

Blade Loads and Response Results

For each of the configurations listed in Table VI, the blade loads and response calculations were performed. For all the cases the same number of azimuthal (eighteen) and radial (eight) blade aerodynamic load points were used. This radial and azimuthal aerodynamic load point spacing was considered to be adequate for determining the radial distribution of the loads through the seventh harmonic of the rotational speed. The number of normal modes used in the response calculation was six. For cases 1 thru 7, the modes listed in Table V for θ_o = 11.75 deg were used, while for case 8 thru 20, the modes given in Table V for θ_o = 13.25 deg were used. These two sets of modes are very similar and only differ because of the small difference in frequency and modal coupling due to the change in collective pitch. In all the cases the nonuniform induced velocity flow field as determined by the deformed wake analysis program was used for these computations.

The blade aerodynamic loads quantities computed by the program include forces parallel and normal to the rotor disk, and the pitching moments about the blade quarterchord. The response quantities which are computed include blade shears, moments, translational and angular response motions of the blade, wake-induced velocities and angles of attack. Also the steady forces and moments and harmonic loads transmitted from rotor to the shaft are calculated. For the various cases, the steady rotor forces, thrust, drag, and torque are listed in Table VII for each rotor of the variable geometry rotor system as well as the resultant lift force, propulsive force, and the total torque needed to drive both the rotors. It should be noted again that all of the resultant forces obtained for the various rotor configurations at a given advance ratio were obtained for the same settings of the control system. Therefore the differences in performance on one VGR configuration compared to another for the same flight conditions

are due to differences in the induced flow field generated by the wake. This allows an evaluation to be made of the independent effects of vertical separation of two rotor systems as well as the effects of azimuthal spacing between the blades of the rotors. In Figure 4, the resultant lift force and the corresponding torque are plotted for the various flight conditions and rotor configurations as listed in Table VI.

Comparison of performance results in steady level flight.- At an advance ratio of 0.2, the conventional six-bladed rotor ($\Delta\bar{z} = 0$, $\Delta\psi = 60^{\circ}$) would require 26,026 meter-newtons of torque to generate a lift force of 84,401 newtons. When the two three-bladed rotors of the VGR system are separated by one chord length without changing the azimuthal spacing between the blades ($\Delta z = 1.0$, $\Delta\psi = 60^{\circ}$) and without altering the control settings, 27,199 meter-newtons of torque would be needed to drive both the rotors and 88,804 newtons of lift force would be obtained. Thus there is an increase of 5.2% in lift force obtained. This increase in resultant lift force obtained is accompanied by an increase in the resultant torque needed to drive the rotor system. In order to compare the computed power requirements of the conventional six-bladed rotor system with those of any VGR configuration of two three-bladed rotors, it is preferable to have the comparison at the same resultant lift value rather than at the same control settings. The torque required to drive the conventional six-bladed rotor to obtain different resultant lift is denoted by the broken line in Figure 4. For $\mu = 0.2$ this curve is obtained by interpolation from the results of case number 2 as listed in Table VII and some other computed data points, while for $\mu = 0.3$, the results for case number 8 in Table VII ($\Delta\bar{z} = 0$, $\Delta\psi = 60^{\circ}$) were used.

Using the configuration of the VGR system corresponding to $\Delta\bar{z} = 1.0$ and $\Delta\psi = 60^{\circ}$ as the basis, the resultant torque needed to obtain a lift force of 88,720 newtons in level flight at $\mu = 0.2$ from the conventional six-bladed rotor is approximately equal to 27,726 meter-newtons (marked by ⊙ in Figure 4). But the required torque of the VGR configuration with $\Delta\psi = 60^{\circ}$ to generate the same lift force of 88,720 newtons in level flight at $\mu = 0.2$ is only 26,323 meter newtons (denoted by ● in Figure 4). Thus this VGR configuration ($\Delta\bar{z} = 1.0$, $\Delta\psi = 60^{\circ}$) would require approximately 5.06 percent less torque as that needed for the standard six-bladed rotor system when both the systems are operating at the same lift. It is noted however, that the standard six-bladed rotor system has to operate at a slightly higher collective setting compared to VGR system in order to carry the same lift at the same flight condition. It is believed that the reason for the beneficial change in the performance characteristics obtained for the VGR is due to the change in the induced velocity

distributions caused by changes in the relationship between the blade and wake positions.

The sketches in Figure 5 illustrate, as an example, the change in the relationship between the blades and two tip vortices for an instantaneous position of the blades for both the conventional coplanar rotor system and the VGR system corresponding to $\Delta\psi = 60^{\circ}$ and $\Delta\bar{z} = 1.0$. Only the side views has been presented, because they clearly illustrate the reorientation of tip vortices of one blade with respect to the rest of blades due to axial spacing of alternate blades.

The plots in Figure 5A present the steady blade aerodynamic loading distribution along the radius of the blade of the rotors for both of the above noted configurations. Comparing the plots of inflow angle $\frac{w}{\Omega R}$, which represent the nondimensionalized component of the velocity perpendicular to the rotor plane including the induced downwash due to wake, versus the radial position on the blade, a reduction in the inflow angle is observed at the outboard sections of the rotor blade when the two three-bladed rotors are separated by one chord. This reduction in inflow angle distribution results in an increase of the aerodynamic lift force distribution at the outboard sections of the blade as seen in the plot of F_Z versus r/R. Comparison of the plot F_X versus r/R indicates the change in the inplane aerodynamic loading distribution for the two cases. There is an overall increase in the inplane force accompanying the increase in the lift force distribution on the blade of the separated rotors as compared to that on the blade of the standard rotor. This results in slightly more torque than for the conventional six-bladed rotor.

The results plotted in Figure 4 also illustrate the effect of variation in the azimuthal spacing ($\Delta\psi$) between the blades of two rotors separated by one chord. At $\mu = 0.2$, a variation in $\Delta\psi$ of $\pm 30^{\circ}$ ($\Delta\psi$ equals 30° to 90°) result in very small changes of resultant steady lift force (variation in less than 1 percent). It is noted that changes in steady loadings due to changes in $\Delta\psi$ only, are associated with the lower of the two rotors of the VGR system as can be seen from the results of the individual rotors listed in Table VII for case numbers 4, 5, and 6. The results listed in Table VII (comparing case numbers 6 and 7) also indicate no change in the steady loadings obtained when the two rotors of the VGR system are separated by a distance beyond one chord.

The performance results as obtained from the blade loads and response program at the higher advance ratio ($\mu = 0.3$) show a similar trend as seen at $\mu = 0.2$. At the advance ratio of 0.3 and at the same control settings, the resultant lift force and

torque as plotted in Figure 4 show a variation in magnitude with the variation in the configuration of the VGR system. The highest value of the lift force obtained is 89,730 newtons when $\Delta\bar{z} = 1.0$ and $\Delta\psi = 70^{\circ}$. Comparing the results of the conventional six-bladed rotor in the steady level flight at an advance ratio of 0.3 with those of the VGR configuration with $\Delta\psi = 60^{\circ}$, $\Delta\bar{z} = 1.0$, a reduction in torque requirements of 3.4% is observed for the separated rotors when both the rotor systems carry the same load of 87,141 newtons.

The similar results obtained in level flight for advance ratios 0.2 and 0.3 may be summarized as follows:

a. the resultant lift force obtained from the separated rotors of the VGR system is, in general, higher than that of the conventional six-bladed rotor system for the same blade control settings on the rotors.

b. the variation in azimuthal spacing between the blades of the two rotors, $\Delta\psi$, has some small but finite effect on the performance results of the lower of the two rotors but has negligible effect on the performance results of the upper rotor.

c. the increase in axial spacing between the two rotors, $\Delta\bar{z}$, beyond one chord length has negligible effect on the performance results.

Performance results in pullup maneuver at $\mu = 0.2$.- The effect of the rotor geometry on the performance of the helicopter in a pullup maneuver at 1.4 "g" load is also illustrated in Figure 4. When the two three-bladed rotors of the VGR system are separated by one chord ($\Delta\bar{z} = 1.0$) and the azimuthal spacing between the blades of the two rotors is maintained at 60° ($\Delta\psi = 60^{\circ}$), approximately 6.4% less torque is required than the conventional six-bladed rotor ($\Delta\bar{z} = 0.0$, $\Delta\psi = 60^{\circ}$) for the same pullup maneuver. When the azimuthal spacing between the blades of the two rotors is increased from 60 degrees ($\Delta\bar{z} = 1.0$, $\Delta\psi = 60^{\circ}$) to 90 degrees ($\Delta\bar{z} = 1.0$, $\Delta\psi = 90^{\circ}$) and the axial spacing between the rotors as well as the control settings of the blades are kept the same, an increase in the resultant lift force of approximately 2.0 percent is obtained accompanied by an increase of 4.25 percent in torque.

Harmonic loads results.- The blade loads program was utilized to determine the radial and azimuthal distribution of periodic loads and to compute the shears and moments transmitted from the rotating blade system to the stationary fuselage system.

The first seven harmonics of blade loads at various radial positions for different configurations and for various flight conditions are plotted in Figures 6 to 25 and 30 to 39. Since different variable geometry configurations have a slightly different magnitude of steady thrust, all the loads have been normalized to a steady thrust of 10,000 lbs. or 44,482 newtons per three-bladed rotor for the purpose of comparison. In the following discussion the blade harmonic loads are compared between the conventional six-bladed rotor system (indicated by the broken lines in the figures) and the various configurations of VGR system (indicated by solid lines) for the same flight condition.

Harmonic loads in steady level flight:- The magnitudes of the various blade loads are shown in Figures 6 to 25 for the various configurations analyzed in a steady level flight condition and at advance ratios of 0.2 and 0.3. The results presented in Figure 6 for $\Delta\bar{z} = 1$ and for various $\Delta\psi$ indicate a significant drop in the magnitude of 1 per rev., 4 per rev., 5 per rev. and 6 per rev. flapwise blade hinge shear force for the blades of the upper of the two rotors of the VGR system compared to corresponding forces on the blades of conventional rotor system. A slight increase in the 3 per rev. blade hinge flapwise shear force is noticed however, when the rotors are separated by a chordlength for all $\Delta\psi$. A variation in the azimuthal spacing ($\Delta\psi$) or in the axial spacing ($\Delta\bar{z}$) of the two rotors does not show any change in the blade harmonic loadings of the upper rotor as seen in Figure 6. For the blades of the lower rotor however, there can be a significant drop in the harmonics of the blade flapwise hinge shear depending upon the azimuthal spacing between the rotors. For example for $\Delta\psi = 30^{\circ}$ there is a significant drop in the 1st, 2nd, 4th, 5th harmonics of the flapwise hinge shears. However for a $\Delta\psi = 60^{\circ}$ a significant drop in the flapwise hinge shears is obtained in only the first harmonic component.

The harmonics of the blade flapwise hinge shear when the rotors are in level flight at $\mu = 0.3$ are sketched in Figures 8 and 9. For the blades of the upper rotor the magnitudes of the harmonic loadings for only one VGR configuration are given at $\mu = 0.3$, because for all other configurations of VGR system the loads are identical in magnitude at this μ. The blade harmonic loadings on the lower rotor, however, (Figure 9) vary with azimuth spacing ($\Delta\psi$), particularly for harmonics above the third.

The effect of advance ratio on the blade flapwise hinge shear can be obtained by comparing the results at $\mu = 0.2$ and $\mu = 0.3$ given in Figures 6 to 9. The decrease in the one per rev. flapwise hinge shear forces obtained when the rotors are

separated by one chord length is less at $\mu = 0.3$ than it is at $\mu = 0.2$, but all the other harmonics show roughly the same trend with $\Delta\psi$ at both the advance ratios. A slightly more detailed analysis of variation in the lower rotor flapwise hinge shear harmonics for various azimuthally spaced configurations indicates that $\mu = 0.2$, there is reduction (compared to $\Delta\bar{z} = 0.0$, $\Delta\psi = 60^{\circ}$) in all but the third harmonic when $\Delta\bar{z} = 1.0$ and $\Delta\psi = 90^{\circ}$. Therefore one might expect that this configuration would be the best as regards blade harmonic flapwise loading. A similar study of the results presented in Figure 9 for $\mu = 0.3$ indicates that the configuration corresponding to $\Delta\bar{z} = 1.0$ and $\Delta\psi = 60^{\circ}$ should result in the least amount of blade harmonic hinge flapwise shears.

The chordwise hinge shear varies in a similar fashion as the flapwise hinge shear for the blades of the upper rotor when the VGR system is in level flight at $\mu = 0.2$, as seen from the results presented in Figure 10. That is, there is some decrease in the magnitude of all the harmonics of chordwise hinge shear except the three per rev. harmonic when the two rotors of the VGR system are separated by one chordlength. Figure 11 presents the variation in the blade chordwise hinge shear of the lower rotor for various rotor phasings. The configuration corresponding to $\Delta\bar{z} = 1.0$ and $\Delta\psi = 90^{\circ}$ show the drop in magnitude for most of the harmonics of blade chordwise hinge shear. It is noted that some variation in the steady chordwise hinge shear is obtained when the azimuthal spacing between the rotors is altered. As previously noted in the discussion of the performance characteristics this results in a slight variation of the steady torque for the same steady thrust.

Unlike the results obtained at $\mu = 0.2$, most of the blade chordwise hinge shear harmonics obtained for $\mu = 0.3$ for both the upper and lower rotors show an increase in magnitude when the rotors are separated by one chord length and the rotor phasing is varied (see Figures 12 and 13). The configuration corresponding to $\Delta\bar{z} = 1.0$ and $\Delta\psi = 60^{\circ}$ among all configurations studied seems to result in the least amount of this increase although it is rather marginal for most harmonics.

Figures 14 and 15 show the plots of the harmonics of the blade pitching moment at the control rod attachment point ($r/R = 0.25$) on the blade for the upper and the lower rotor respectively for level flight at $\mu = 0.2$. All the blade pitching moment harmonics except steady for the blades of upper rotor show some drop in magnitude when the rotors are separated for this flight condition. But the VGR configuration with $\Delta\bar{z} = 1.0$

and $\Delta\psi = 60^{o}$ indicates significant drop in all the harmonics and may be considered the best as far as blade pitching moment loads are concerned. Except for the one per rev., the 7 per rev. harmonic of blade pitching moment is significantly larger than the rest as the first torsion mode of the blade is very close to the 7Ω (see Table IV). For level flight at $\mu = 0.3$, the blade pitching moment harmonic on the blade at the control rod attachment point $r/R = 0.25$ as presented in Figures 16 and 17, are of higher magnitude compared to those at $\mu = 0.2$ as might be expected but no significant drop in the one per rev. pitching moment forces is achieved as it was at $\mu = 0.20$. A further analyses of results presented in Figure 17 for the lower rotor indicates that at an advance ratio of 0.30 the VGR configuration with $\Delta\bar{z} = 1.0$ and $\Delta\psi = 70^{o}$ may be the best as far as the blade pitching moment loads are concerned.

Figures 18 to 21 present the flapwise bending moment harmonic loadings at the blade radial location corresponding to $r/R = 0.282$ for various rotor configurations in level flight at different advance ratios. The radial location of the blade at which the maximum bending moment occurs varies from configuration to configuration due to variations in the spanwise loading distribution, but for discussion purposes only the data at radial location $r/R = 0.282$ will be presented. This radial location on the blade corresponds to where the maximum steady bending moment occurs for the standard six-bladed rotor system. At $\mu = 0.2$, for the upper rotor, a decrease in the magnitude of all the harmonics of flapwise bending moment except the steady third and seventh per rev. is noticed for the various VGR configuration when these loads are compared with those of the standard six-bladed rotor system. But at $\mu = 0.3$, for the upper rotor blades (Figure 20), a drop in blade flapwise bending moment is obtained for only steady, second, fourth and fifth harmonics. The first, third, sixth and seventh harmonics of blade flapwise bending moment show significant rise in magnitude. For the lower rotor blades the magnitude of all the harmonics are generally higher and vary appreciably depending upon the configuration (Figure 21). This variation is primarily due to the fact that the spanwise loading distribution on the blade gets altered due to change in rotor induced flow field caused by modification of the rotor geometry as discussed before in the performance results.

The various harmonics of chordwise bending moment of the blade at $r/R = 0.282$ are plotted in Figures 22 to 25 for various level flight conditions. At $\mu = 0.2$, for the blades of upper rotor, all the harmonics of chordwise bending moment except the third harmonic are significantly lower in magnitude for all the configurations with $\Delta\bar{z} > 1.0$ when compared to those of the coplanar six-bladed rotor. At $\bar{\mu} = 0.3$, however, only the second, third and fourth harmonics of blade chordwise bending moment are lower

in magnitude for separated rotors when compared to those of the coplanar rotors. In addition, the first, sixth and seventh harmonics of blade chordwise bending moment vary insignificantly with the change in the geometry of rotors.

The harmonic shears and moments transmitted from the rotating blade system to the stationary fuselage system for the different configurations are presented in Figures 26 and 28 for level flight at $\mu = 0.2$ and in Figures 27 and 29 for level flight at $\mu = 0.3$. These plots show the variation in the 3 per rev. and 6 per rev. forces and moments transmitted to the fuselage, with the change in azimuthal spacing $\Delta\psi$ between the blades of the two three-bladed rotors spaced apart by a distance equal to one chord or more. For the conventional six-bladed rotor system, no 3 per rev. thrust, pitching moment or rolling moment is transmitted to the stationary fuselage system (indicated by the 'x') from the rotating blade system. But when the two three-bladed rotors are separated, there is residual 3 per rev. shears and moments transmitted from the rotating blade system to the stationary fuselage system due to unequal loadings on the two rotors and/or due to azimuthal spacing between the two rotors.

The pitching and rolling moment components transmitted to fuselage as presented in Figures 26 thru 29 are the resultant moments in stationary coordinate system about the center of the hub. The 3 per rev. moments are due to 2 per rev. and 4 per rev. blade thrust components at the hinge (multiplied by hinge offset) and the 6 per rev. moments are due to 5 per rev. and 7 per rev. blade thrust components at the hinge. If the rolling and pitching moments about the center of gravity of the fuselage are desired, additional components should be added to the already computed moments about the hub. These additional components are obtained by multiplying the resultant 3 and 6 per rev. rotor lateral and longitudinal forces in stationary coordinate system by the appropriate offset distances. The 3 per rev. rotor forces are due to 2 and 4 per rev. blade inplane shears and the 6 per rev. inplane rotor forces which come from 5 and 7 per rev. blade inplane shears are computed and have been presented in Figures 26 thru 29, 'x' and 'Δ' indicate the magnitudes of 3 per rev. and 6 per rev. transmitted loads respectively corresponding to the standard six-bladed rotor. The resultant 3 per rev. thrust and inplane shear forces and 3 per pitching and rolling moments about the hub locations, transmitted from the blades to stationary shaft system, as is clear from Figures 26 and 27, are strongly dependent upon the azimuthal spacing between the blades of the rotors, being very large when $\Delta\psi$ is 30 degrees or 90 degrees and being small when $\Delta\psi$ is close to 60 degrees.

As indicated by the results presented in Figures 26 and 27, the variation of 3 per rev. forces and moments with $\Delta\psi$ at $\mu = 0.3$ is much more pronounced than at $\mu = 0.2$ and among all

the configurations of the VGR system with separated rotors, the one with $\Delta\psi$ close to 60^{o} will generally result in the smallest amount of harmonic loads being transmitted to the fuselage, when the system is in level flight at high advance ratios. It is believed that one way of reducing the high magnitude of 3 per rev. transmitted thrust obtained for some VGR configuration may be the use of differential collective for the upper and lower rotors.

The results presented in Figures 28 and 29 indicate that the 6 per rev. transmitted shears and moments are also strongly dependent on the azimuthal spacing between the blades of the two rotors $\Delta\psi$. At the lower advance ratio ($\mu = 0.2$), the 6 per rev. transmitted thrust magnitudes are lower for the rotors separated by one chord length than for the standard six-bladed rotor. But at $\mu = 0.3$, the VGR configurations with $\Delta\bar{z} = 1.0$ have more 6 per rev. transmitted thrust than the conventional six-bladed rotor system. At $\mu = 0.2$, it seems that the configuration with $\Delta\bar{z} = 1.0$ and $\Delta\psi = 90$ degrees may be the one with the lowest amount of overall 6 per rev. forces and moments transmitted to the fuselage, while at $\mu = 0.3$ the configuration corresponding to $\Delta\bar{z} = 1.0$ and $\Delta\psi = 60^{o}$ may result in the least amount of 6 per rev. transmitted loads.

Blade harmonic loads in pullup maneuver:- The variations in blade harmonic loads with different configurations of VGR system in pullup maneuver at 1.4 "g" factor and at $\mu = 0.2$ are illustrated in Figures 30 to 38. The plots in Figure 30 indicate that a reduction in the magnitudes of steady, one per rev. two per rev., five per rev. and seven per rev. harmonics of the blade flapwise hinge shear of the upper rotor can be achieved by separating the two rotors by one chord length. The third per rev., fourth per rev. and sixth per rev. harmonics, however, show an increase in magnitude. The magnitude of various blade hinge flapwise shear harmonics on the lower rotor vary with $\Delta\psi$ (Figure 31). For the configuration corresponding to $\Delta\bar{z} = 1.0$ and $\Delta\psi = 90^{o}$ all the blade hinge flapwise shear harmonics are lower in magnitude than those for the standard six-bladed rotor system. Therefore this configuration may be considered the best as far as the blade flapwise shear loads are concerned.

The steady, one per rev., two per rev. harmonics of blade chordwise hinge shear of the upper rotor for all configurations with separated rotors, are smaller in magnitude, while the three per rev. harmonic is slightly higher in magnitude than that of the conventional six-bladed rotor (Figure 32). The fourth through the seventh harmonic do vary somewhat but their magnitude is so small that they can be ignored. A study of the data presented in Figure 33 also indicates that the VGR configuration

with $\Delta\bar{z} = 1.0$ and $\Delta\psi = 60^{\circ}$ may be the one with the lowest blade chordwise hinge shear loads on the lower rotor. The same conclusion is drawn from the results of blade pitching moment loads presented in Figures 34 and 35, while only the steady, first per rev., fourth per rev., fifth per rev. and sixth per rev. harmonics of blade pitching moment load at $r/R = 0.25$ show decrease in magnitude for the upper rotor, all the important harmonics except the two per rev. are reduced in magnitude for the lower rotor. An examination of Figures 36 and 37 which presents the magnitudes of flapwise bending moment harmonics on the blade at $r/R = 0.282$ for various VGR configurations, indicates that the configuration corresponding to $\Delta\bar{z} = 1.0$ and $\Delta\psi = 90^{\circ}$ has the least amount of flapwise bending harmonic loads on the blade. For this configuration all the harmonics of flapwise bending moment on blades of lower rotor and all but third, fourth and seventh harmonics on blades of upper rotor are smaller in magnitude than the corresponding harmonics on rotors in the coplanar configuration. The configuration with $\Delta\bar{z} = 1.0$ and $\Delta\psi = 60^{\circ}$ has higher magnitudes of third per rev., fourth per rev., fifth per rev. and sixth per rev. flapwise bending moment loads on the lower rotor than those on the blades of coplanar configuration.

The harmonics of chordwise bending moment on the blade at $r/R = 0.282$ are given in Figures 38 and 39 for the three configurations studied in pullup maneuver at 1.4 "g" load. For chordwise bending moment loads also the configuration with $\Delta\bar{z} = 1.0$ and $\Delta\psi = 90^{\circ}$ seems to be the one with the least amount of resultant inplane moments. For the blades of lower rotor in the above configuration, all the harmonics of chordwise bending moment except steady are lower in magnitude than those on the blades corresponding to standard six-bladed rotor. But for blades of upper rotor of configuration with $\Delta\bar{z} = 1.0$ and $\Delta\psi = 90^{\circ}$, the third per rev., fourth per rev., sixth per rev. and seventh per rev. chordwise bending moment harmonics are higher in magnitude compared to those on blades of a coplanar rotor. Since the moments for $\Delta\psi = 60^{\circ}$ are basically the same the evaluation of the best configuration must be made on the basis of the results for the lower rotor.

A study of 3 per rev. loads transmitted to fuselage and presented in Figure 40, however, indicates that the configation with $\Delta\bar{z} = 1.0$ and $\Delta\psi = 60^{\circ}$ may be a better one than the configuration with $\Delta\bar{z} = 1.0$ and $\Delta\psi = 90^{\circ}$, if the criterion is to minimize the 3 per rev. transmitted loads. The 6 per rev. loads transmitted from the blades to the stationary fuselage system for various configurations in the same pullup maneuver

are given in Figure 41. It may be noted that there is no significant difference in the 6 per rev. transmitted loads for the standard six-bladed rotor and VGR configuration with $\Delta\bar{z} = 1.0$ and $\Delta\psi = 60^{o}$. However, for the configuration with $\Delta\bar{z} = 1.0$ and $\Delta\psi = 90^{o}$, the 6 per rev. transmitted rolling and pitching moments in the fixed system will be reduced by a factor of two but the 6 per thrust being transmitted to the fixed fuselage system will be increased by a factor of approximately 3.

Rotor Noise Prediction Results

For each of the configurations and flight conditions listed in Table IV, the noise spectrum at one observer location was obtained utilizing the noise prediction program (Reference 9). On the basis of Reference 10 the microphone position (observer location) for all cases was taken to be 68.6 m in front, 53.3 m below and 28.7 m to the right (advancing side) with respect to rotor hub. Moreover, the relative position of the microphone with respect to the rotor hub was maintained since it was assumed that the microphone moved with the helicopter.

The required distributions of angles of attack, inflow angles, and flow velocities were obtained from the output of the blade loads program for each of the configurations considered and thus the computations include the effects of the nonuniform wake induced flow. Each blade was represented by 16 radial stations acting as locations for sources of sound.

The sound pressure at the microphone was computed as the function of time using a time interval of 10^{-3} seconds and the number of intervals used was 1052. Both the rotational noise and the noise created by vortex shedding was included in the prediction, but ground reflection effects were neglected.

Figure 42 illustrates, as an example, the variation of sound pressure with time of the rotational noise from the conventional six-bladed rotor system (case 2 in Table VI) in level flight at $\mu = 0.2$. When the spectrum analysis of the pressure-time history data in Figure 42 is obtained utilizing a fast Fourier transform, a plot shown in Figure 43 results which presents the variation of SPL in DB as the function of the frequency in Hz. The effective band width was approximately 1 Hz over the frequency range of 0 to 512 Hz.

Figures 44 to 48 are plots of SPL versus frequency for various configurations of VGR system in level flight at $\mu = 0.2$ when both the rotational and vortex shedding noise contributions are included. Similar plots for the various VGR configurations of the aircraft in level flight at $\mu = 0.3$ are presented in

Figures 49 to 57. Similarly Figures 58 thru 60 illustrate the variations of SPL in terms of dB versus the frequency in Hz for the different VGR configurations studied when the helicopter is in a pullup maneuver.

For the six-bladed rotor operating at approximately 200 rpm (or 21.29 rad/sec), the blade passage frequency is approximately 20 Hz, while for each of the three-bladed rotors operating individually at the same rpm the blade passage frequency is approximately 10 Hz.

Figure 44 presents the noise spectrum of the conventional six-bladed rotor at an advance ratio $\mu = 0.20$. The significant peaks and their harmonic number in terms of the blade passage frequency of the three-bladed rotor have been identified. As can be seen the odd harmonics that would be associated with a three-bladed helicopter rotor are not apparent and the even harmonics associated with a six-bladed rotor dominate the spectrum. When the two three-bladed rotor systems are separated by one chordlength but the blade phasing are those of the six-bladed single rotor (i.e. $\Delta\psi = 60$ degrees) the characteristics of the spectrum are changed significantly as shown in Figure 45. In case of this rotor configuration ($\Delta\bar{z} = 1.0$, $\Delta\psi = 60^{\circ}$) the odd harmonics of the blade passage frequency (10 Hz) associated with a three-bladed rotor seem to dominate. Even though the envelope of the peaks is about 5 dB higher for the separated rotors ($\Delta\bar{z} = 1.0$, $\Delta\psi = 60^{\circ}$) than that for the coplanar configuration ($\Delta\bar{z} = 0.0$, $\Delta\psi = 60^{\circ}$), it cannot be assumed that the configuration with $\Delta\bar{z} = 1.0$, $\Delta\psi = 60^{\circ}$ would be noisier than the configuration with $\Delta\bar{z} = 0.0$, $\Delta\psi = 60^{\circ}$ because of differences in characteristics at higher frequency end of the spectrum. For the rotor configurations with $\Delta\bar{z} = 1.0$ and $\Delta\psi = 60 \pm 30^{\circ}$ (Figures 46 and 47), the noise spectrum contains a mix of peaks at frequencies which are both the odd and even multiples of 10 Hz and thus it cannot be stated for sure that the rotors would sound more like a three-bladed or a six-bladed rotor configuration. However, since at the low frequency end of the spectrum, the 3, 4, 5, 6 and 7th harmonic of a three-bladed configuration seem to dominate, it is expected that the entire six-bladed rotor configuration ($\Delta\bar{z} = 1.0$, $\Delta\psi = 60 \pm 30^{\circ}$) would sound more like a three-bladed rotor and might be noisier than the six-bladed coplanar configuration since the envelopes of the peaks are about 3 dB higher.

Figure 48 presents the spectrum for $\Delta\psi = 90$ degrees and a rotor separation of one and one-half chordlengths, $\Delta\bar{z} = 1.5$. Comparison of these results with those presented in Figure 46 indicates that the additional half of a chord of rotor separation did not alter the acoustic signature of the rotors.

The acoustic spectrum for the standard coplanar rotor at an advance ratio $\mu = 0.30$ is shown in Figure 49. As can be seen, the even harmonics again dominate as they should for a six-bladed rotor system and the envelope of the peaks are approximately 3 dB higher than they were at an advance ratio $\mu = 0.20$. The spectrum for the separated rotor with $\Delta\psi = 60$ degrees (Figure 50) that was predicted for an advance ratio of $\mu = 0.30$ is very similar to that obtained at $\mu = 0.20$ except that the fourth harmonic blade passage is higher relative to the third and fifth than it was at $\mu = 0.20$. The spectrum for $\Delta\psi = 30$ and 90 degrees that were predicted at an advance ratio of $\mu = 0.30$ (Figures 55 and 56 respectively) are very similar to those predicted for those configurations at $\mu = 0.20$ except that the first and second harmonics are much larger with respect to the third and fourth than they were at $\mu = 0.20$.

The spectrums presented for $\Delta\psi = 40$, 50, and 80 degrees shown in Figures 53, 51, and 54 respectively, all show a consistant sequence of even and odd harmonics and thus it is suspected that all of these six-bladed configurations would sound like a three-bladed rotor. For $\Delta\psi = 70$ degrees the absence of the fourth harmonic of the blade passage frequency might make this configuration the quietest of all of the configurations and since only the third and fifth harmonics dominate, the rotor characteristic signature may be a peculiar one to an observer.

Comparison of the spectrums presented in Figures 56 and 57 shows that increasing the separation between the rotors from 1.5 to 2.0 chordlengths did not have any apparent effect on the noise characteristics of the rotor system.

The acoustic spectrum for the conventional six-bladed rotor in pullup maneuver at 1.4 "g" factor is presented in Figure 58. The spectrum at low frequency level is similar to those for the steady level flight conditions with even harmonics dominating the spectrum. The envelope of peaks in pullup maneuver flight condition is approximately 4 dB higher than it is for level flight at $\mu = 0.2$. Also for the separated rotors having $\Delta\psi = 60$ degrees the spectrums are similar in pullup maneuver (Figure 59) and in level flight at $\mu = 0.2$, with the envelope of peaks being only 3 dB higher for the maneuver flight condition. It may be noted that for the pullup flight condition the envelope of peaks in case of the separated rotors with $\Delta\psi = 60$ degrees is of the same level as that of the conventional coplanar rotor. For the separated rotors the envelope peak occurs at 5th harmonic of blade passage, while for the coplanar rotor it is at 4th harmonic of the blade passage. The spectrum of the separated rotors with $\Delta\psi = 90$ degrees in a pullup maneuver presented in Figure 60 indicates that it would sound more like a three-bladed rotor, because the 3rd, 4th, 5th, 6th and 7th harmonics of three-bladed rotor seem to dominate the spectrum.

The envelope of peaks for this configuration is approximately 5 dB lower than that of the conventional coplanar rotor.

It is believed that the general effect of rotor separation on the acoustic output of the six-bladed rotor is to make it sound more like a three-bladed rotor than a six-bladed rotor. In addition it is believed that for some of the $\Delta\psi$'s the rotor might be quieter subjectively than the standard coplanar configuration. This type of subjective evaluation could be undertaken if the predicted pressure time histories are put on audio tape and a subjective evaluation conducted.

CONFIGURATIONS FOR TEST

On the basis of the results obtained and discussed in the previous sections some test configurations can be identified and suggested to investigate experimentally the effects of rotor configurations on blade loads, performance, fuselage vibrations and noise output.

Some of the parameters to be considered for this experimental investigation are:

1. Axial spacing between the rotors, Δz
2. Azimuthal spacing between the blades of the two rotors, $\Delta\psi$
3. Advance ratio, μ
4. Differential collective pitch of the two rotors
5. Differential radius of the blades of the two rotors
6. Rotor tip speed

For the present investigation the effects of only the first three above mentioned parameters were studied and the rotor characteristics that were considered were performance, blade dynamic loads, transmitted loads and the rotor noise output. The variation of the vertical spacing Δz beyond one chord had negligible effect on all of these characteristics and therefore test to evaluate the effect should be limited. At a given Δz, the variation in the azimuthal spacing between the blades of two rotors $\Delta\psi$ results in significant variations in the performance and blade loads of only the lower of the two rotors. If blade instrumentation is limited, it should be concentrated on the lower blade set. Since the transmitted loads and noise output vary significantly with $\Delta\psi$, it is recommended that the effect of $\Delta\psi$ should be investigated experimentally in great detail.

Even though the effect of geometry on performance and noise output of VGR system indicate the same trends at both of the advance ratios that were studied, the variation in blade harmonic loads and the loads transmitted to fuselage with variation in geometry differed significantly at $\mu = 0.2$ and $\mu = 0.3$. Therefore it is recommended that the experimental investigation of blade loads and fuselage vibration should be conducted for at least three advance ratios in the range $0.20 \leq \mu \leq 0.30$.

The effect of differential collective and differential radius on the performance of VGR system in hover was investigated experimentally and results have been presented in Reference 4. While no significant benefit in performance was obtained by varying these parameters in hover (Reference 4), it is expected that in forward flight and in steady pullup maneuvers the effect of these configuration parameters may be significant as regards balancing the loads carried by the two rotors and to reduce the fuselage vibrations by controlling transmitted loads.

It is believed that the benefits achievable by the VGR rotor might be more pronounced at high tip speeds and therefore it is recommended that the experimental investigation consider determining the effect of tip speeds on the benefits that are achievable. In order to maximize the efficiency of experimental investigation it is believed that a theoretical study should be carried out prior to the test to study the effects of differential collective, differential radius and tip speed on the performance, blade loads, transmitted loads and noise output of VGR system in forward flight and pullup maneuvers. The results of this theoretical investigation could be utilized to determine the degree of benefit that could be realized by the variation of these parameters and the range over which they should be varied.

CONCLUSIONS AND RECOMMENDATIONS

The performance, blade loads and acoustic characteristics of a variable geometry-rotor (VGR) system consisting of six blades were investigated in steady level flight and in steady pullup maneuvers. The investigation considered the independent effects of vertical separation of two three-bladed rotor systems as well as the effects of azimuthal spacing between the blades of the two rotors. The following are specific conclusions obtained from the comparison of the predicted results of various configurations of the VGR system,

1. Axial spacing of alternate blades offers a significant performance advantage relative to a conventional rotor configuration for steady state flight and steady pullup maneuver conditions. This performance advantage does not show any further improvement with an increase in axial spacing beyond one chord.

2. Variation in the azimuth spacing between the blades of two separated rotors has a small effect on the overall performance of the rotor system in forward flight.

3. The gain in performance obtained when the rotors are axially spaced is due to improvement in the induced flow field of the rotor caused by the change in the wake orientation relative to the individual blades.

4. The performance and blade loads of only the lower of the two rotors depend on azimuthal spacing between the blades of two rotors. The performance and blade loads of the upper rotor change negligibly with the change in azimuthal spacing for the VGR system in forward flight or in a pullup maneuver.

5. The magnitude of the different harmonics of blade shears and moments vary appreciably with the geometry of VGR configuration as well as with the flight condition. At $\mu = 0.3$, the configuration with $\Delta\bar{z} = 1.0$ and $\Delta\psi = 60^{\circ}$ seems to have the lowest harmonic of blade loading. At $\mu = 0.2$ or in a pullup maneuver at 1.4 "g" factor, overall flapwise shear loads are minimum for $\Delta\bar{z} = 1.0$ and $\Delta\psi = 90^{\circ}$, while the overall blade pitching moment loads are lowest for $\Delta\bar{z} = 1.0$ and $\Delta\psi = 60^{\circ}$.

6. The three per rev. and the six per rev. loads transmitted from the rotating blades to the fixed fuselage system vary significantly with the variation in $\Delta\psi$. Among all the configurations of VGR system studied, the one with $\Delta\bar{z} = 1.0$ and $\Delta\psi = 60^{\circ}$ results in overall the lowest amount of shears and moments being transmitted to the fuselage when the helicopter is in level flight at $\mu = 0.3$ or in a pullup maneuver with a 1.4 "g" load factor. At $\mu = 0.2$, however, the configuration with $\Delta\bar{z} = 1.0$ and $\Delta\psi = 90^{\circ}$ transmits the least amount of oscillatory loads.

7. The general effect of rotor separation on the acoustic output of the six-bladed rotor is to make it sound more like a three-bladed rotor than a six-bladed rotor. Some VGR configurations with separated rotors might be quieter subjectively than the conventional coplanar rotor. This however, has to be verified by making an audio tape of the predicted pressure time histories and conducting a subjective evaluation.

On the basis of the results that were obtained in the present study it is recommended that additional analyses be conducted to investigate the following:

1. The effect of differential collective on the performance, blade loads, transmitted loads and acoustic characteristics of VGR system.

2. The effect of differential radius on the performance, blade loads, transmitted loads and acoustic characteristics of VGR system.

3. The effect of tip speed on the benefits that are achievable from a VGR system.

4. The effect of advance ratio should be studied more completely by conducting calculations at $\mu = 0.25$ and for an advance ratio $\mu < 0.20$.

5. A subjective evaluation of the noise output of the various VGR configurations should be undertaken. This can be achieved by creating an audio tape of the predicted pressure time histories.

REFERENCES

1. Miller, R.H.: Unsteady Airloads on Helicopter Rotor Blades. Fourth Cierva Memorial Lecture, The Royal Aeronautical Society, October 1963.

2. Piziali, R.A.; and DuWaldt: Computation of Rotary Wing Harmonic Airloads and Comparison with Experimental Results. AHS Eighteenth Annual National Forum, Washington, D.C., May 1962.

3. Sadler, S. Gene : Development and Application of a Method for Predicting Rotor Free Wake Positions and Resulting Rotor Blade Air Loads. NASA CR-1911, December 1971.

4. Landgrebe, Anton J.; and Bellinger, Dean E.: Experimental Investigation of Model Variable-Geometry and Ogee Tip Rotors. NASA CR-2275, February 1974.

5. Landgrebe, Anton J.; and Bellinger, Dean E.: Experimental Investigation of Model Variable-Geometry and Ogee Tip Rotors. 29th Annual National Forum of AHS, May 1973.

6. Gessow, Alfred; Crim, Almer D.: A Method for Studying the Transient Blade-Flapping Behavior of Lifting Rotors at Extreme Operating Conditions. NACA TN-3366, January 1955. The equations given in this technical note were used in NASA Computer Program D0865.

7. Sadler, S. Gene : Blade Frequency Program for Nonuniform Helicopter Rotors, With Automated Frequency Search. NASA CR-112071, 1972.

8. Sadler, S. Gene : Main Rotor Free Wake Geometry Effects on Blade Air Loads and Response for Helicopters in Steady Maneuvers. NASA CR-2110, September 1972.

9. Johnson, Kevin H.: Development of a Technique for Realistic Prediction and Electronic Synthesis of Helicopter Rotor Noise. USAAMRDL Technical Report 73-8, March 1973.

10. Lowson, M.V.; Ollerhead, J.B.: Studies of Helicopter Rotor Noise. USAAVLABS Technical Report 68-60, January 1969.

TABLE I

CHARACTERISTICS OF FUSELAGE
AND ROTOR USED

Gross weight, newtons	80 958
Parasite drag, meters^2	2.3226
Blade radius, R, meters	9.4488
Blade twist (linear), deg	-8.0
Tip speed, meters/sec	201.17
Hinge offset (flap and lag), percent R	3.4
Blade root pocket cutout, percent R	25
Number of blades	6
Solidity	.094

TABLE II

BLADE PROPERTIES

I	Section Length	EIX	EIY	EIZ	IX,IY	Mass	$\Delta\phi$	ϵ	ΔLZ	ZA
	m	N-m^2	N-m^2	N-m^2	N-sec^2-m	N-sec^2/m	deg	m	m	m
1	.0000	14.34 x 10^5	11.49 x 10^6	114.9 x 10^5	0.0000	28.660	.000	.0000	.0000	.0000
2	.2883	2.4880	6.9430	114.9000	4.9870	26.430	.000	.0265	.0381	.0381
3	.1524	2.4880	2.8140	57.4400	.6915	10.870	.000	.0265	.0000	.0381
4	.1524	2.4880	2.3510	12.9300	.3023	5.706	.000	.0265	.0000	.0381
5	.5334	2.4880	1.0210	2.0700	.1803	7.618	.000	.0265	.0000	.0381
6	.6096	1.3430	.8678	.9009	.1029	5.268	.000	.0280	.0013	.0394
7	.6096	.4587	.8513	.8596	.1267	6.626	-.258	.0280	.0000	.0394
8	.6096	1.1780	.8224	.7728	.1235	6.728	-.516	.0280	.0000	.0394
9	.6096	1.1780	.7893	.7315	.1095	6.305	-.516	.0280	.0000	.0394
10	.6096	1.1780	.7645	.6984	.1038	6.129	-.516	.0280	.0000	.0394
11	.6096	.8761	.7232	.6364	.0958	5.896	-.516	.0293	.0013	.0406
12	.6096	.8348	.7191	.5868	.0916	5.721	-.516	.0293	.0000	.0406
13	.6096	.8348	.6943	.5662	.0859	5.502	-.516	.0293	.0000	.0406
14	.6096	.8348	.6447	.5290	.0785	5.444	-.516	.0293	.0000	.0406
15	.6096	.7521	.6116	.4752	.0748	5.444	-.516	.0293	.0000	.0406
16	.6096	.7232	.5786	.4339	.0683	5.254	-.516	.0293	.0000	.0406
17	.6096	.7232	.5744	.3802	.0745	5.765	-.516	.0293	.0000	.0406
18	.6858	.7232	.5744	.3306	.0931	7.209	-.581	.0293	.0000	.0406

TABLE III

RESULTS OF PERFORMANCE ANALYSIS

Flight Condition	g-level	μ	Ω $\frac{rad}{sec}$	$\dot{\alpha}$ $\frac{rad}{sec}$	Pitch Angles, deg[b] θ_o	A_c	B_c	Flap Angles, deg[c] β_o	β_1	β_2	α_s deg	ρ $\frac{N\text{-}sec^2}{m4}$
Level	1.0	0.2	21.29	0.0	11.75	0.0	0.26	4.536	-.889	-2.88	-4.81	515.38
Level	1.0	0.3	21.29	0.0	13.25	0.0	0.48	4.578	-1.29	-4.84	-8.90	515.38
Pull-up	1.4	0.2	21.29	.098	13.62	0.0	0.07	6.574	-1.35	-3.59	-4.97	515.38
Pull-up	1.8	0.2	21.29	.196	15.83	0.0	-.13	8.664	-1.93	-4.73	-5.60	515.38
Level	1.0	0.2	21.29	0.0	11.14	0.0	-.22	4.472	-.917	-2.70	-4.64	515.38
Level[a]	1.0	0.2	21.29	0.0	12.71	0.0	0.35	5.595	-1.057	-3.426	-4.98	515.38

[a]At 10 percent higher load.

[b]Pitch Angle = $\theta_o + A_c \sin\psi + B_c \cos\psi$

[c]Flap Angle = $\beta_o + \beta_1 \sin\psi + \beta_2 \cos\psi$

TABLE IV

CASE NUMBERS AND CONFIGURATIONS

Case No.	Flight Condition	Advance Ratio	$\dot{\alpha}$ rad/sec	α_s deg	Configuration $\Delta\bar{z}$	Configuration $\Delta\psi$ deg	Pitch Angles θ_o deg	Pitch Angles A_c deg	Pitch Angles B_c deg	Load Percent Full
1	Level	0.2	0.0	-4.60	-	-	11.14	0.0	-0.22	50
2	Level	0.2	0.0	-4.81	0.0	60	11.75	0.0	0.26	100
3	Level	0.2	0.0	-4.98	0.0	60	12.71	0.0	0.35	110
4	Level	0.2	0.0	-4.81	1.0	30	11.75	0.0	0.26	100
5	Level	0.2	0.0	-4.81	1.0	60	11.75	0.0	0.26	100
6	Level	0.2	0.0	-4.81	1.0	90	11.75	0.0	0.26	100
7	Level	0.2	0.0	-4.81	1.5	90	11.75	0.0	0.26	100
8	Level	0.3	0.0	-8.90	0.0	60	13.25	0.0	0.48	100
9	Level	0.3	0.0	-8.90	1.0	30	13.25	0.0	0.48	100
10	Level	0.3	0.0	-8.90	1.0	40	13.25	0.0	0.48	100
11	Level	0.3	0.0	-8.90	1.0	50	13.25	0.0	0.48	100
12	Level	0.3	0.0	-8.90	1.0	60	13.25	0.0	0.48	100
13	Level	0.3	0.0	-8.90	1.0	70	13.25	0.0	0.48	100
14	Level	0.3	0.0	-8.90	1.0	80	13.25	0.0	0.48	100
15	Level	0.3	0.0	-8.90	1.0	90	13.25	0.0	0.48	100
16	Level	0.3	0.0	-8.90	1.5	90	13.25	0.0	0.48	100
17	Level	0.3	0.0	-8.90	2.0	90	13.25	0.0	0.48	100
18	Pull-up	0.2	.098	-4.97	0.0	60	13.62	0.0	0.07	140
19	Pull-up	0.2	.098	-4.97	1.0	60	13.62	0.0	0.07	140
20	Pull-up	0.2	.098	-4.97	1.0	90	13.62	0.0	0.07	140
21	Pull-up	0.2	.196	-5.60	0.0	60	15.83	0.0	- .13	180

TABLE V

BLADE FREQUENCIES AND MODE SHAPES

Ω = 21.2903 rad/sec, θ_o = 11.75 deg

FULLY ARTICULATED

Frequency ω		Tip Deflections			Mode
rad/sec	$x\frac{1}{\Omega}$	v	-w	Φ	Type
5.1031	0.2397	1.0	-9.5500	- .01510	Lead-lag
21.8566	1.0266	1.0	.0953	- .01170	Flapping
54.2262	2.5470	1.0	- .0954	- .00382	1st Elas. Flap
68.3614	3.2109	1.0	6.3200	- .02390	1st Elas. Edge
96.6103	4.5378	1.0	- .0741	.01150	2nd Elas. Flap
144.7190	6.7974	1.0	.1370	-4.60000	1st Elas. Tor.

TABLE VI

BLADE FREQUENCIES AND MODE SHAPES

Ω = 21.2903 rad/sec, θ_0 = 13.25 deg

FULLY ARTICULATED

Frequency ω		Tip Deflections			Mode
rad/sec	$x\frac{1}{\Omega}$	v	-w	ϕ	Type
5.1014	0.2396	1.0	-7.5800	- .01430	Lead-lag
21.8563	1.0266	1.0	0.1210	- .01170	Flapping
54.1785	2.5448	1.0	- .1010	- .00381	1st Elas. Flap.
68.3973	3.2126	1.0	6.0300	- .02300	1st Elas. Edge
96.5896	4.5368	1.0	- .0747	- .01150	2nd Elas. Flap.
144.6932	6.7962	1.0	.1380	-4.62000	1st Elas. Tor.

TABLE VII

HELICOPTER PERFORMANCE

Case No.	Rotor thrust N		Rotor drag N		Torque m-N		Resultant forces N		Resultant Torque
	Upper Rotor	Lower Rotor	Upper Rotor	Lower Rotor	Upper Rotor	Lower Rotor	Lift + Up	Propulsive + For	m-N
1	36 444	-	165	-	13 265	-	36 342	2 758	13 265
2	42 311	42 311	436	436	13 013	13 013	84 401	6 223	26 026
3	50 056	50 056	320	320	23 904	23 904	99 787	8 047	47 809
4	45 114	43 832	672	734	13 677	13 522	88 804	6 058	27 199
5	45 118	43 811	672	636	13 677	12 646	88 720	6 147	26 323
6	45 114	43 201	672	556	13 679	12 889	88 106	6 183	26 548
7	45 141	43 232	672	556	13 671	12 849	88 168	6 183	26 518
8	43 037	43 037	863	863	23 970	23 970	84 770	11 610	47 939
9	44 175	46 110	1 081	970	24 508	25 262	89 516	11 939	49 771
10	44 211	44 251	1 081	1 072	24 519	24 436	87 728	11 552	48 953
11	44 211	44 304	1 081	1 045	24 517	25 251	87 781	11 588	49 768
12	44 180	43 699	1 081	992	24 508	23 986	87 141	11 543	48 494
13	44 211	46 279	1 085	1 023	24 519	25 375	89 730	11 917	49 894
14	44 215	44 402	1 085	1 112	24 520	24 675	87 888	11 534	49 195
15	44 215	44 246	1 085	1 036	24 521	25 056	87 723	11 588	49 577
16	44 224	44 295	1 081	1 036	24 512	25 095	87 786	11 597	49 605
17	44 224	44 313	1 085	1 041	24 510	25 099	87 808	11 597	49 609
18	54 682	54 682	11	11	28 742	28 742	108 955	9 457	57 484
19	55 327	54 655	93	4	28 341	25 500	109 577	9 435	53 841
20	55 323	56 443	93	222	28 345	27 785	111 375	9 359	56 128

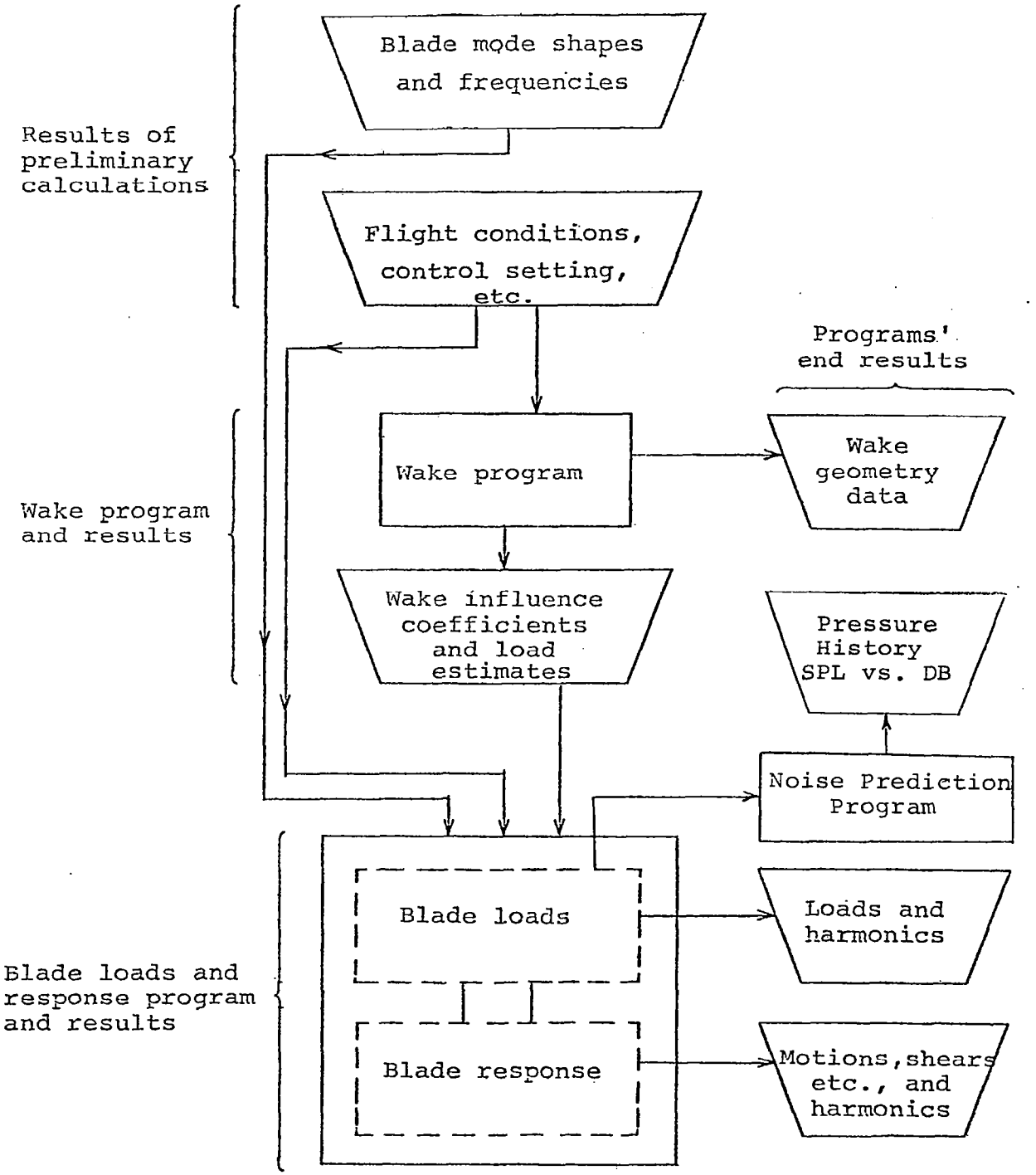

Figure 1. Program usage flow diagram

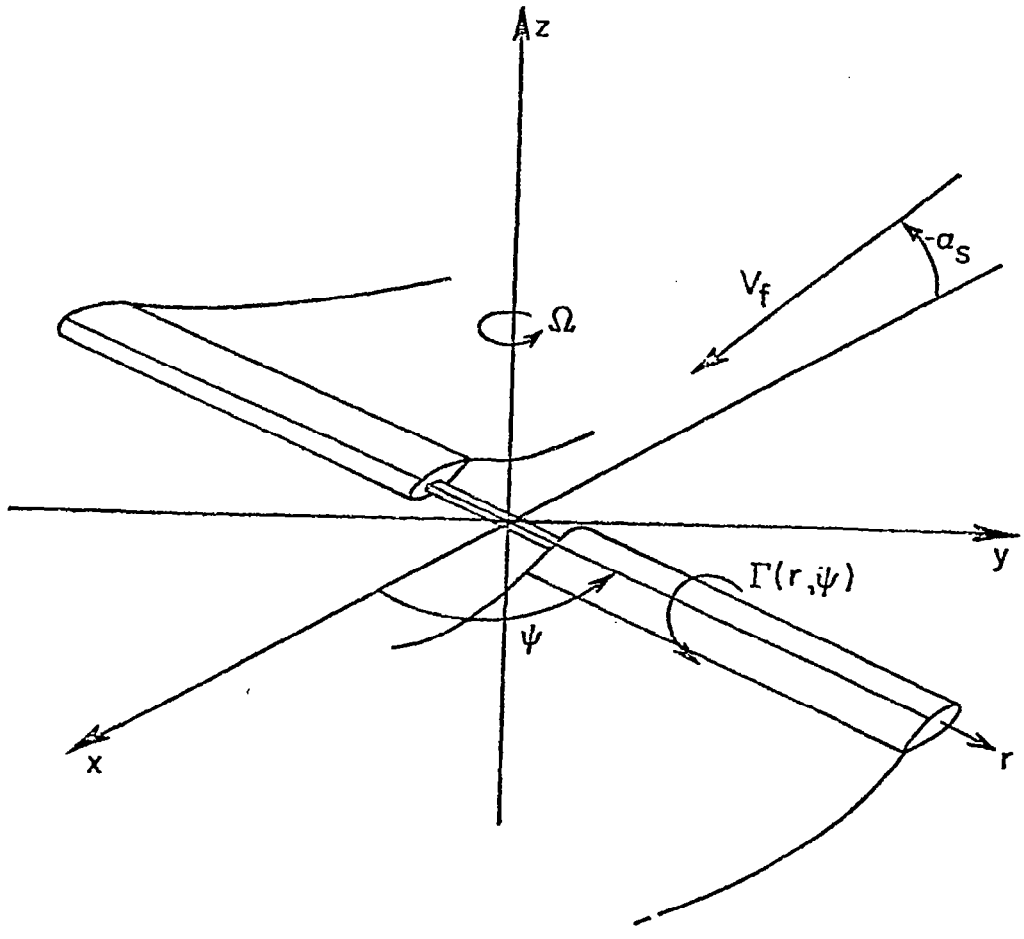

Figure 2. Rotor system coordinates

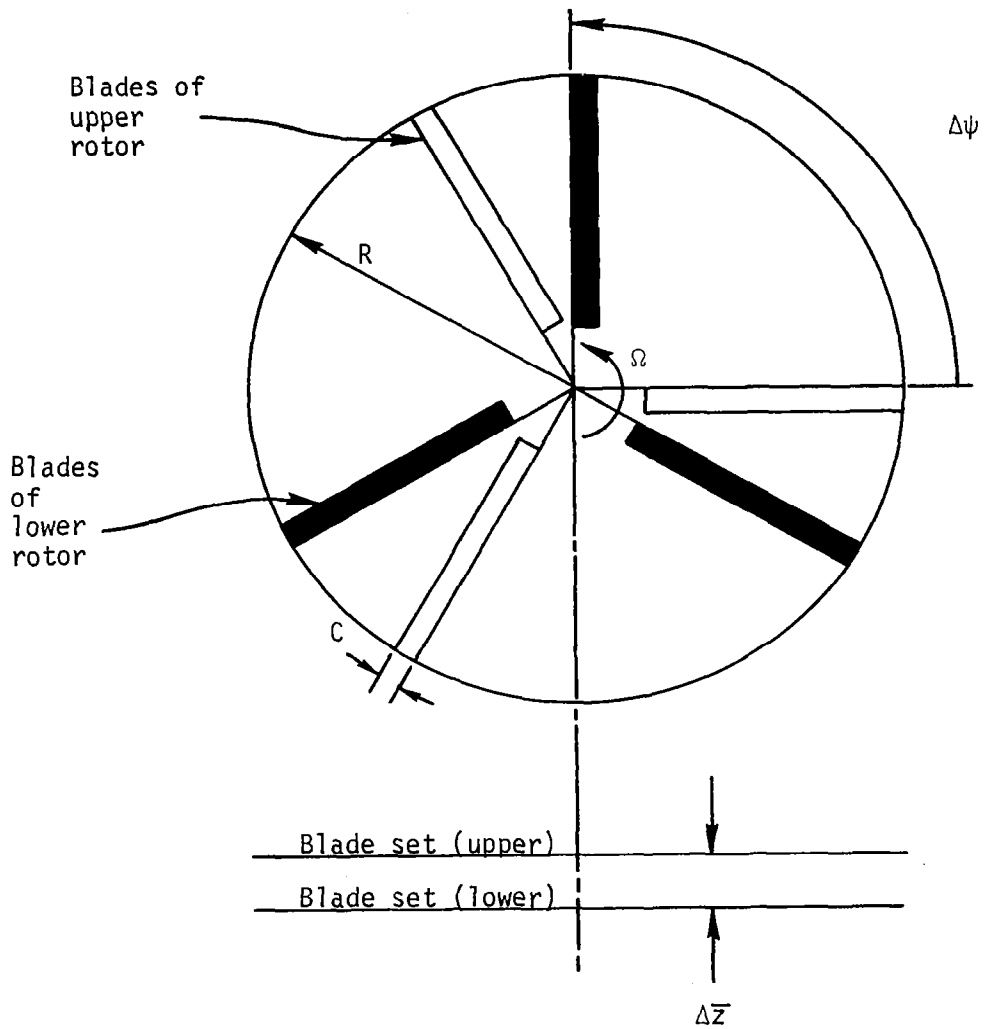

Figure 3. Schematic diagram of variable geometry rotor

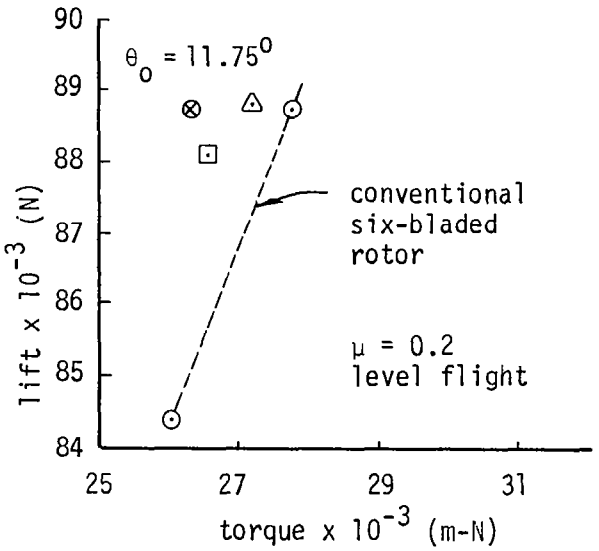

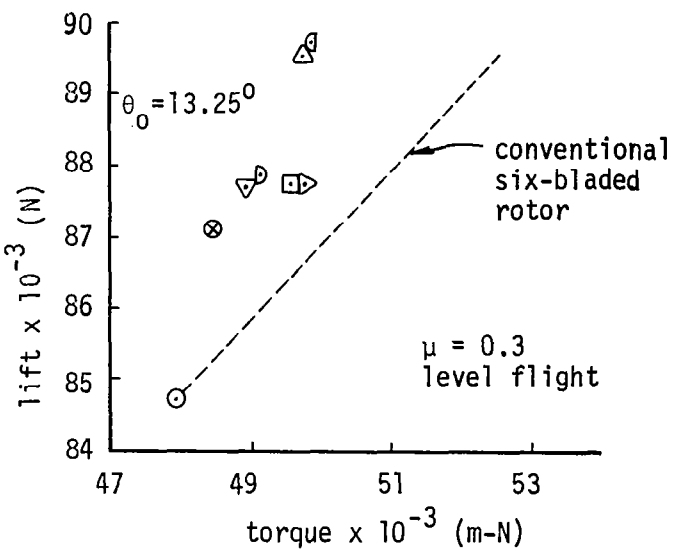

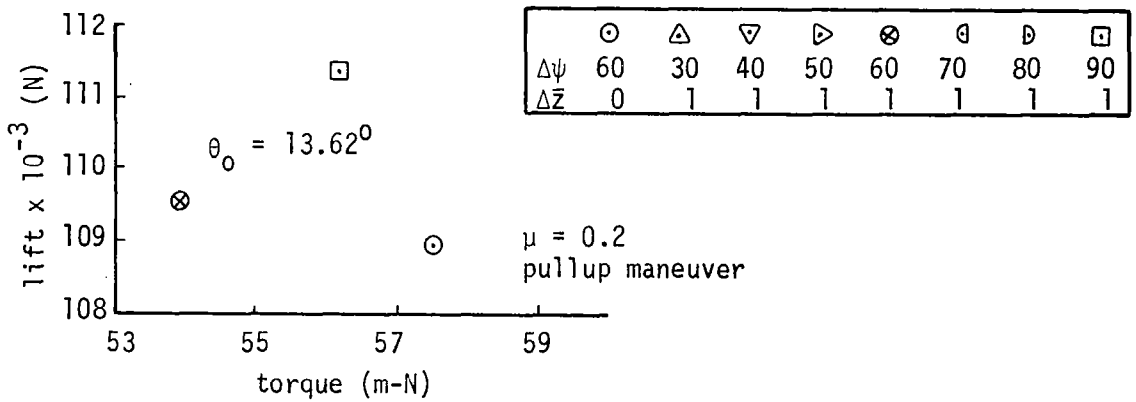

Figure 4. Performance results

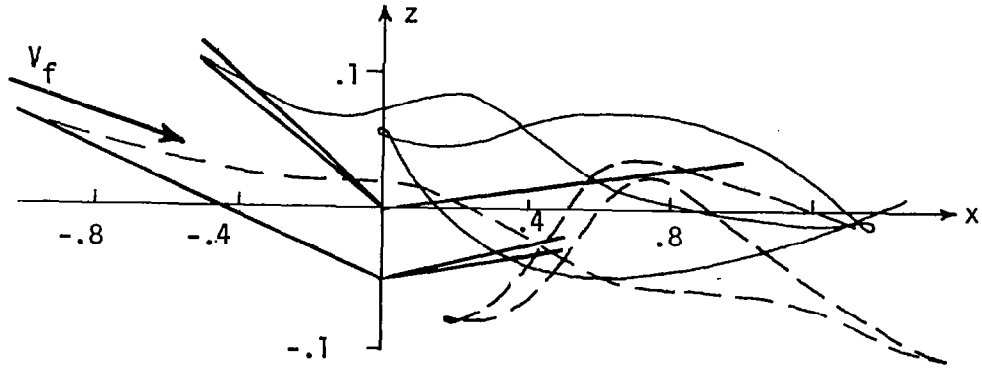

Two Tip Vortices, one from Upper Rotor (Blade at $\psi = 120^o$) and one from Lower Rotor (Blade at $\psi = 180^o$), $\mu = 0.2$, $\Delta\bar{z} = 1$, $\Delta\psi = 60^o$

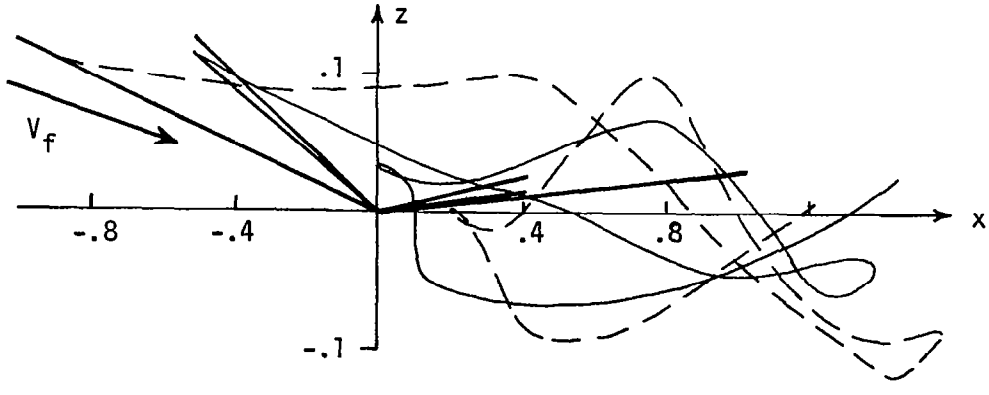

Two tip Vortices, from Blades at 120^o and at 180^o Azimuth Positions, $\mu = 0.2$, Standard Six-bladed Rotor

Figure 5. Tip Vortices

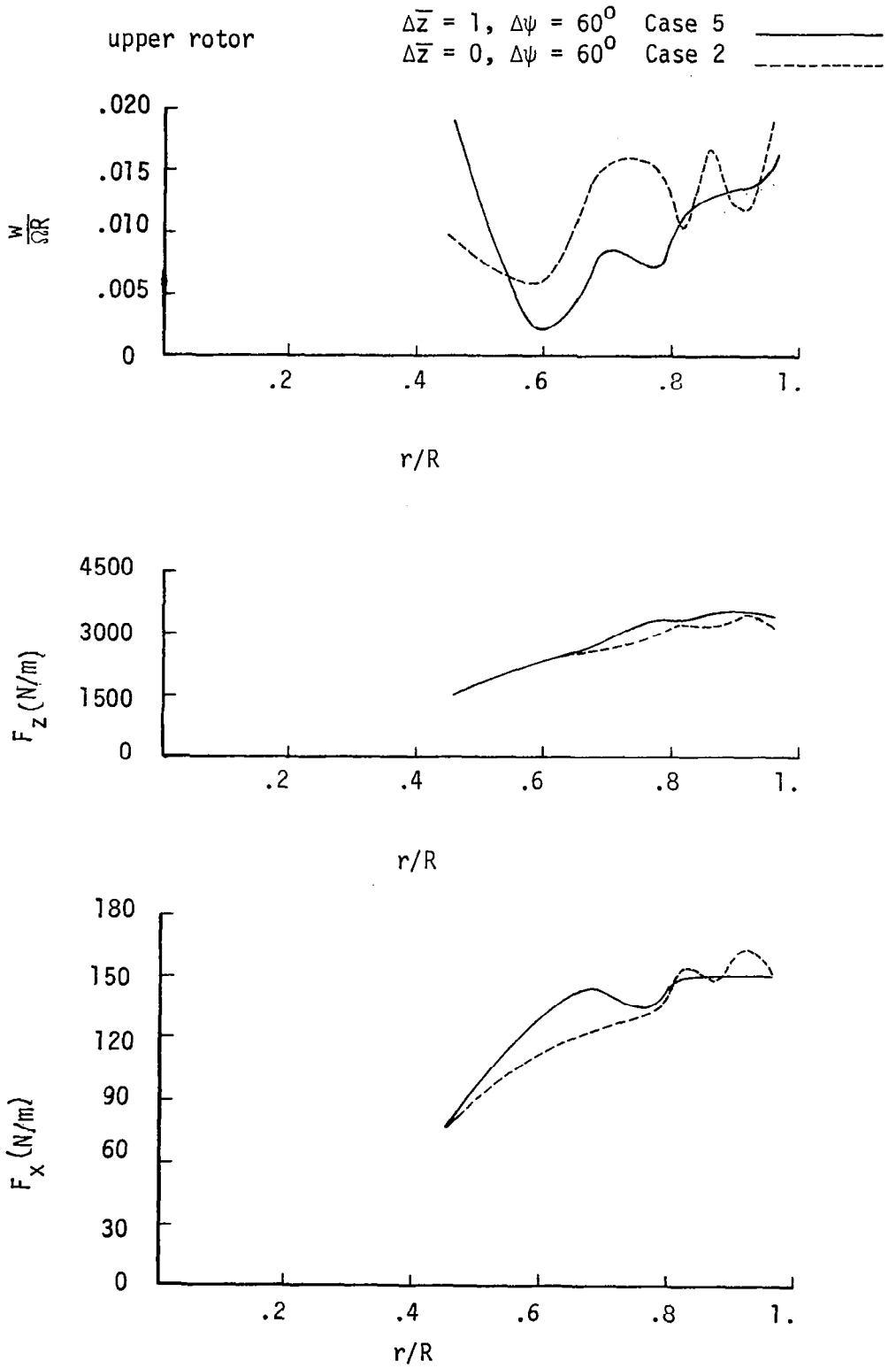

Figure 5A. Spanwise distribution of steady inflow velocity and aerodynamic loads μ = 0.20

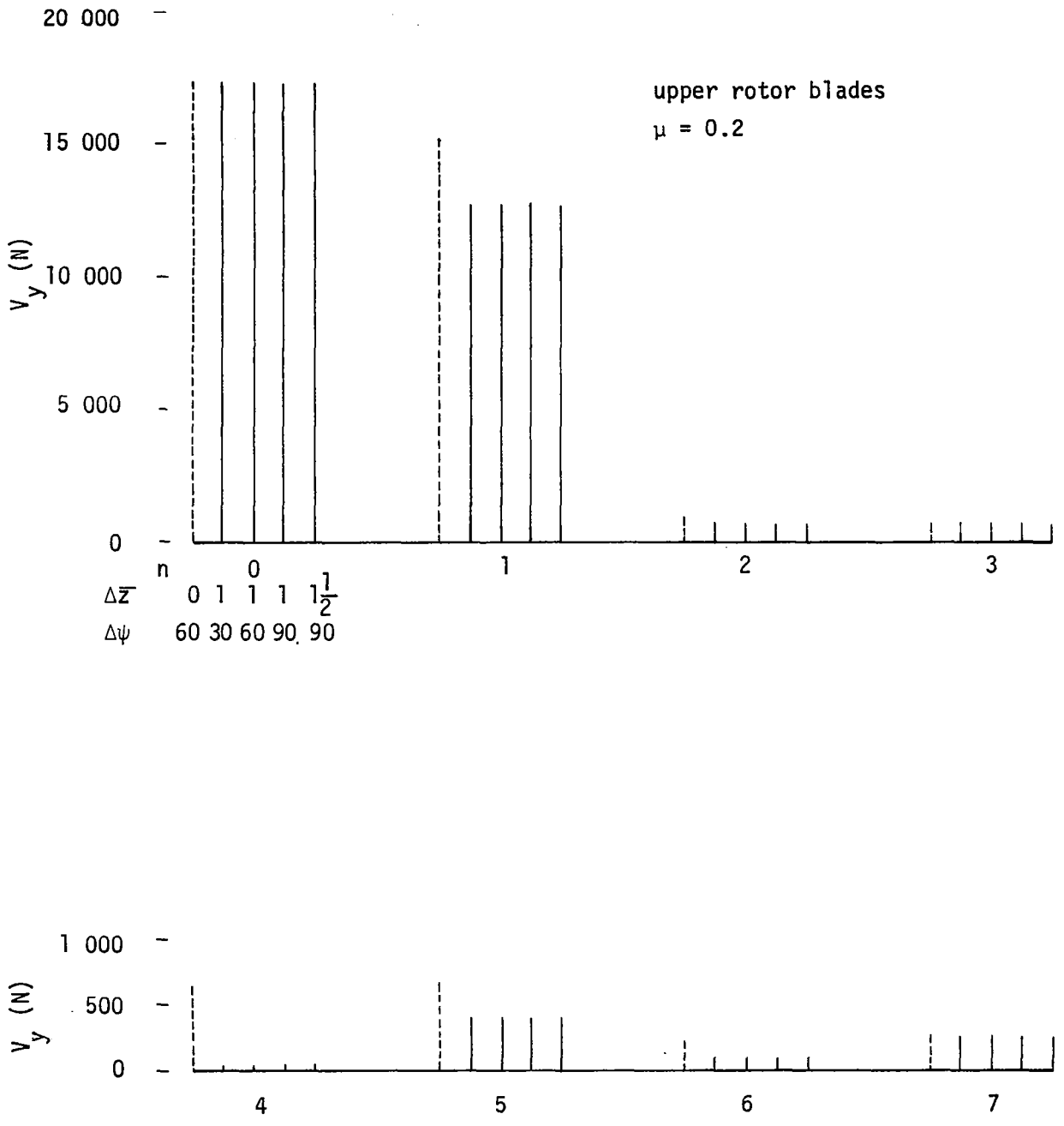

Figure 6. Harmonics of flapwise hinge shear for various VGR configurations

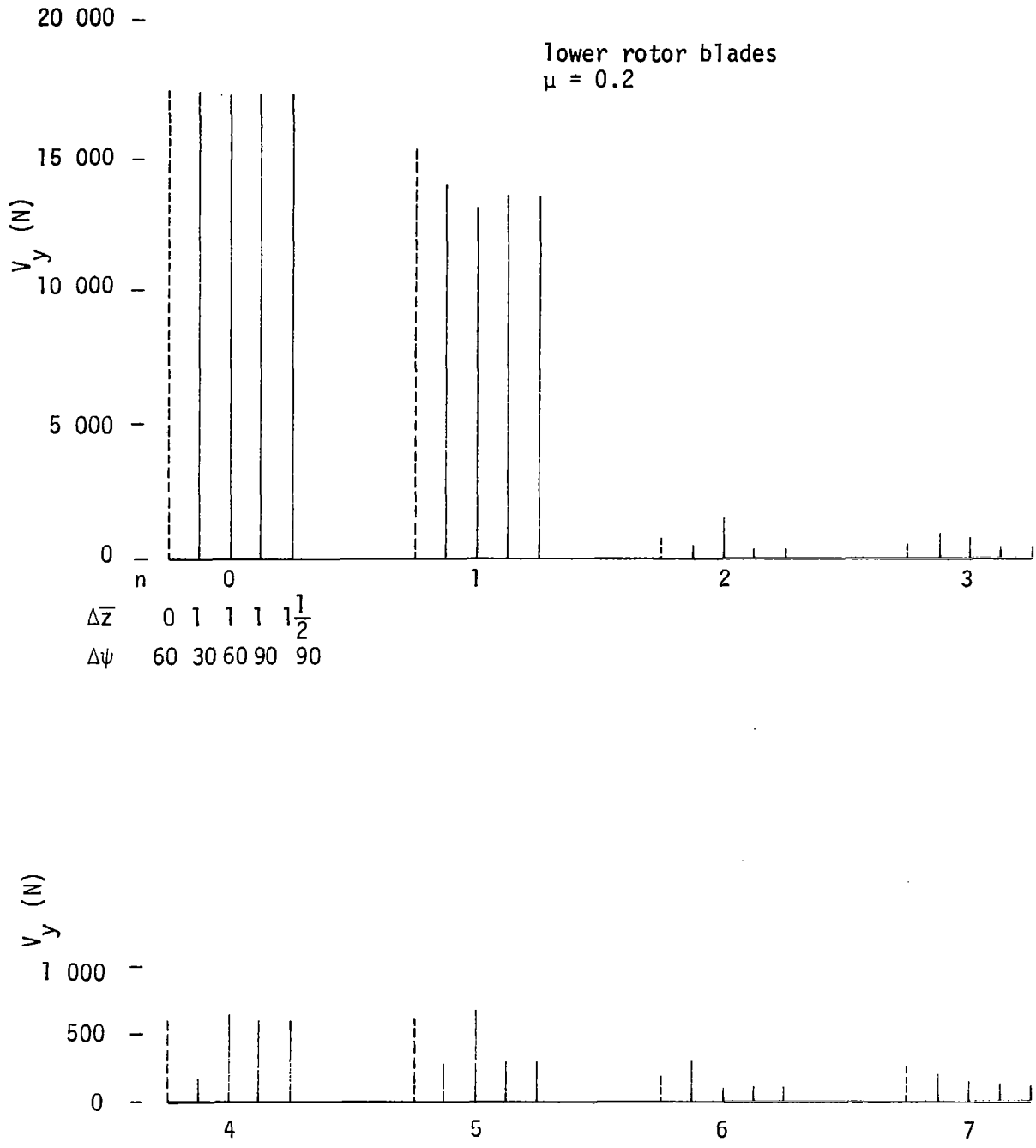

Figure 7. Harmonics of flapwise hinge shear for various VGR configurations

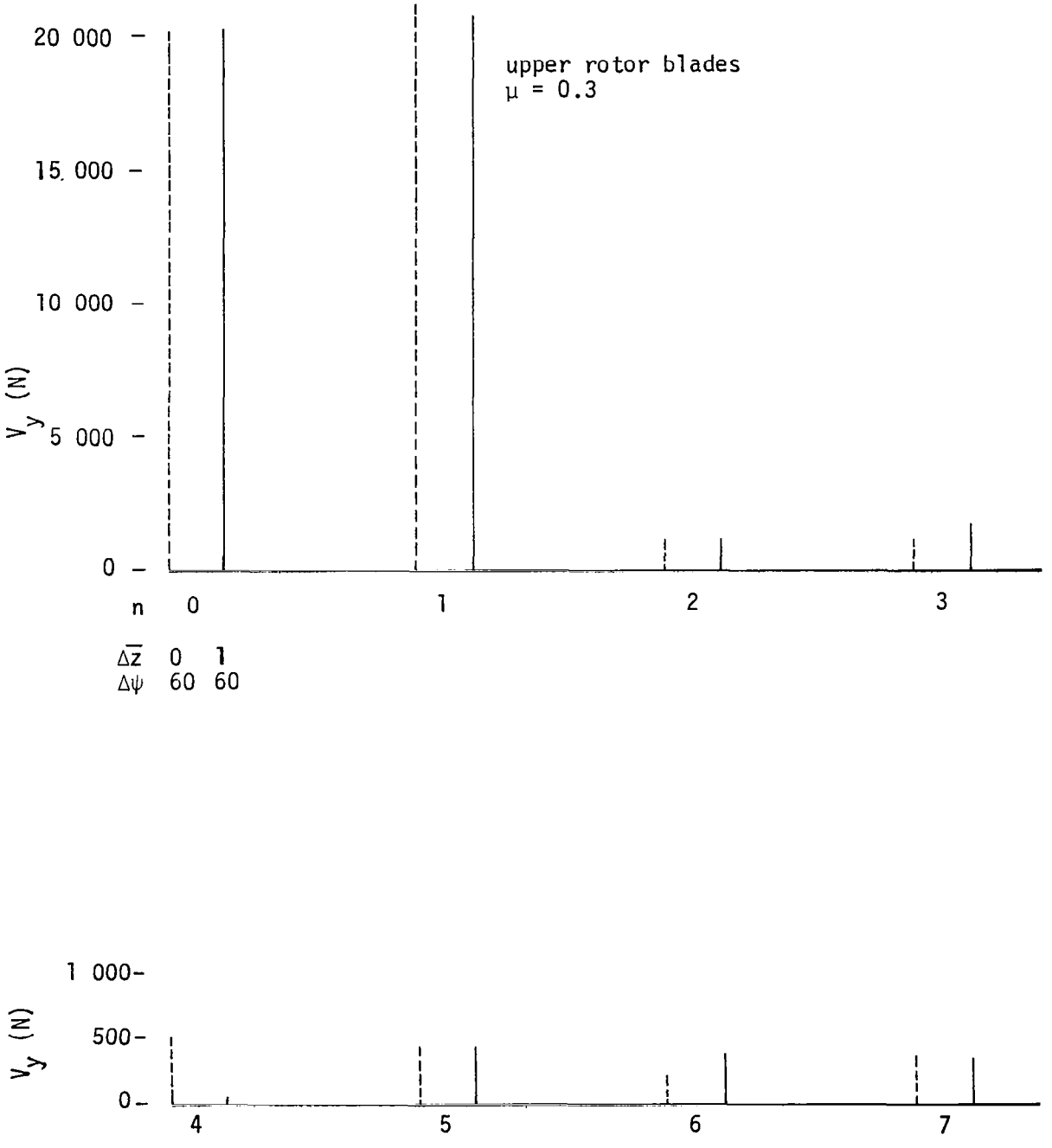

Figure 8. Harmonics of flapwise hinge shear for various VGR configurations

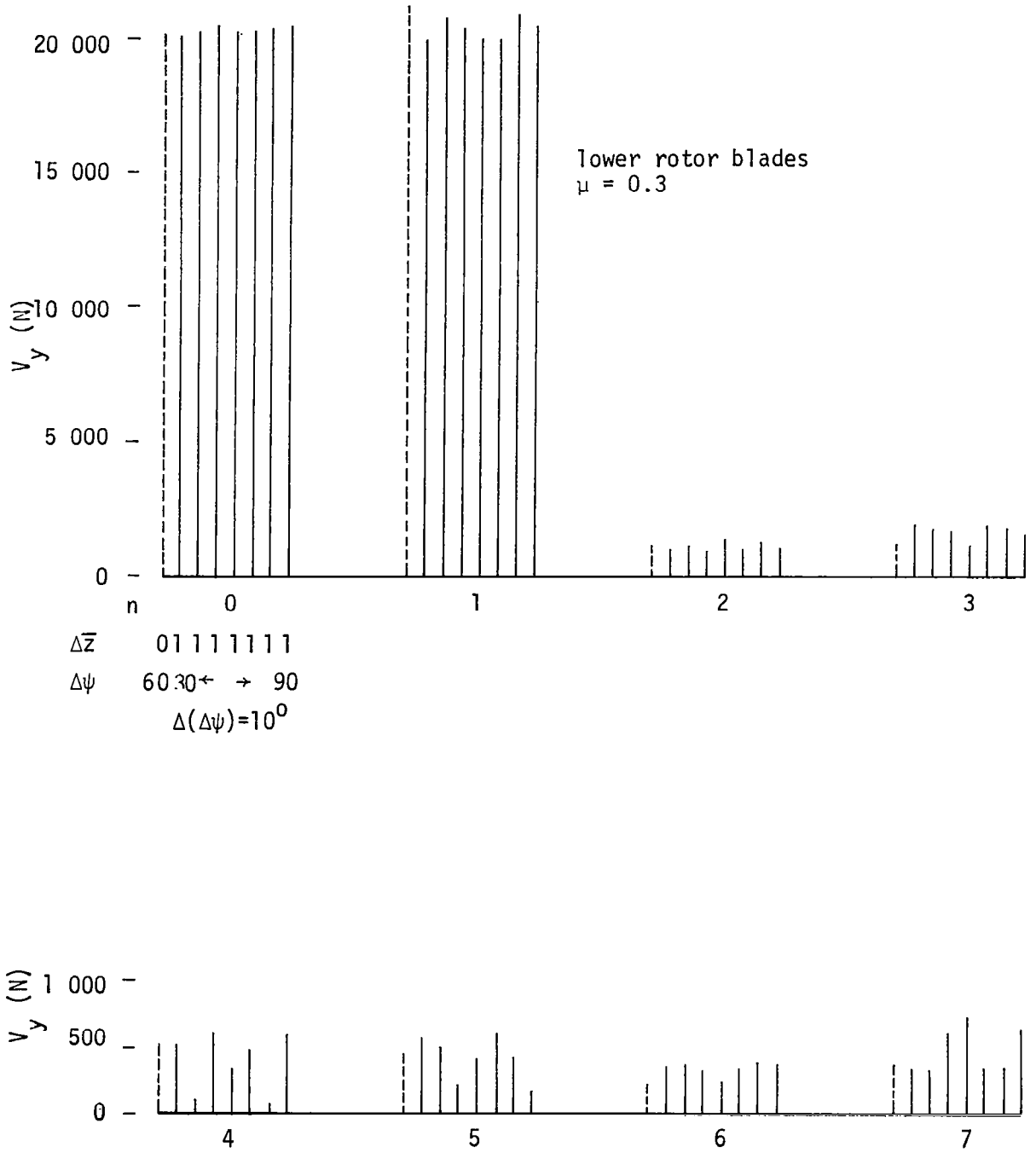

Figure 9. Harmonics of flapwise hinge shear for various VGR configurations

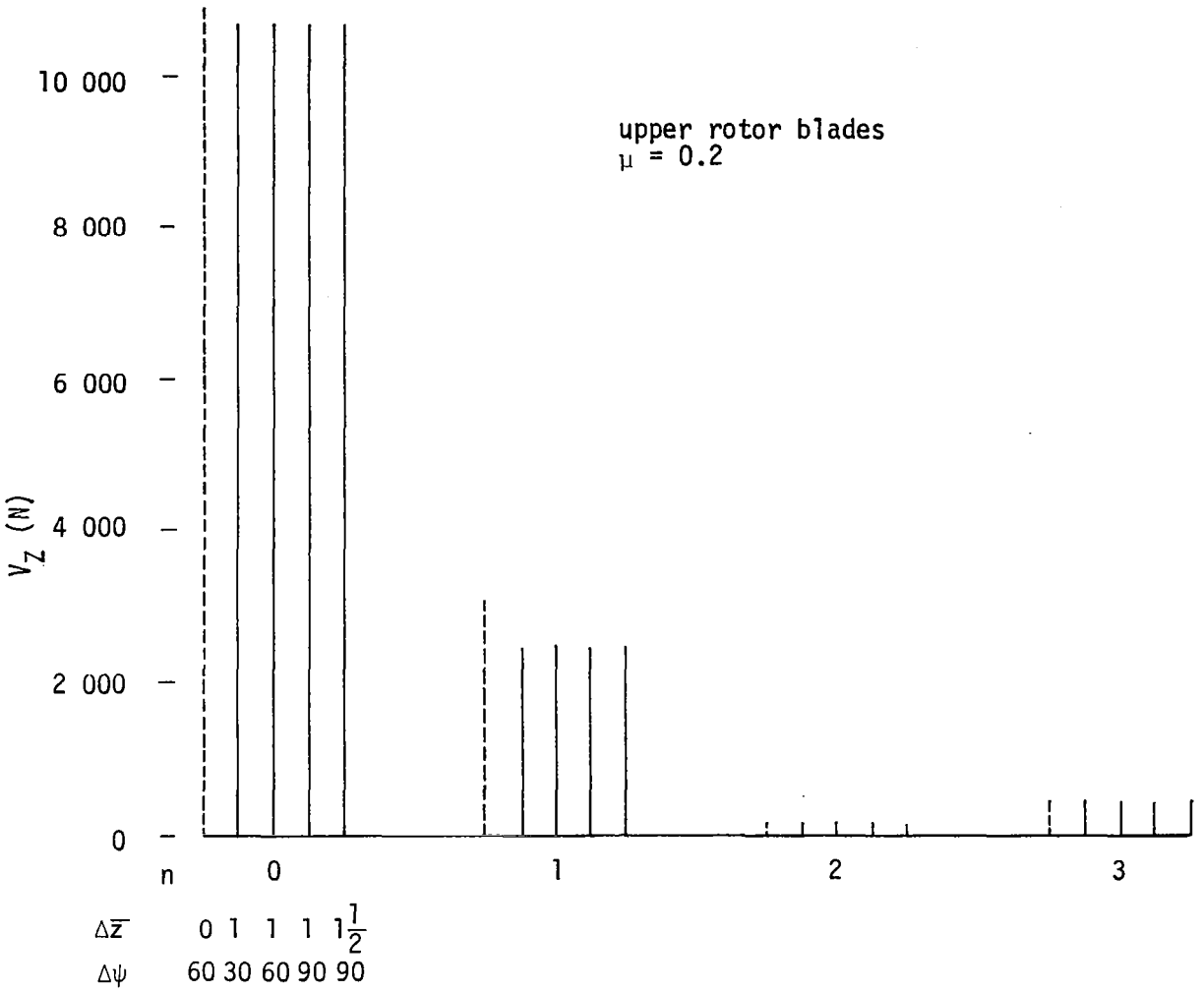

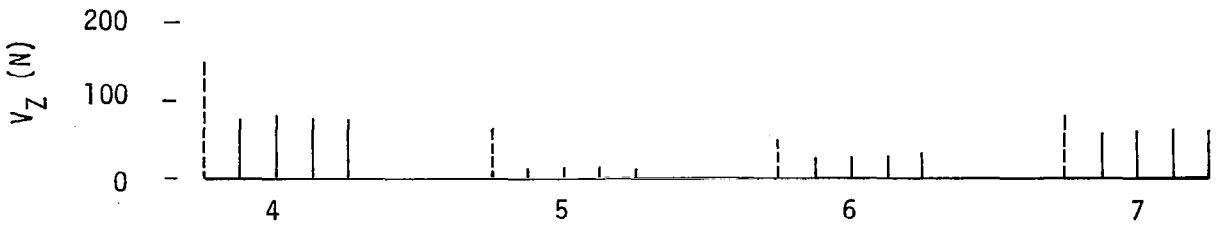

Figure 10. Harmonics of chordwise hinge shear for various VGR configurations

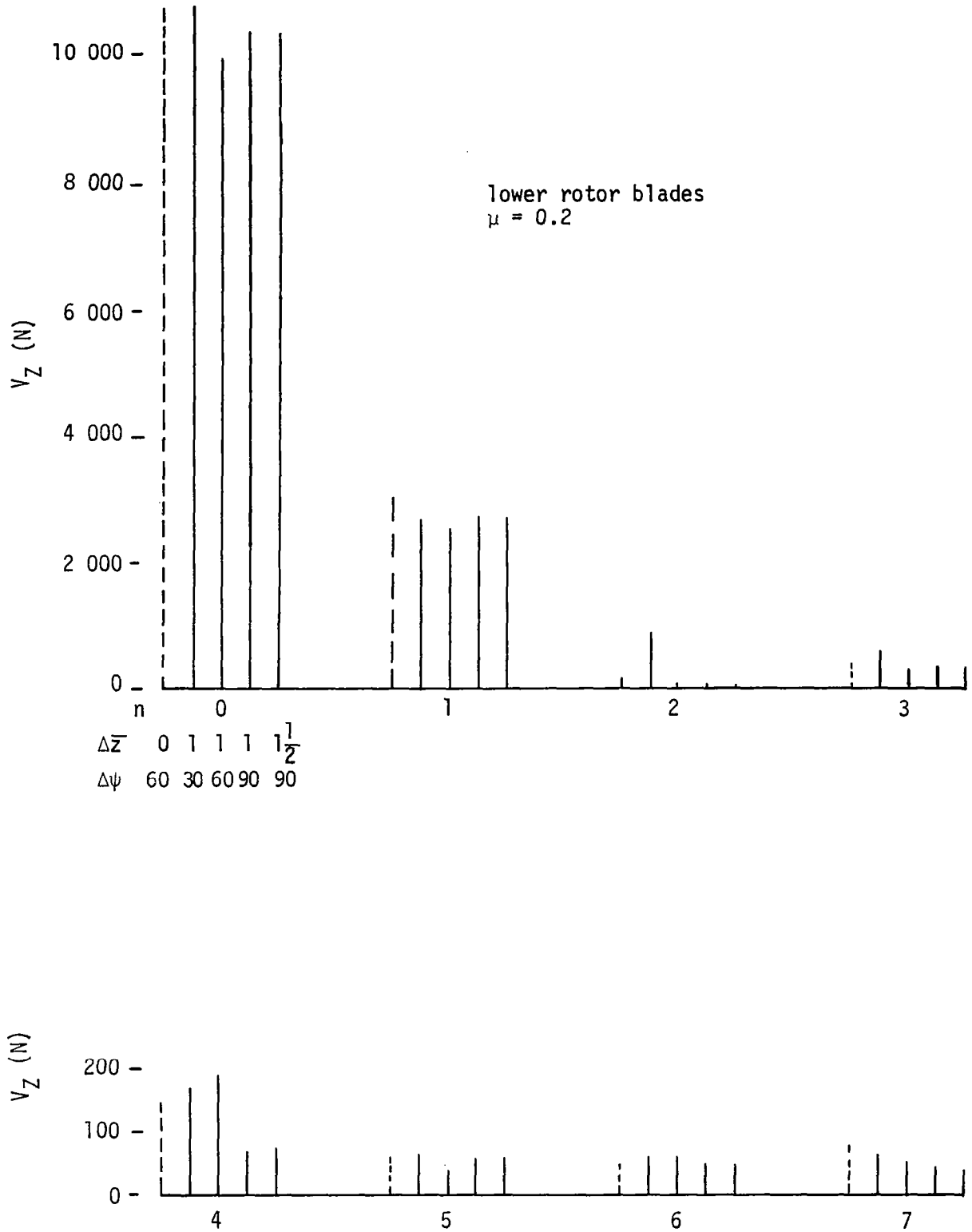

Figure 11. Harmonics of chordwise hinge shear for various VGR configurations

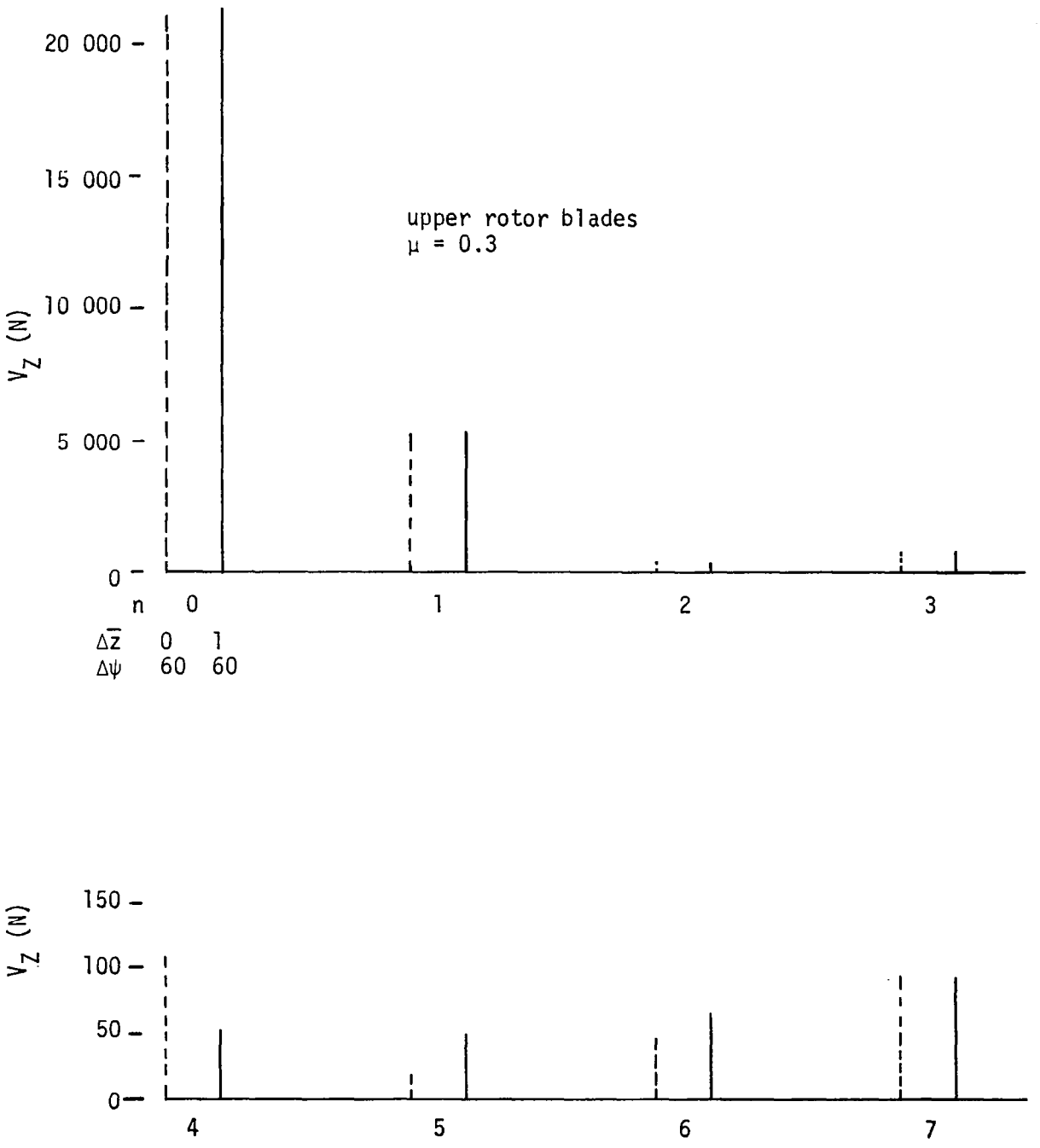

Figure 12. Harmonics of chordwise hinge shear for various VGR configurations

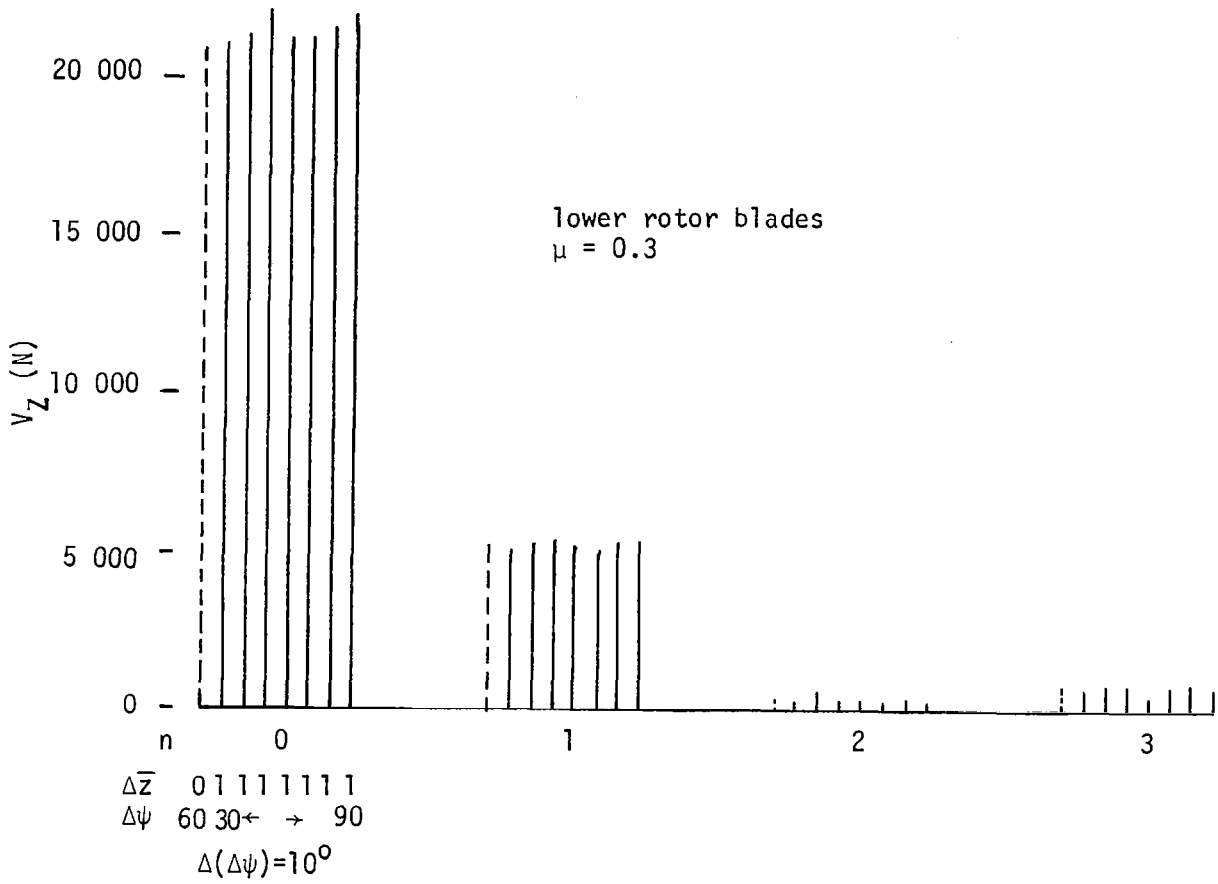

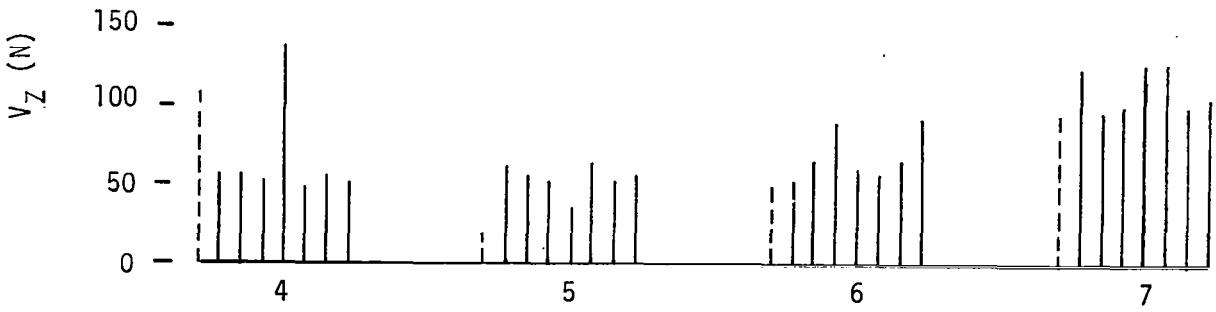

Figure 13. Harmonics of chordwise hinge shear for various VGR configurations

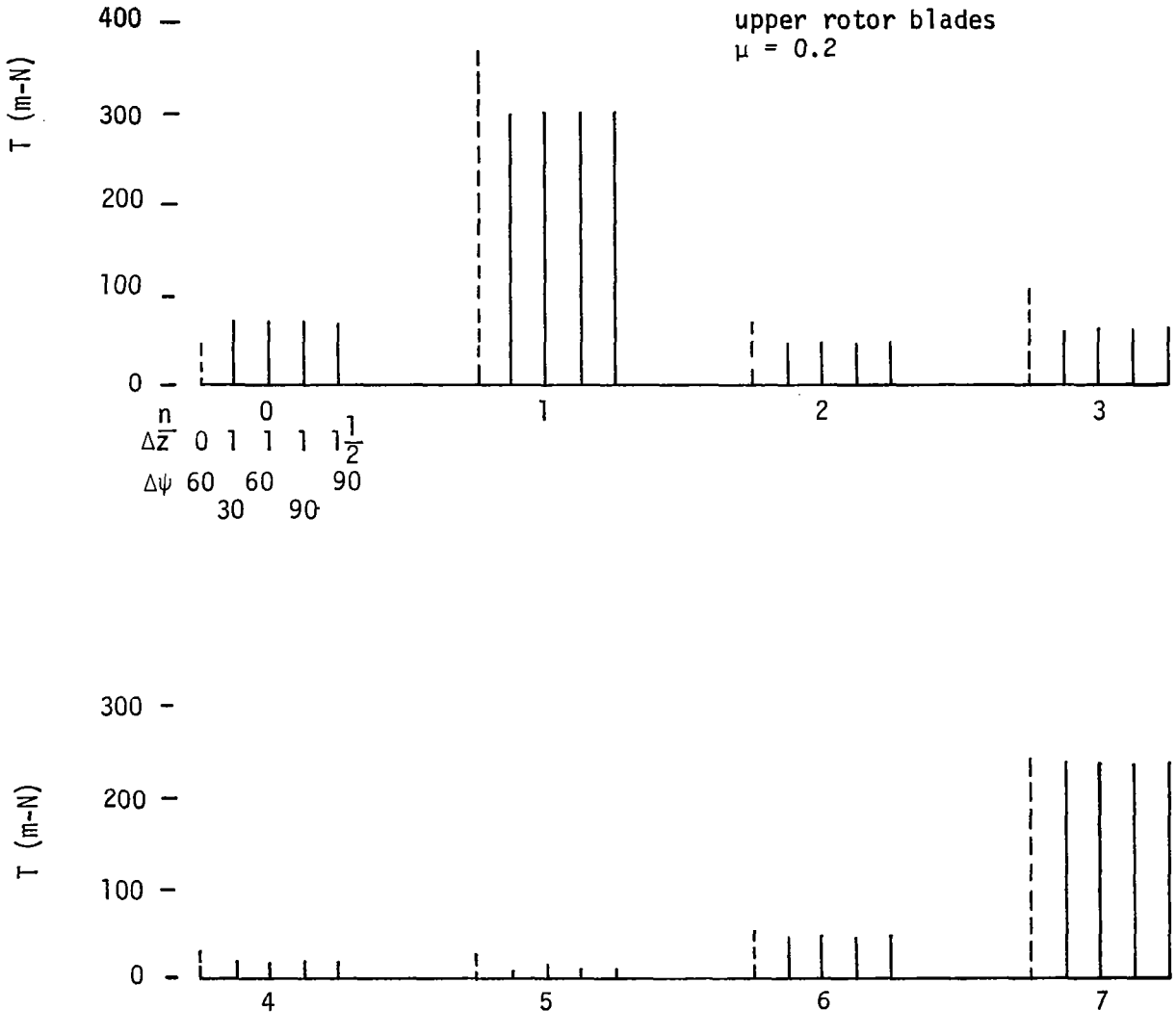

Figure 14. Harmonics of blade pitching moments at r/R =0.25 for various VGR configurations

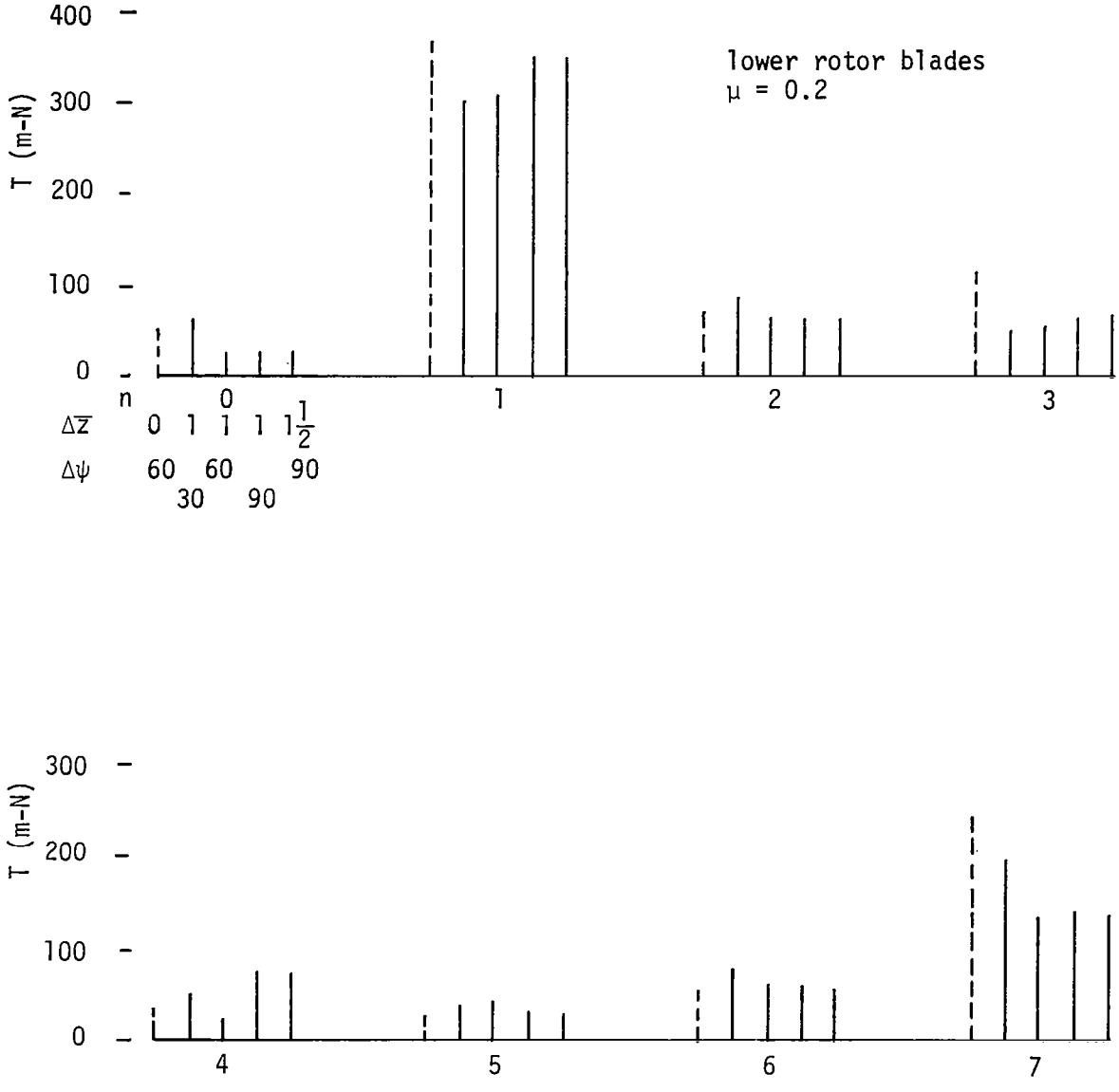

Figure 15. Harmonics of blade pitching moments at r/R =0.25 for various VGR configurations

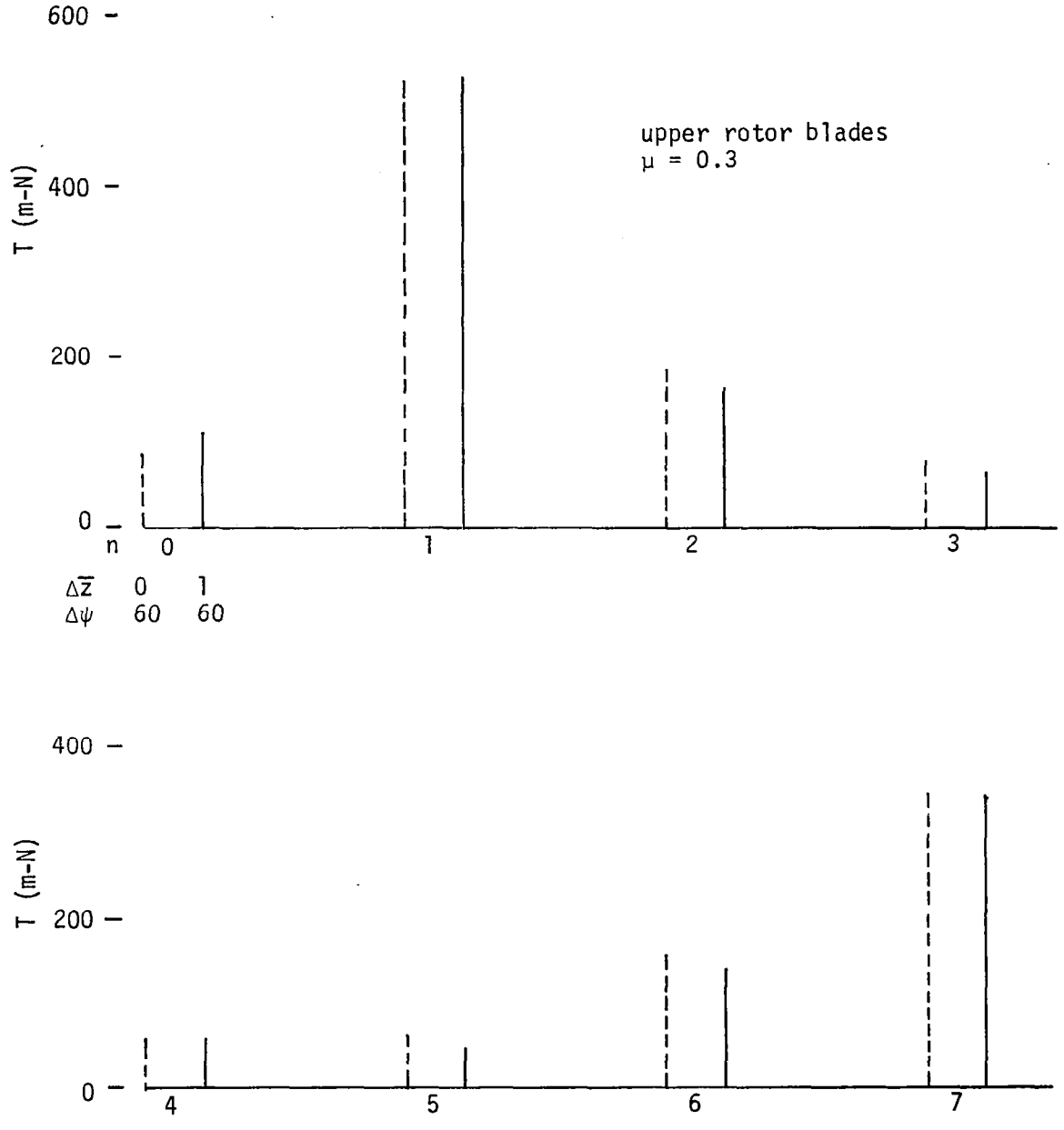

Figure 16. Harmonics of blade pitching moments at r/R =0.25 for various VGR configurations

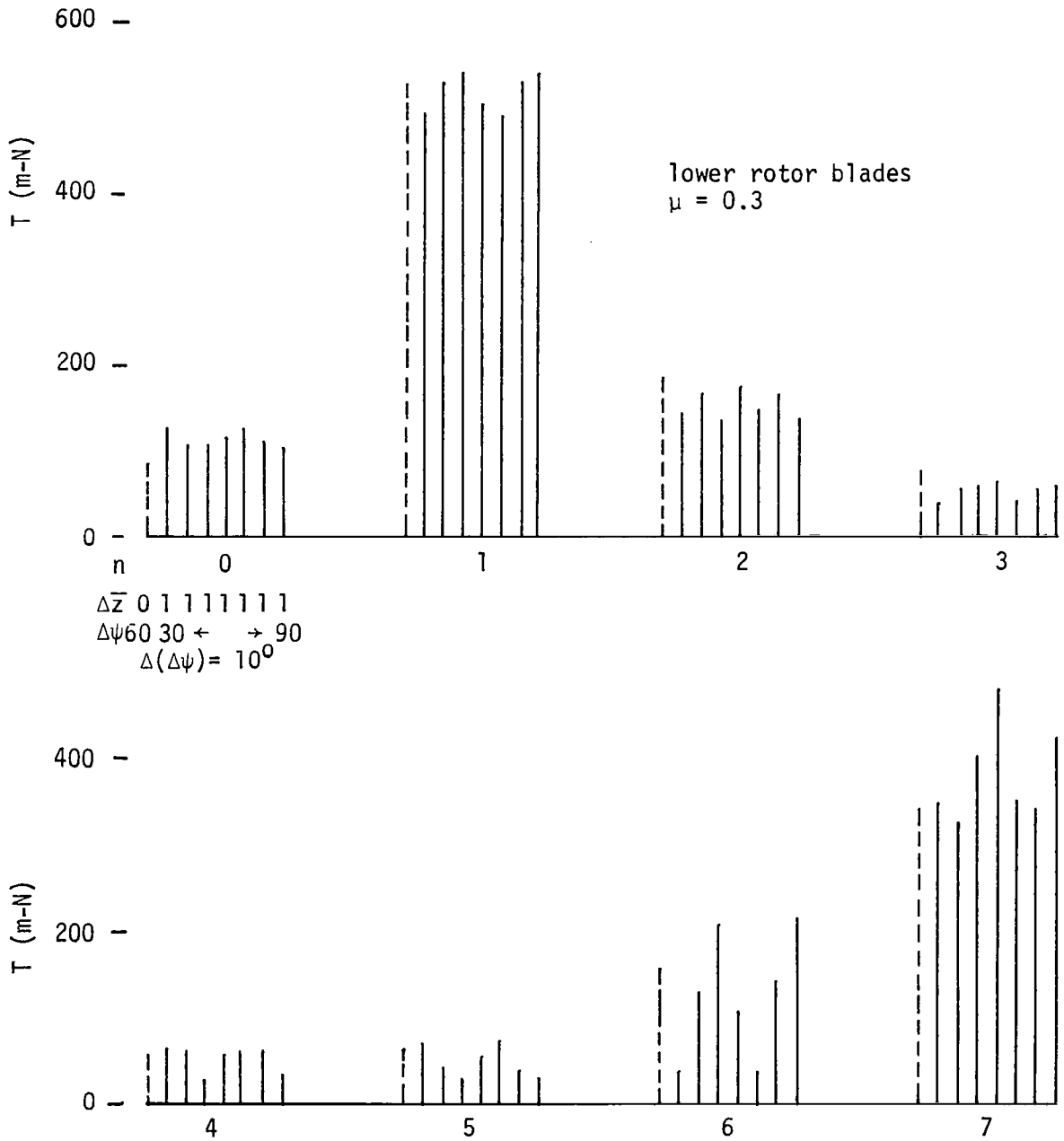

Figure 17. Harmonics of blade pitching moments at r/R =0.25 for various VGR configurations

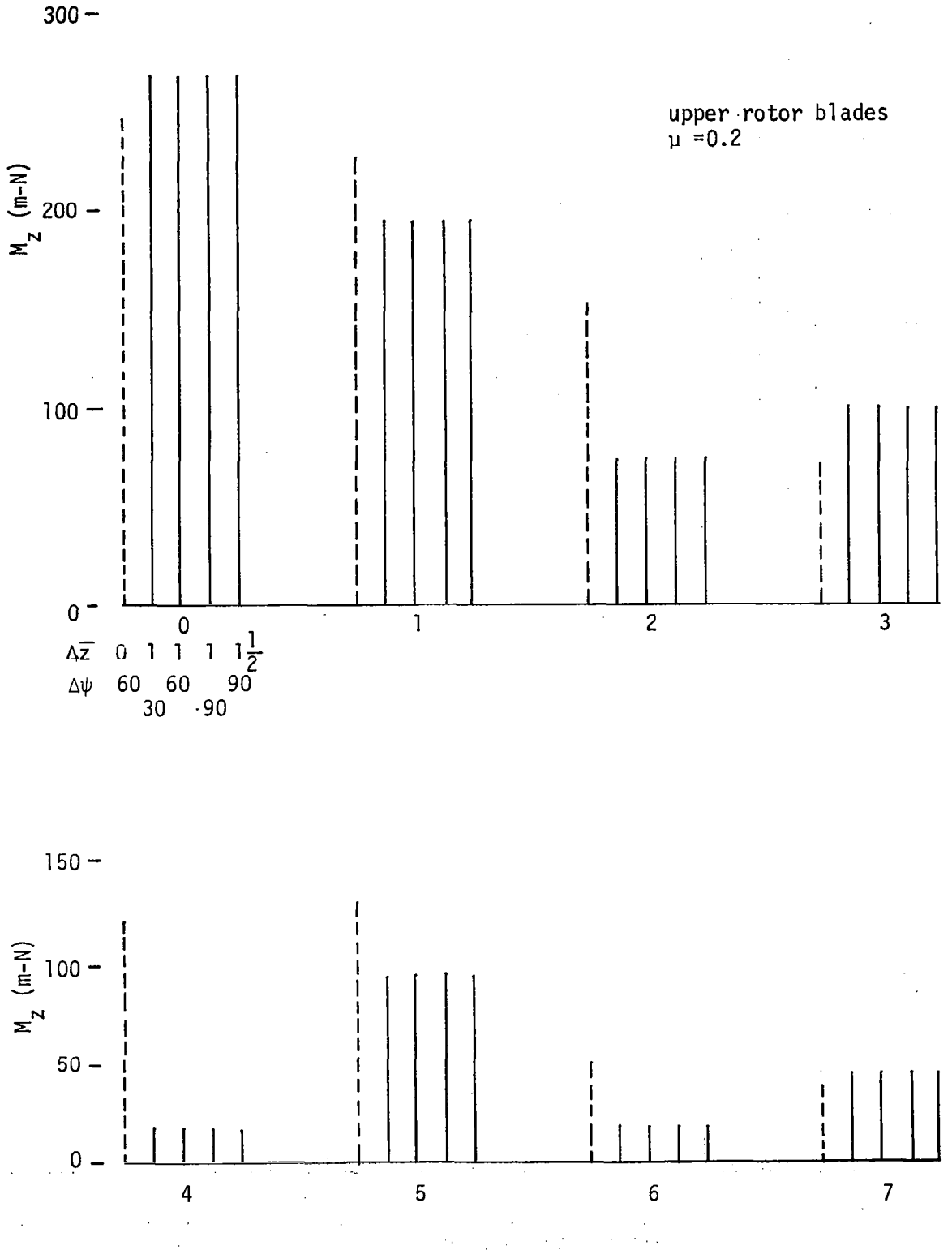

Figure 18. Harmonics of flapwise bending moments at r/R = 0.282 for various VGR configurations

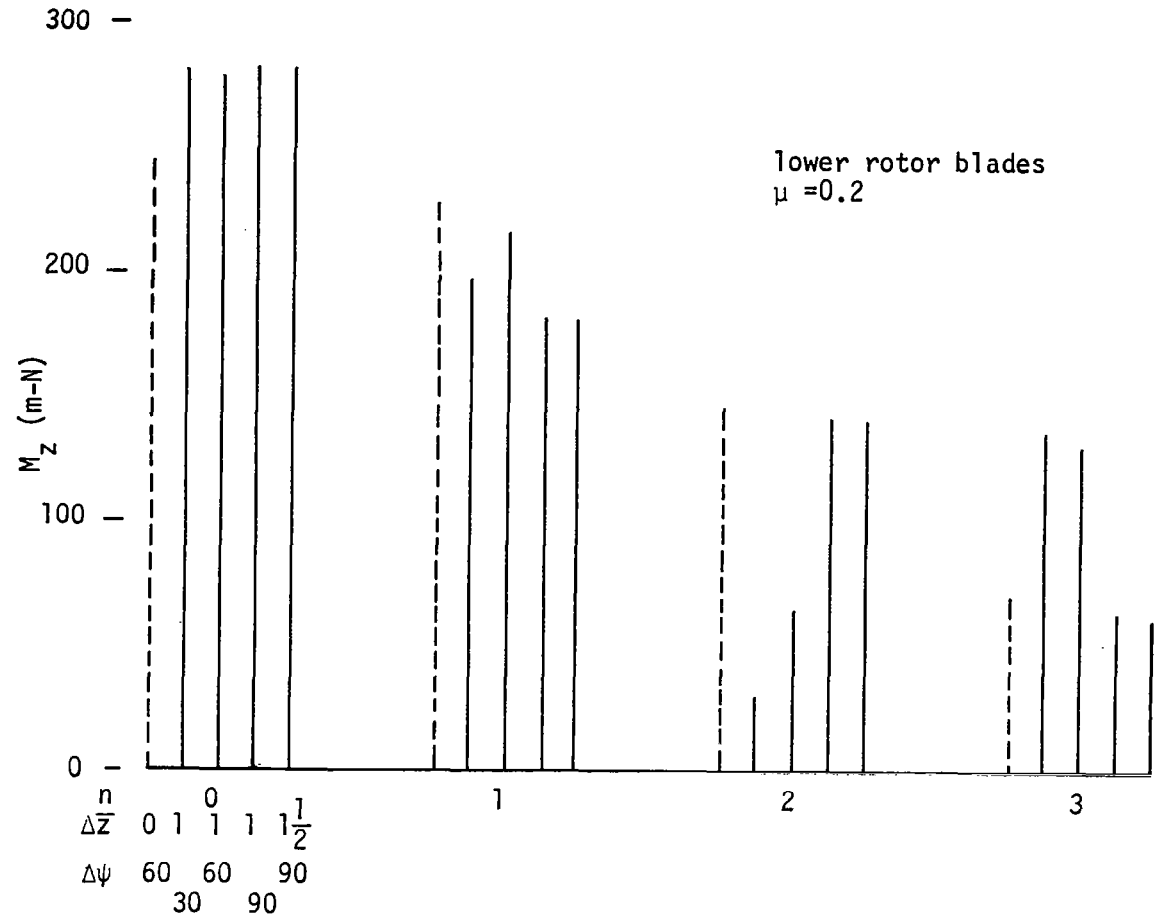

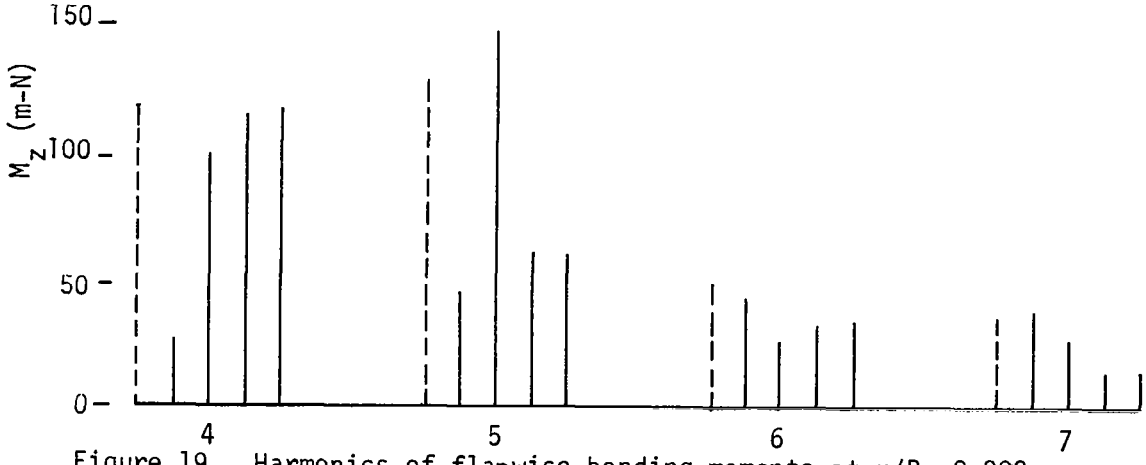

Figure 19. Harmonics of flapwise bending moments at r/R =0.282 for various VGR configurations

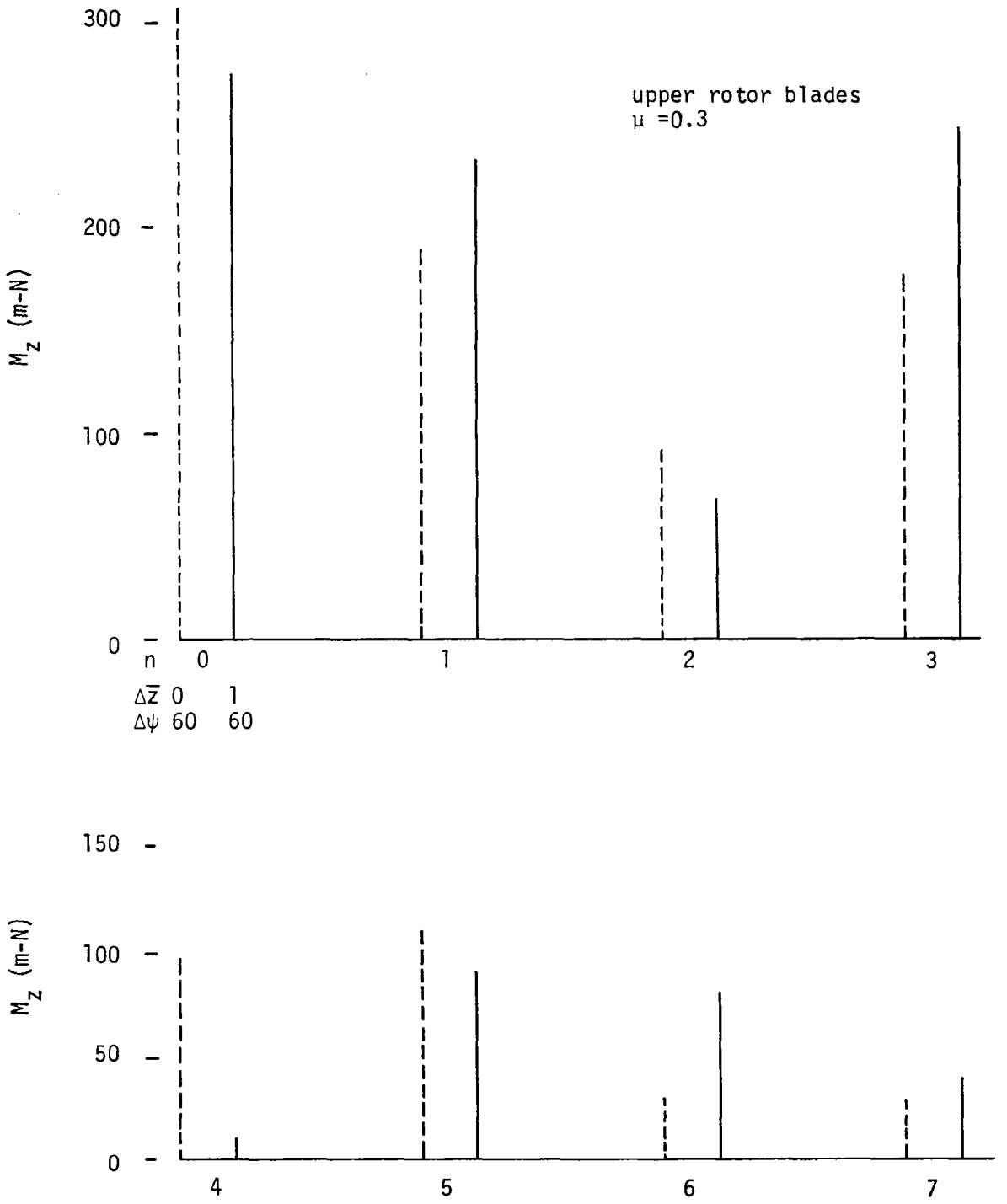

Figure 20. Harmonics of flapwise bending moments at r/R =0.282 for various VGR configurations

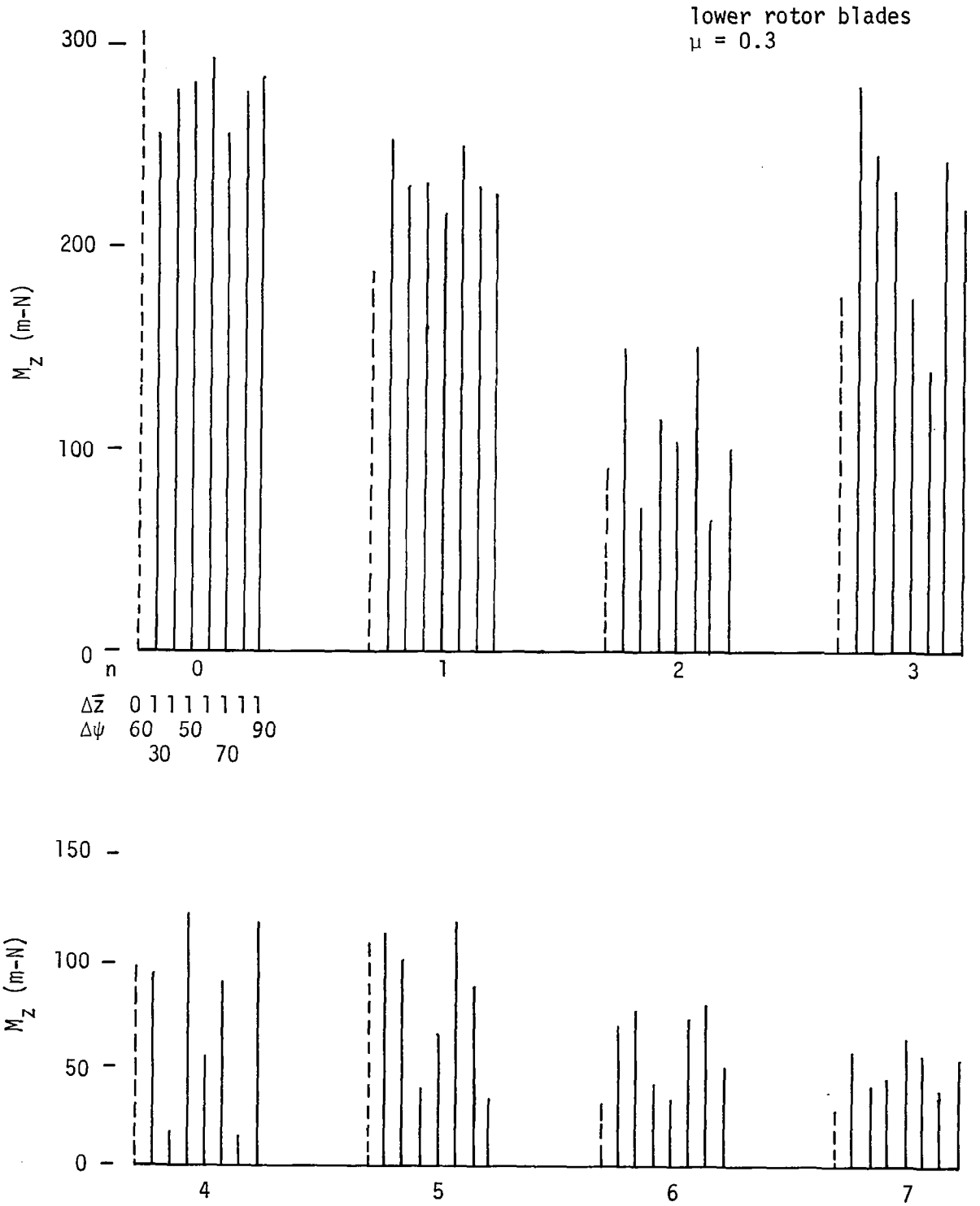

Figure 21. Harmonics of flapwise bending moment at r/R =0.282 for various VGR configurations

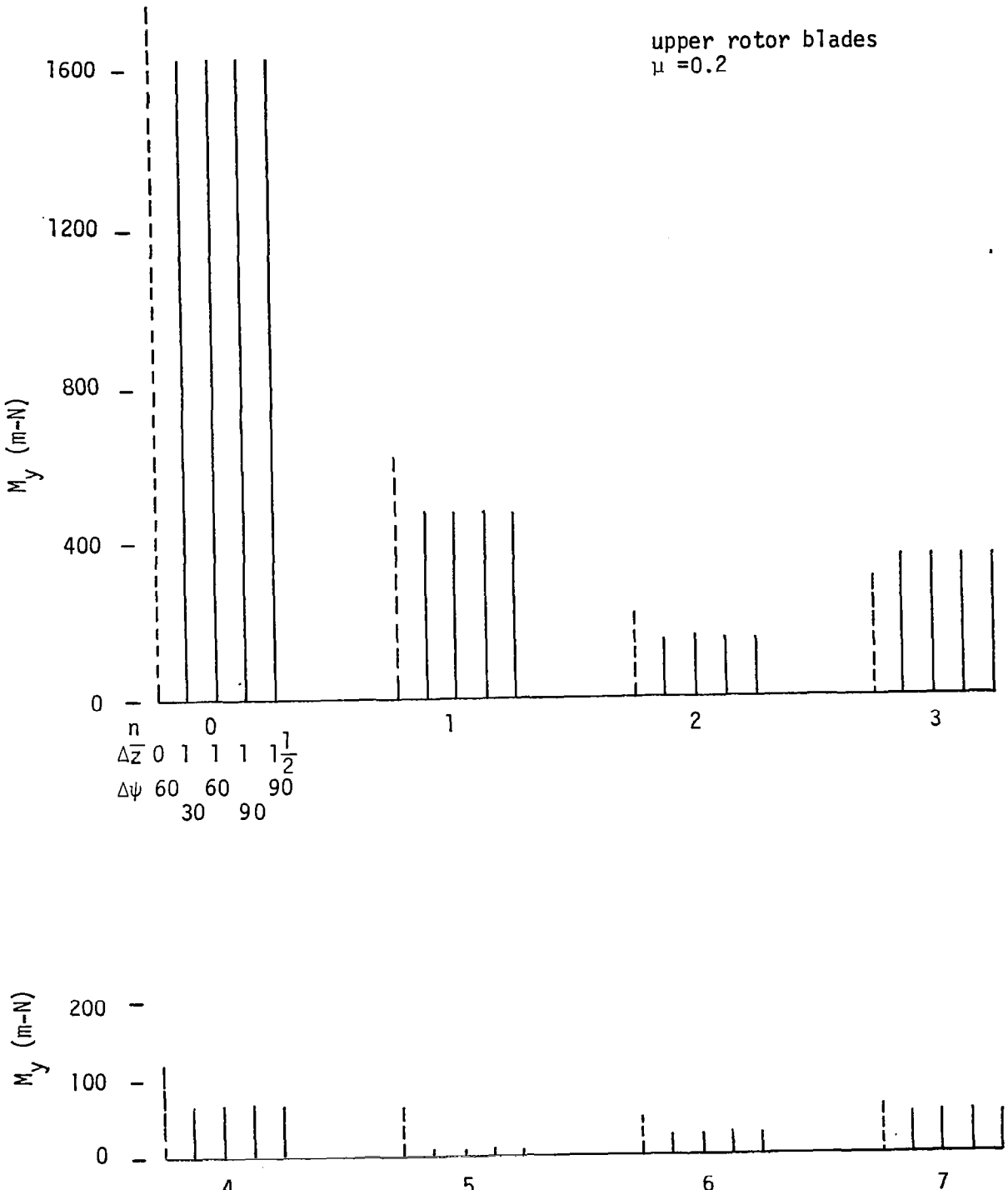

Figure 22. Harmonics of chordwise bending moment at r/R =0.282 for various VGR configurations

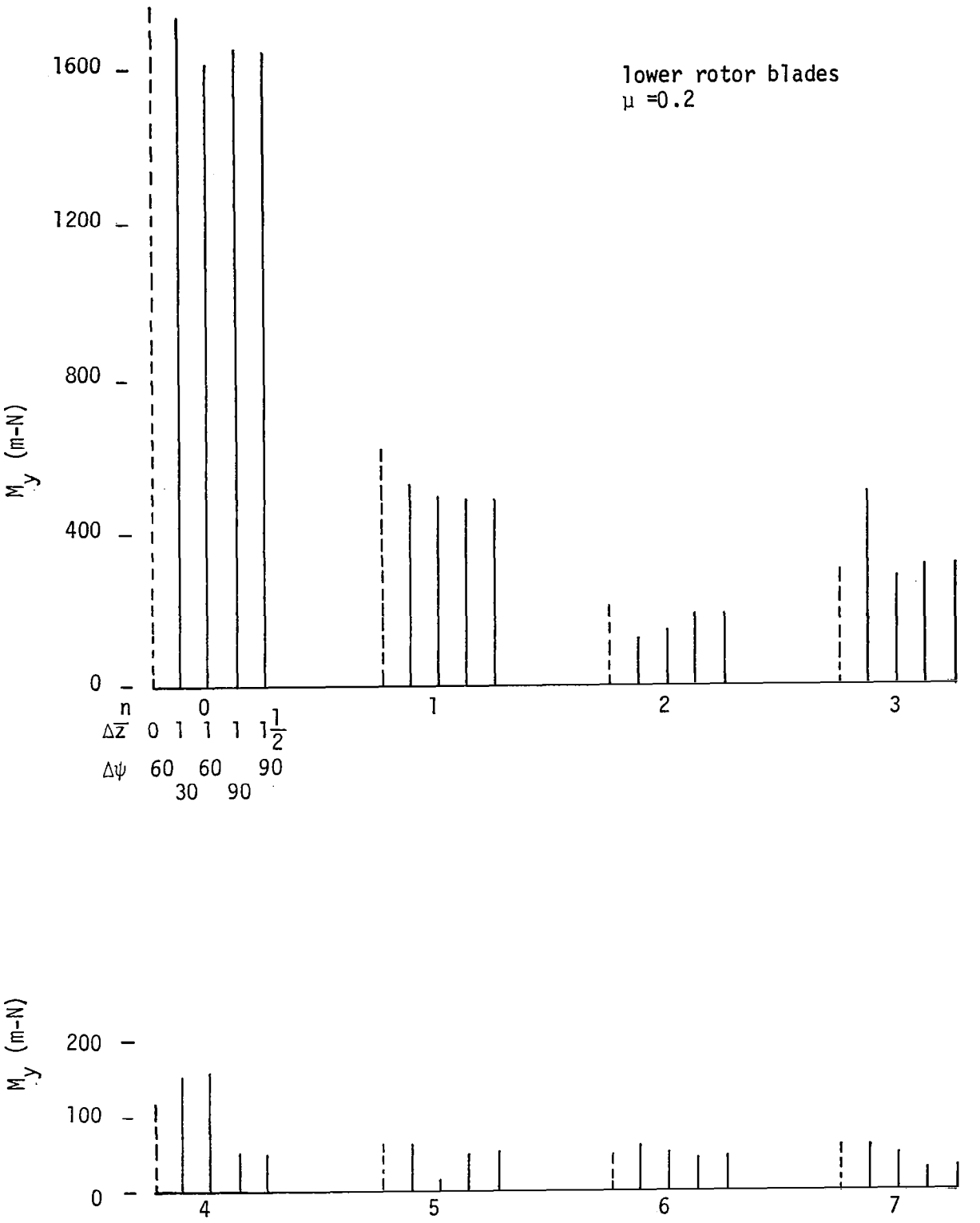

Figure 23. Harmonics of chordwise bending moment at r/R =0.282 for various VGR configurations

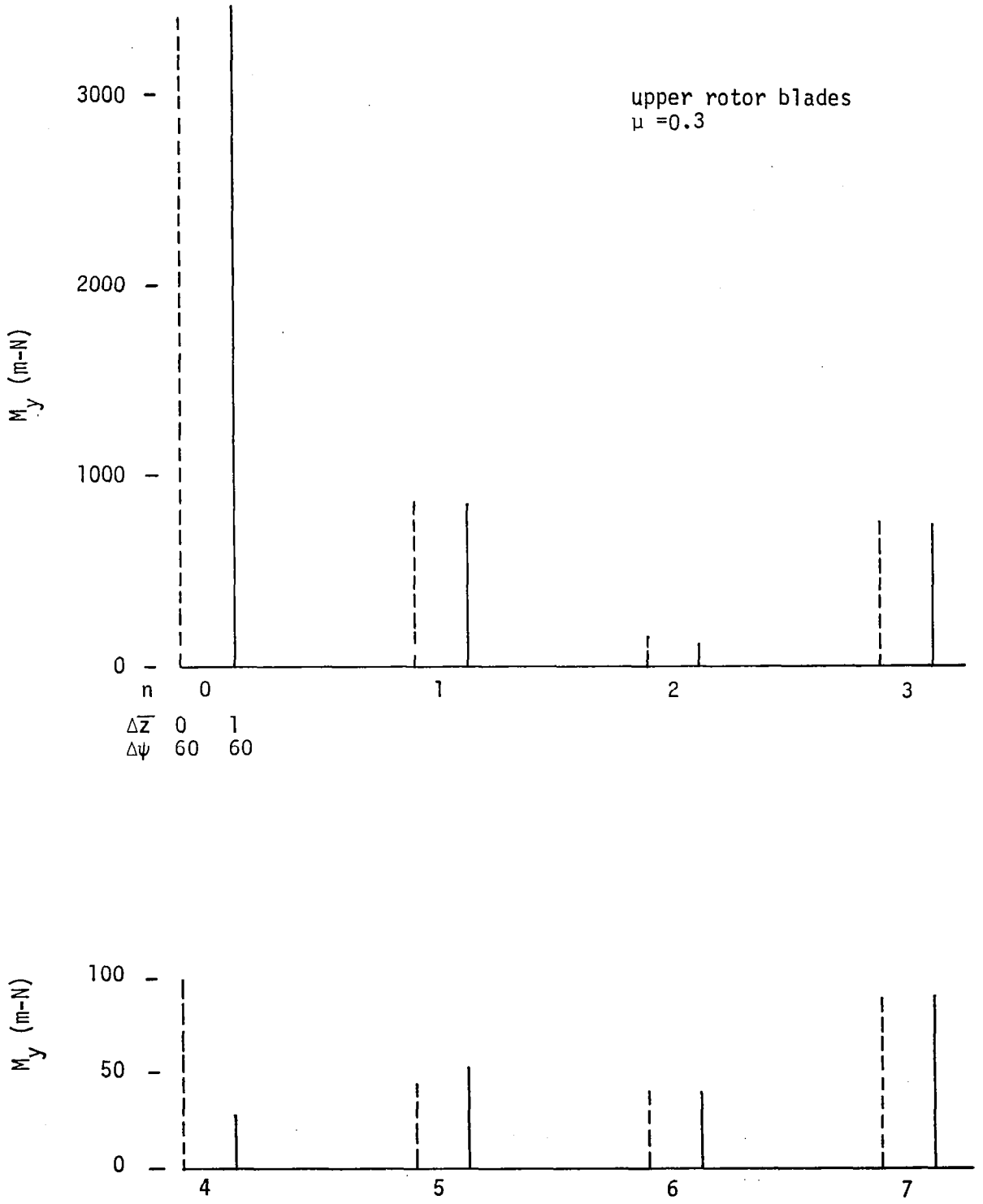

Figure 24. Harmonics of chordwise bending moment at r/R =0.282 for various VGR configurations

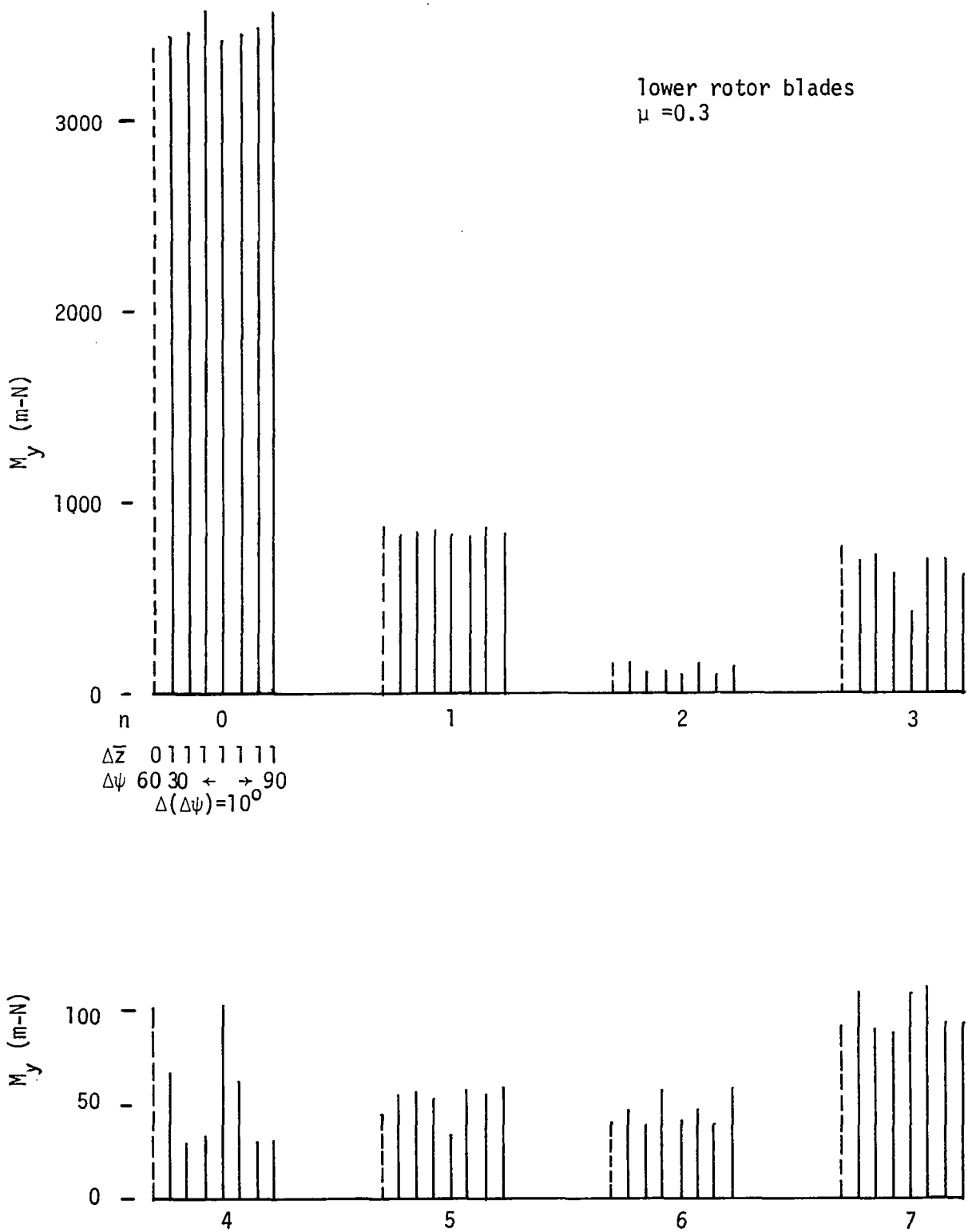

Figure 25. Harmonics of chordwise bending moment at r/R =0.282 for various VGR configuration

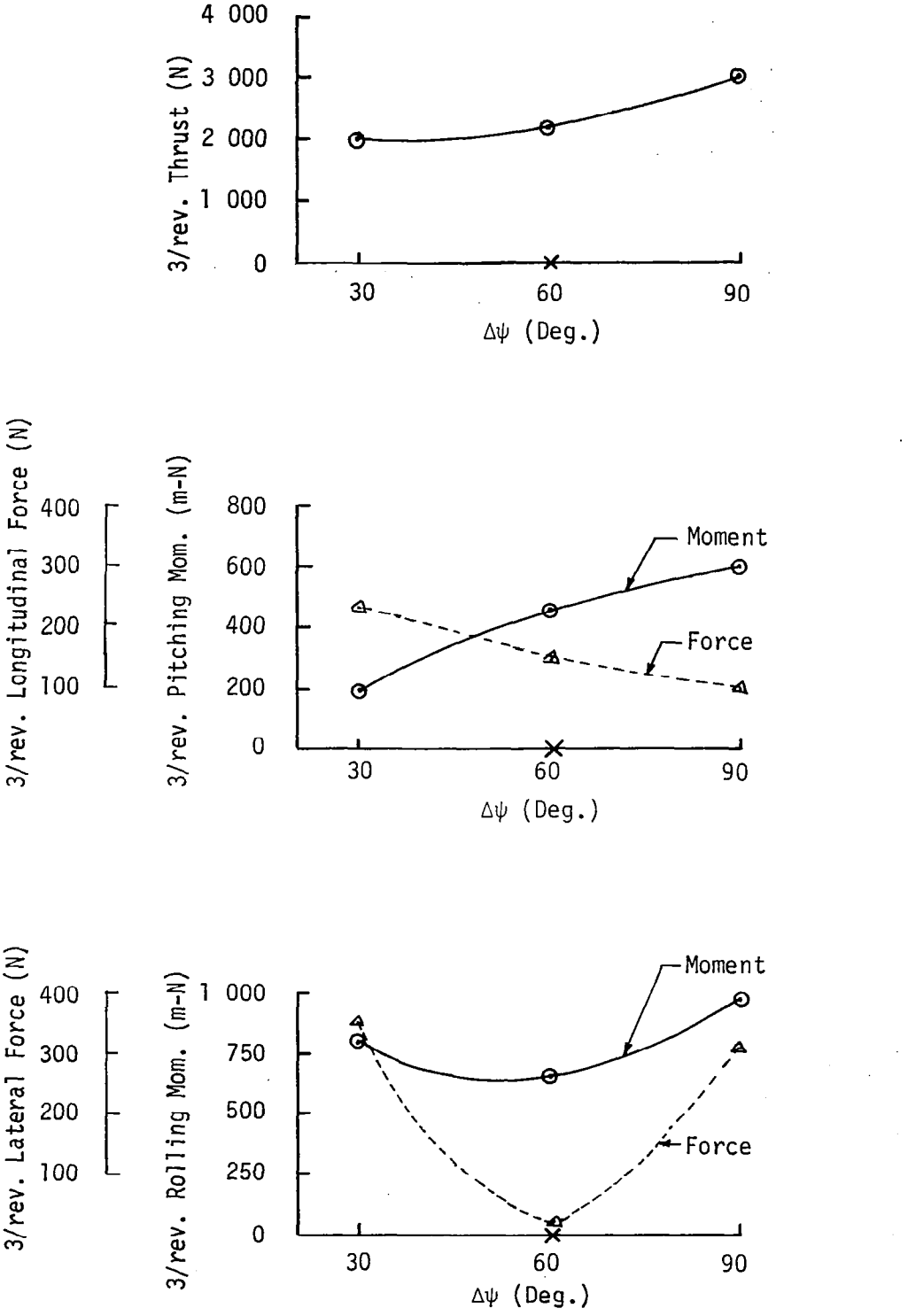

Figure 26. 3 per rev. transmitted loads versus azimuthal spacing, $\Delta\psi$, μ =0.2

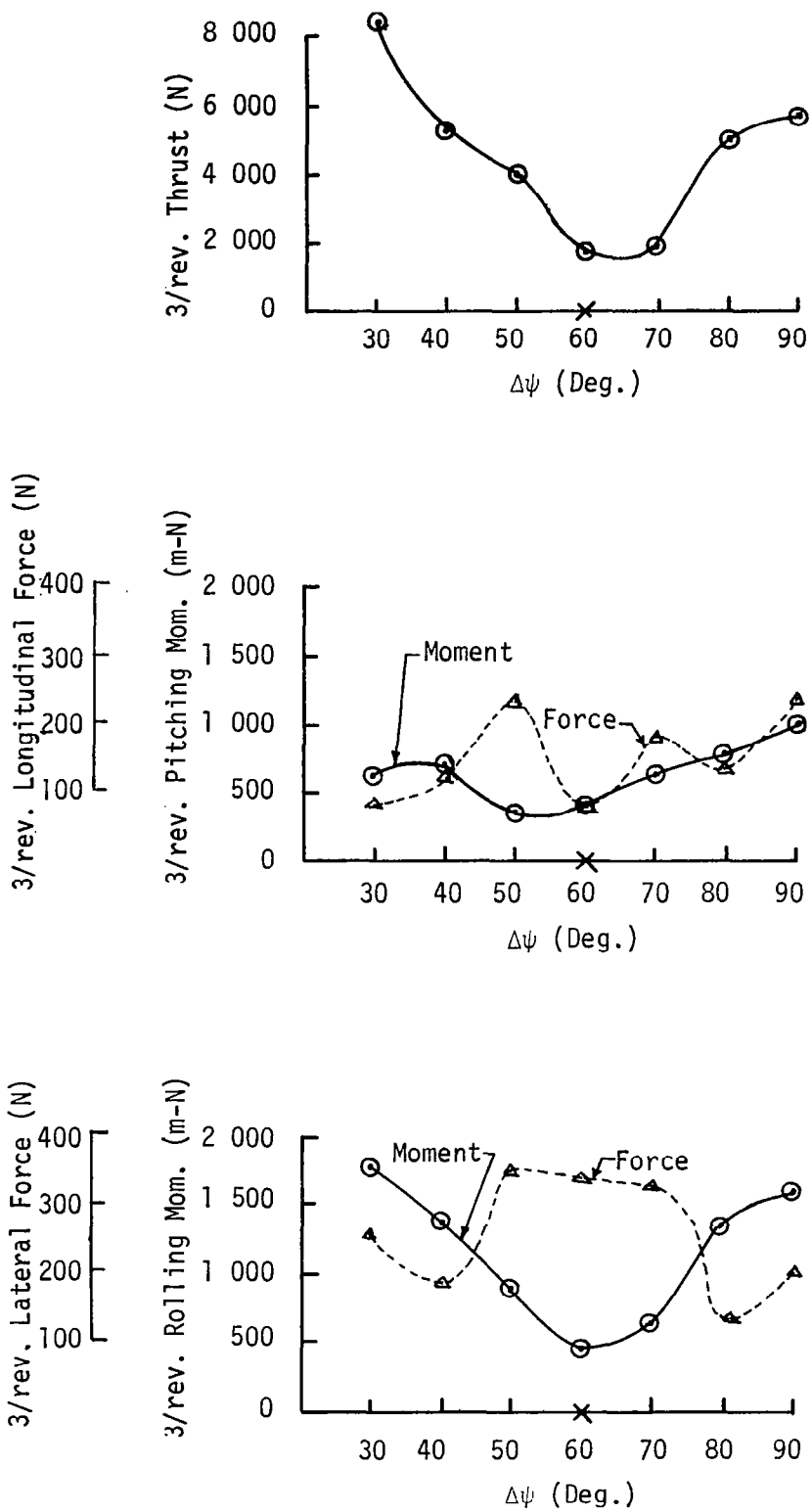

Figure 27. 3 per rev. transmitted loads versus azimuthal spacing, $\Delta\psi$, μ =0.3

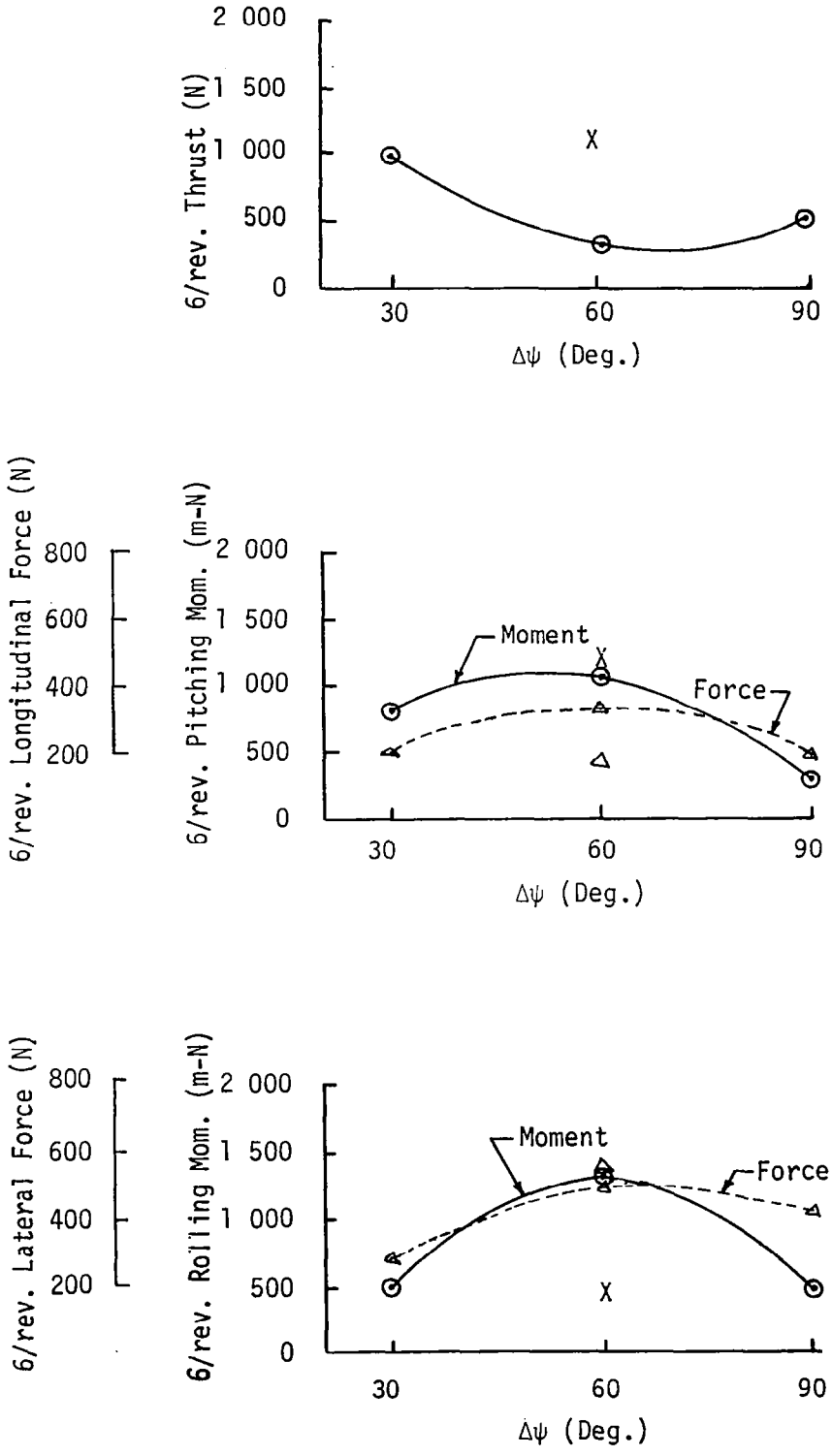

Figure 28. 6 per rev. transmitted loads versus azimuthal spacing, $\Delta\psi$, μ =0.2

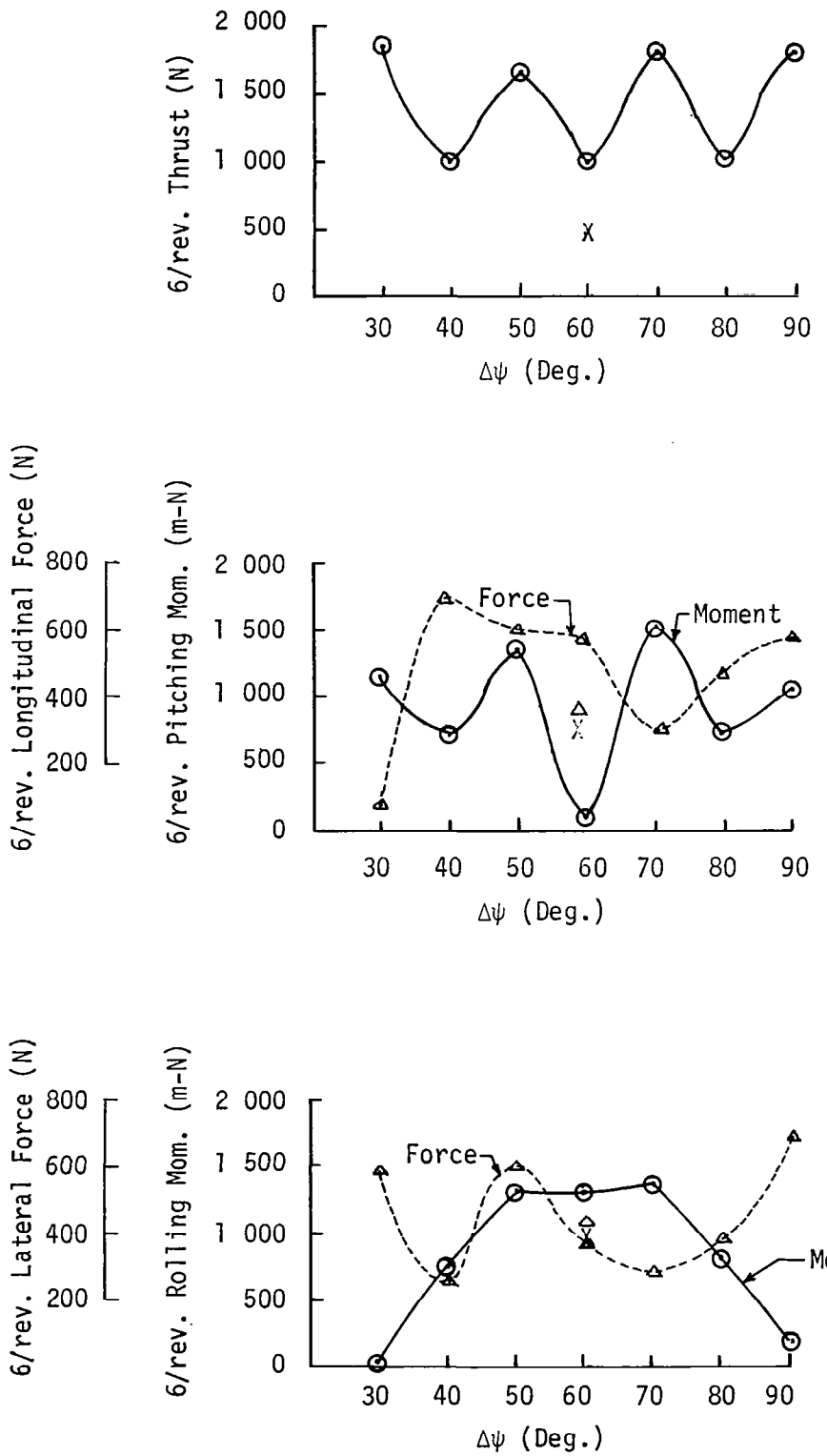

Figure 29. 6 per rev. transmitted loads versus azimuthal spacing, $\Delta\psi$, μ =0.3

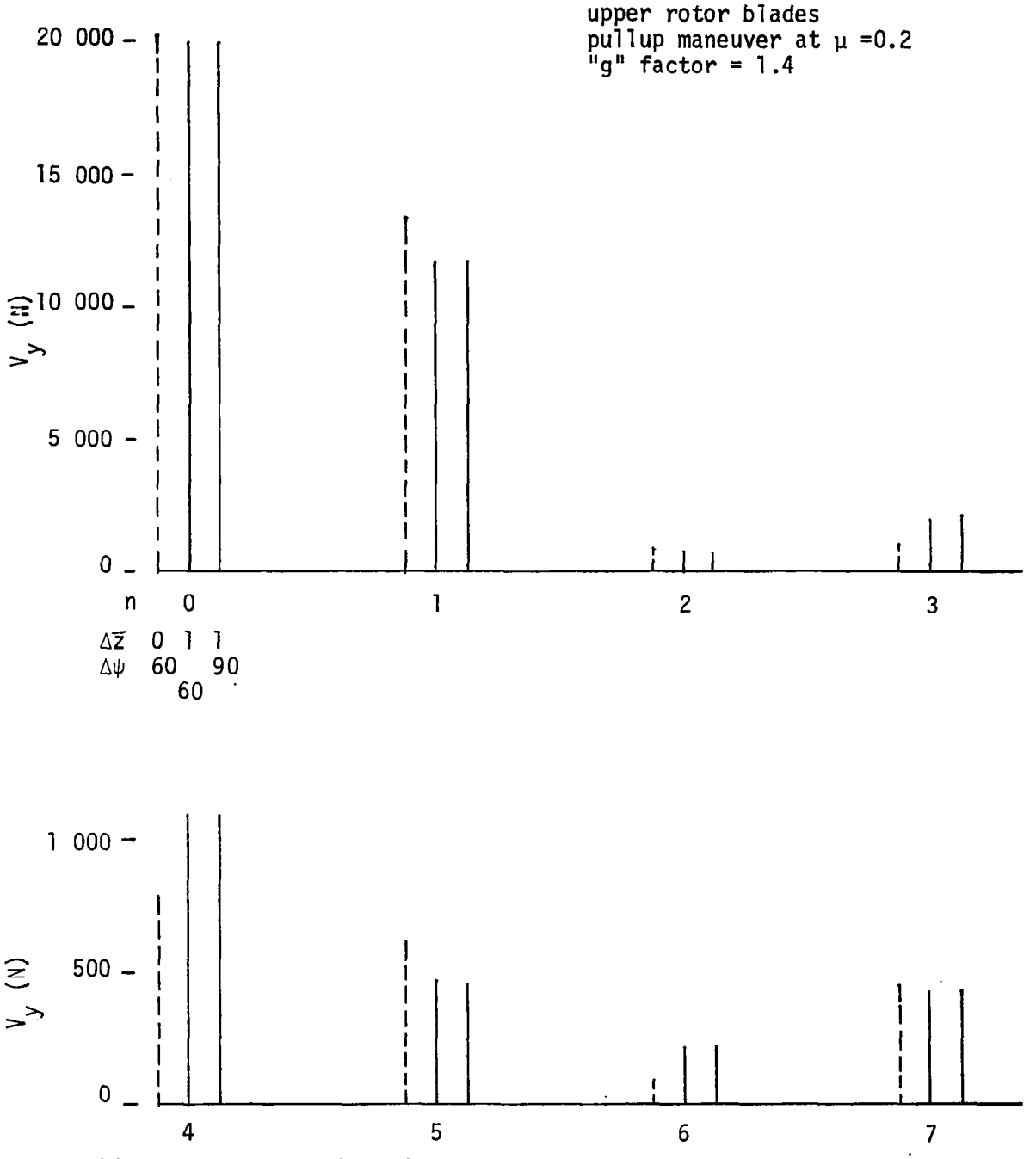

Figure 30. Harmonics of flapwise hinge shear for various VGR configurations

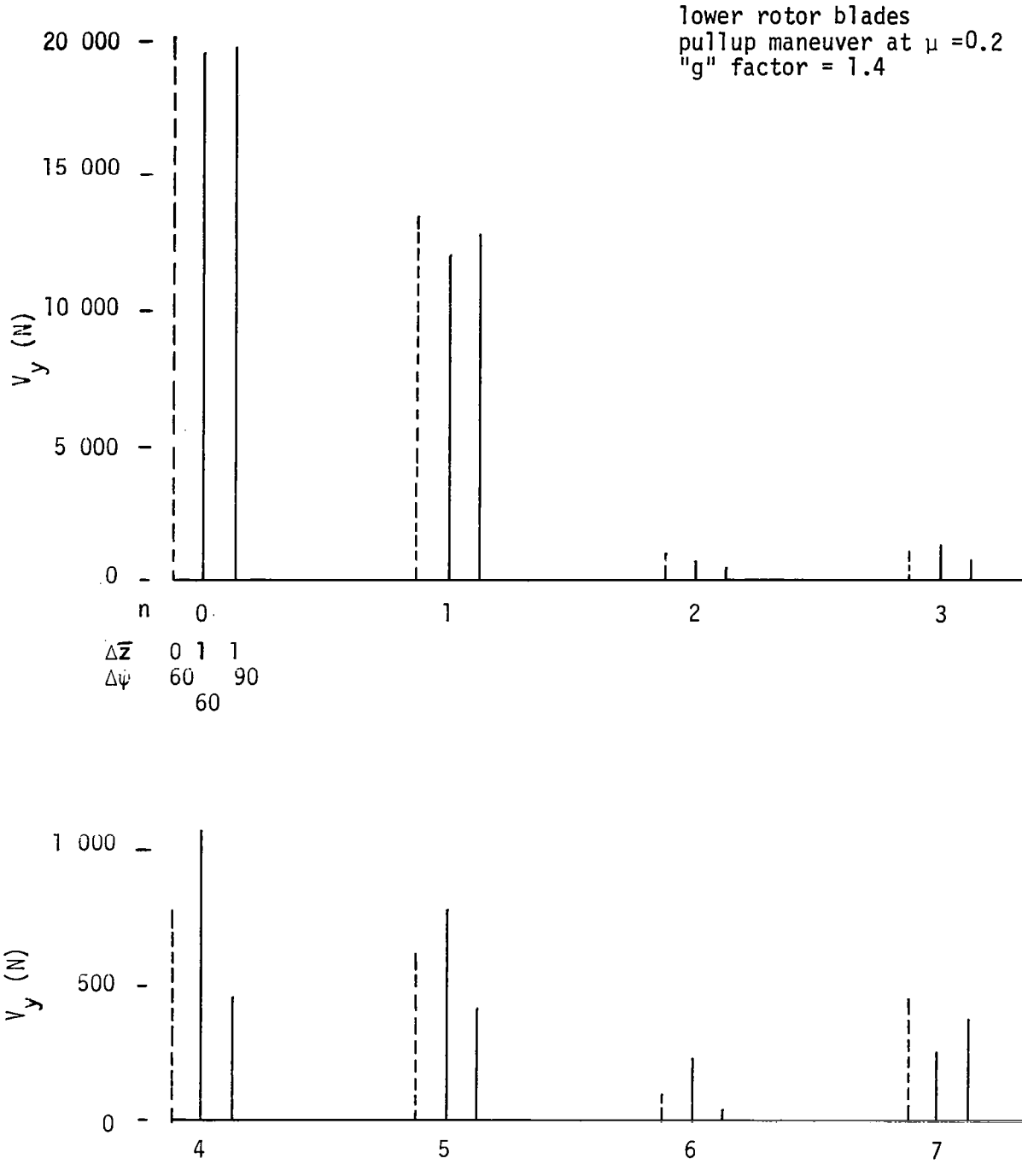

Figure 31. Harmonics of flapwise hinge shear for various VGR configurations

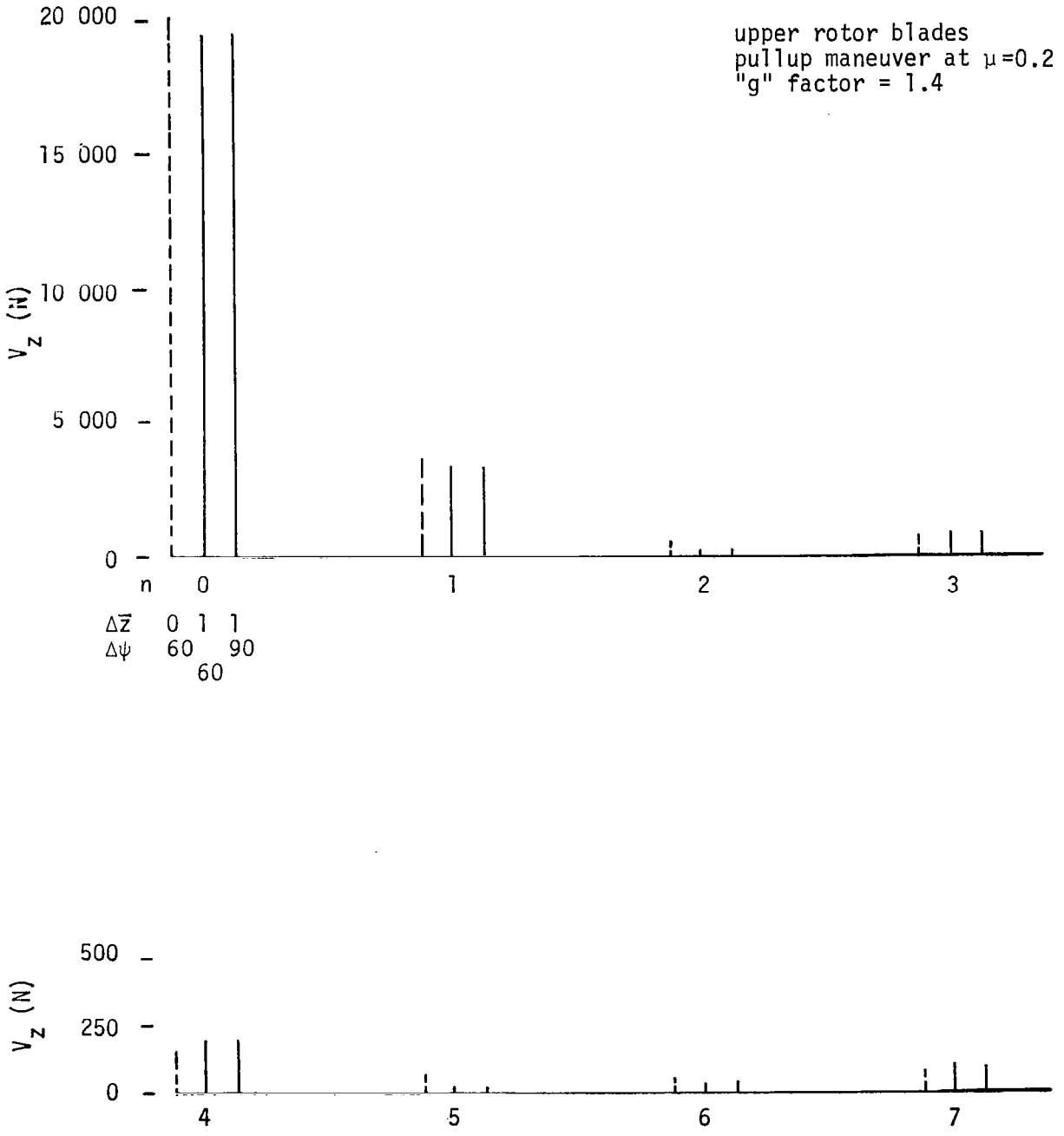

Figure 32. Harmonics of chordwise hinge shear for various VGR configurations

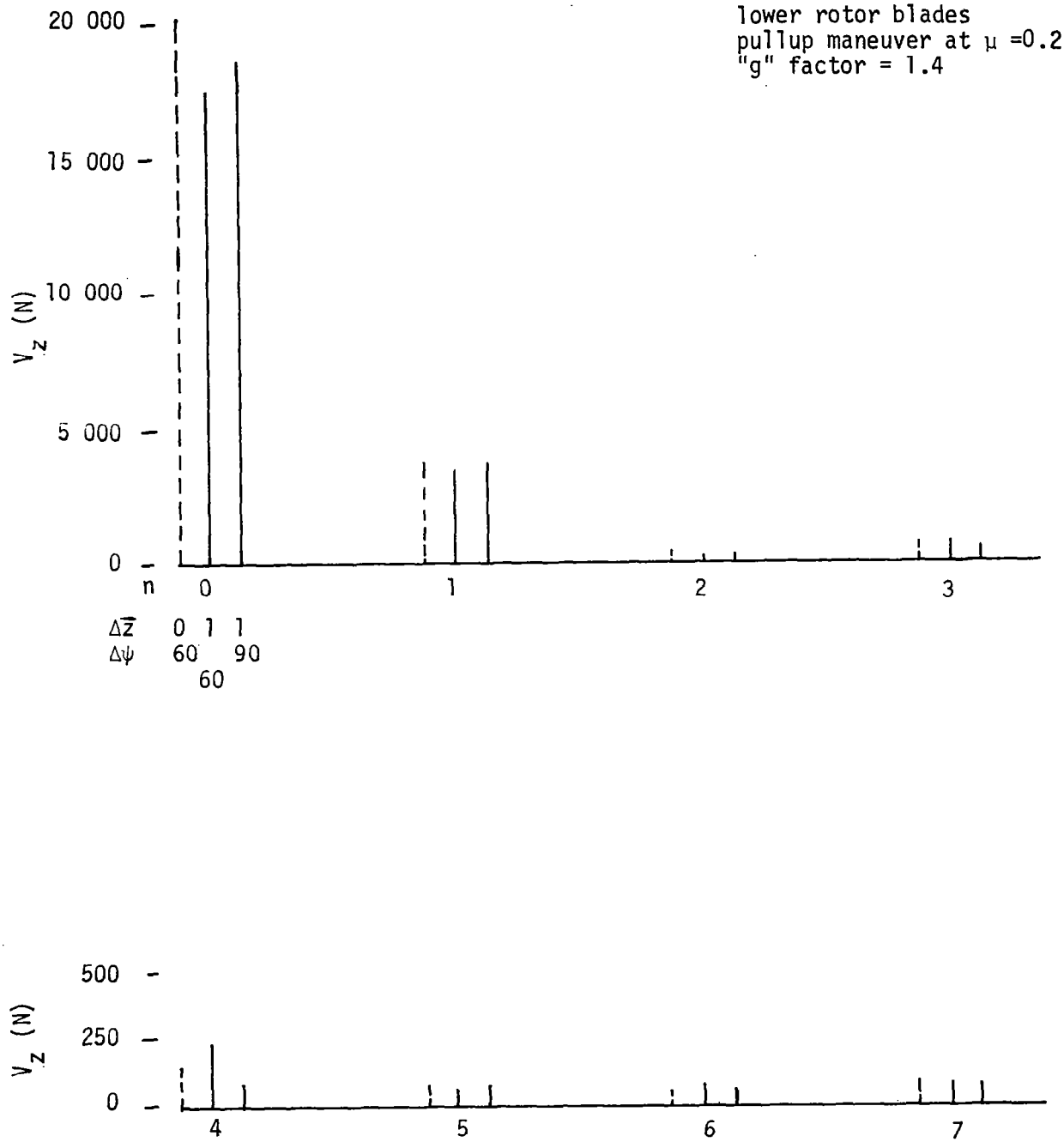

Figure 33. Harmonics of chordwise hinge shear for various VGR configurations

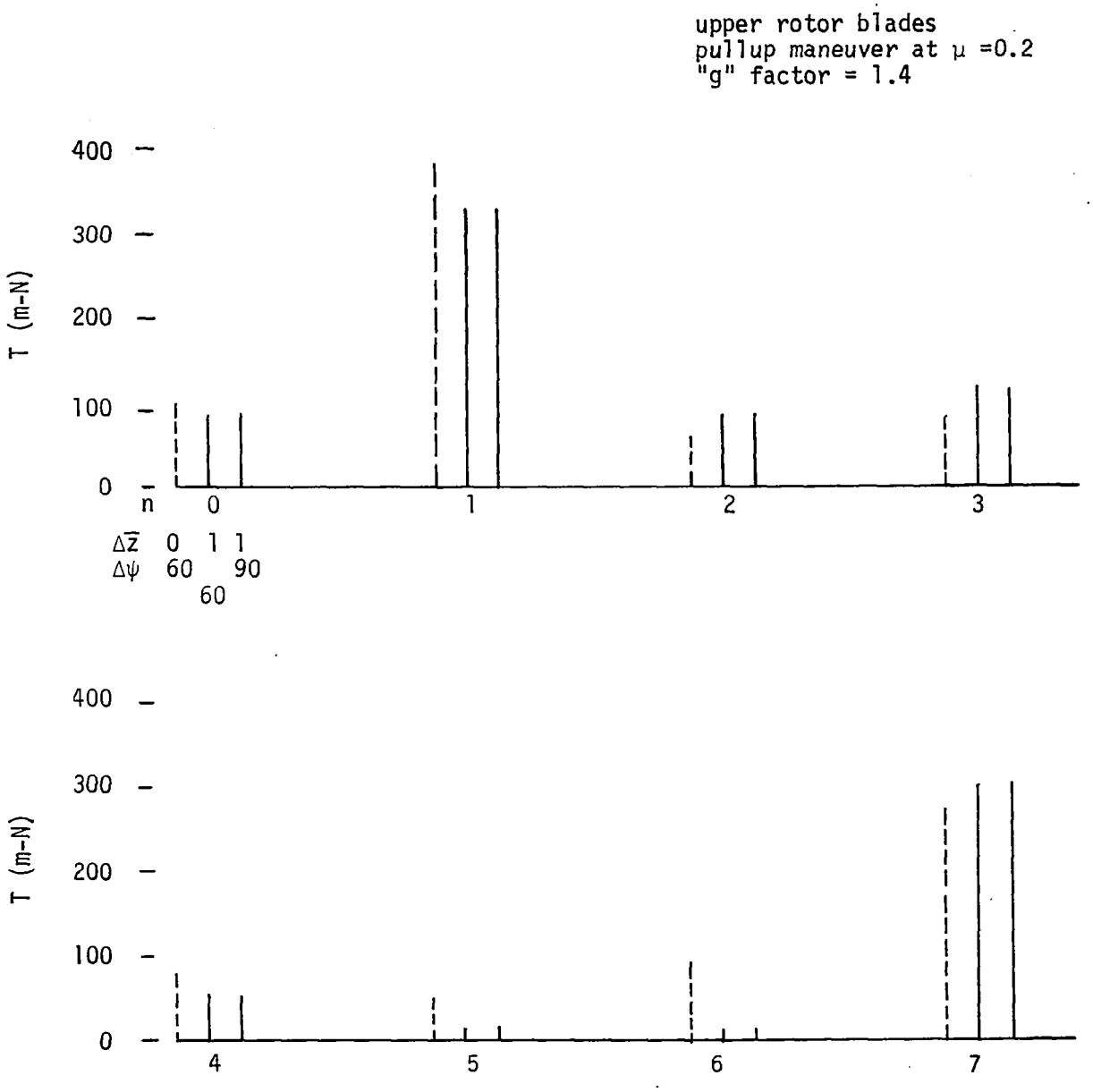

Figure 34. Harmonics of blade pitching moment at r/R =0.25 for various VGR configurations

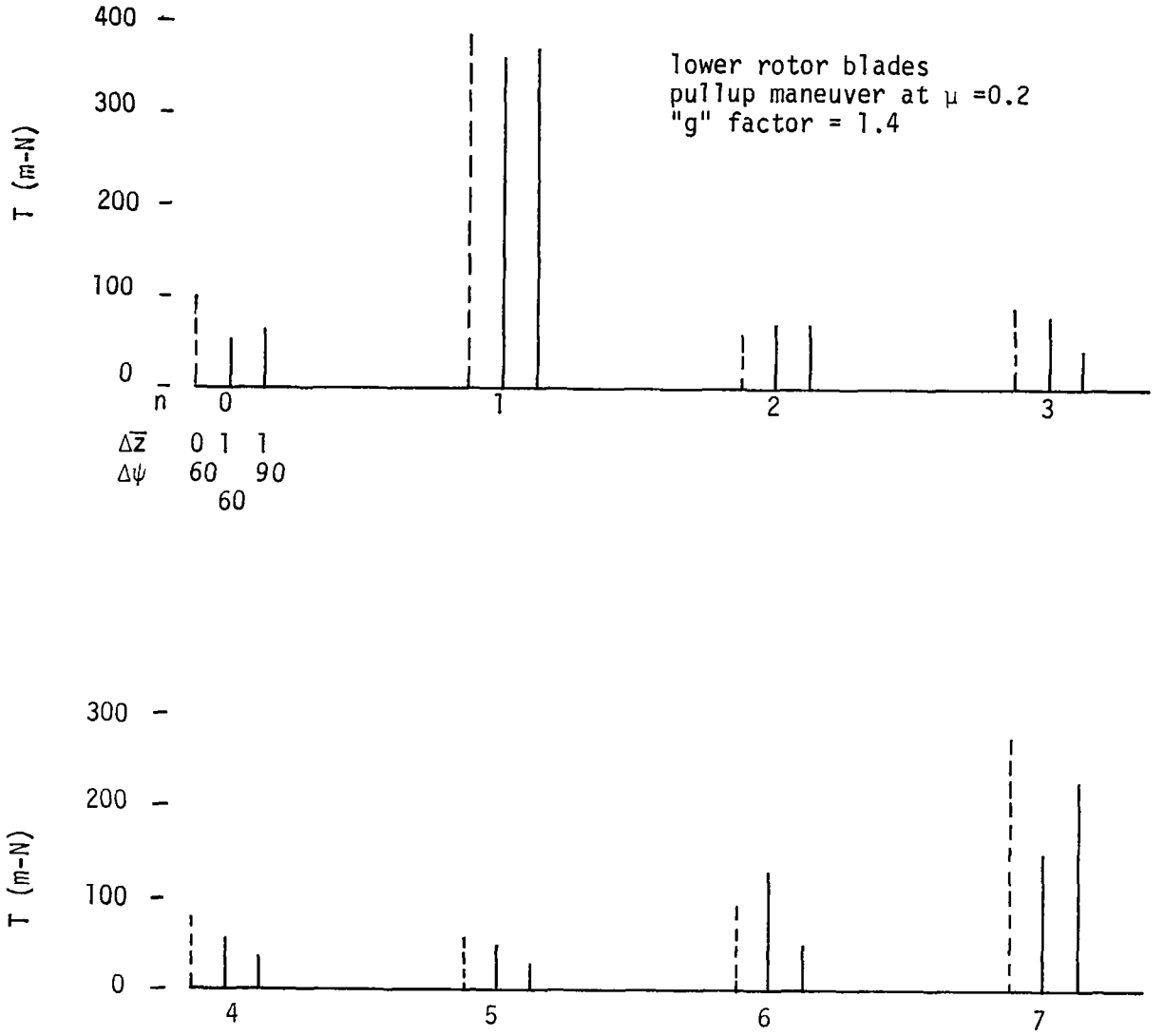

Figure 35. Harmonics of blade pitching moment at r/R =0.25 for various VGR configurations

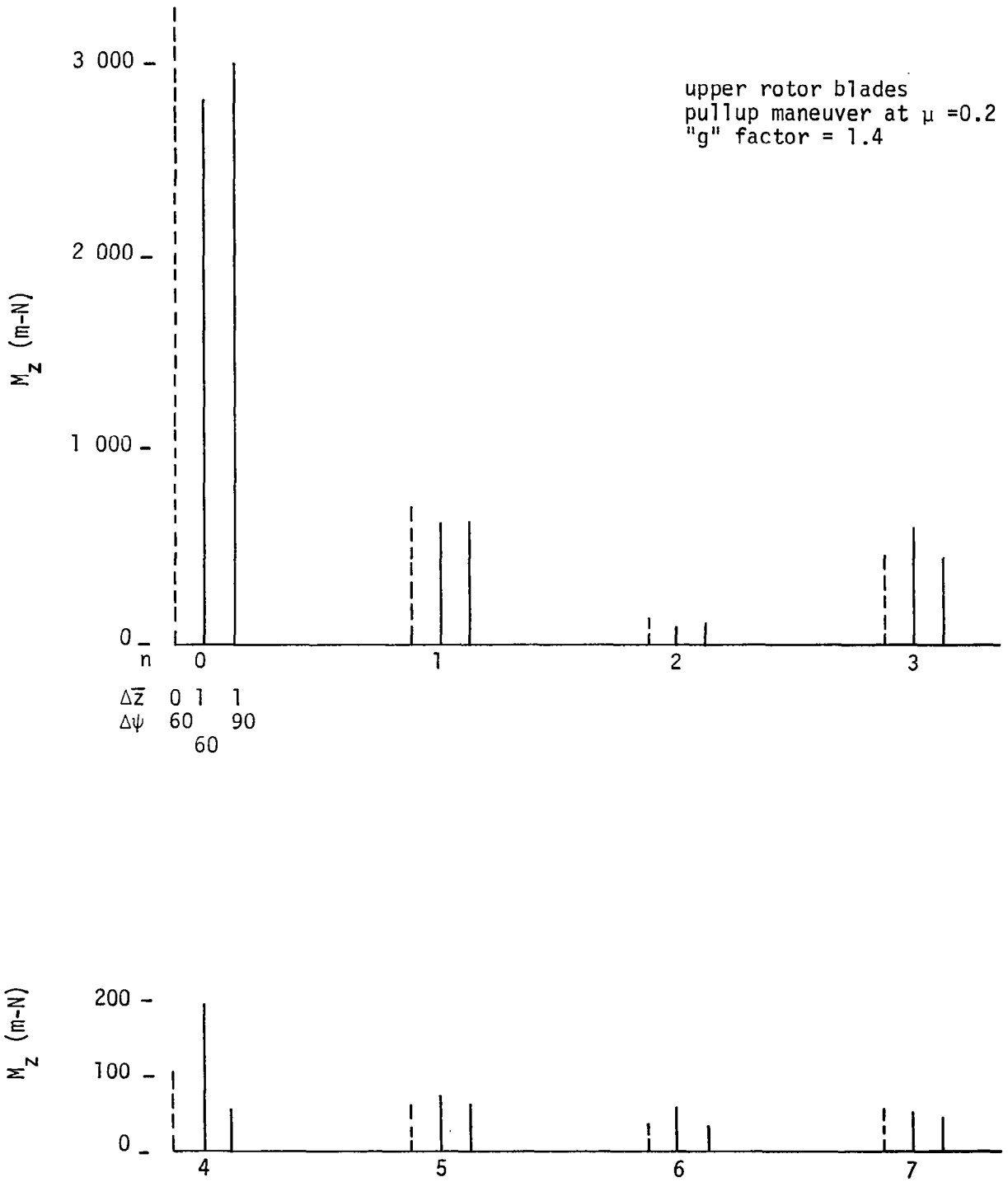

Figure 36. Harmonics of flapwise bending moment at r/R =0.282 for various VGR configurations

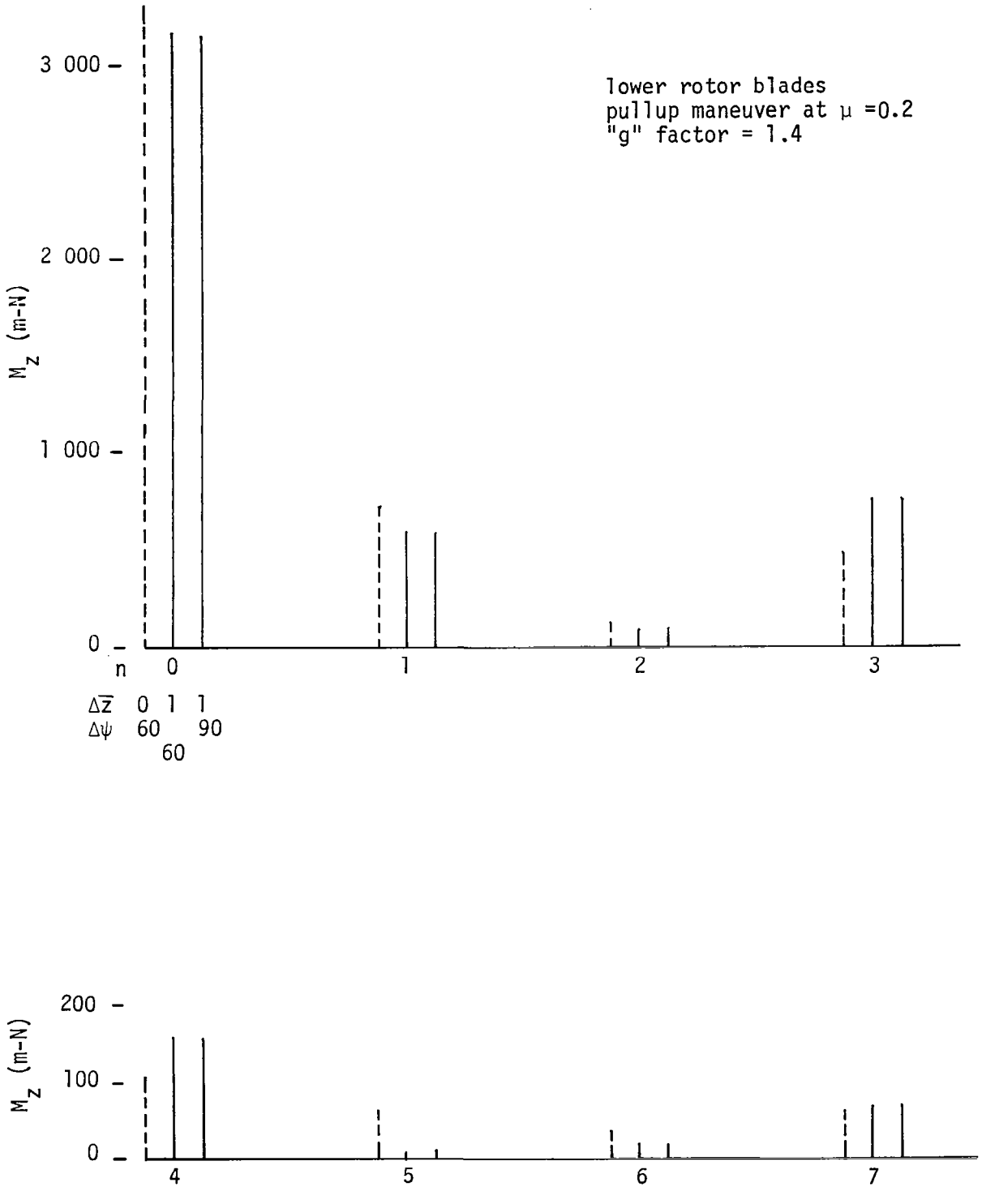

Figure 37. Harmonics of flapwise bending moment at r/R =0.282 for various VGR configurations

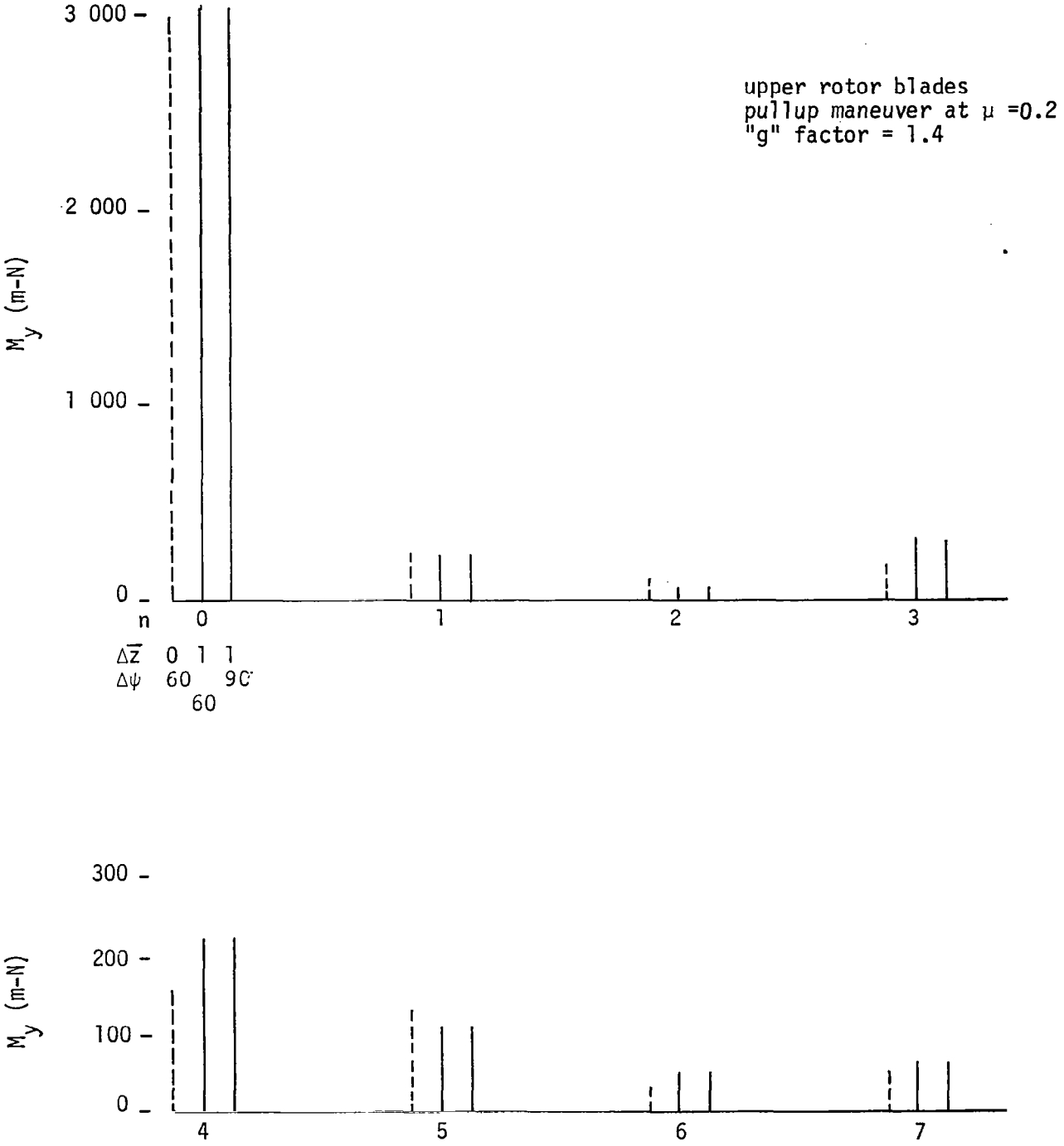

Figure 38. Harmonics of chordwise bending moment at r/R =0.282 for various VGR configurations

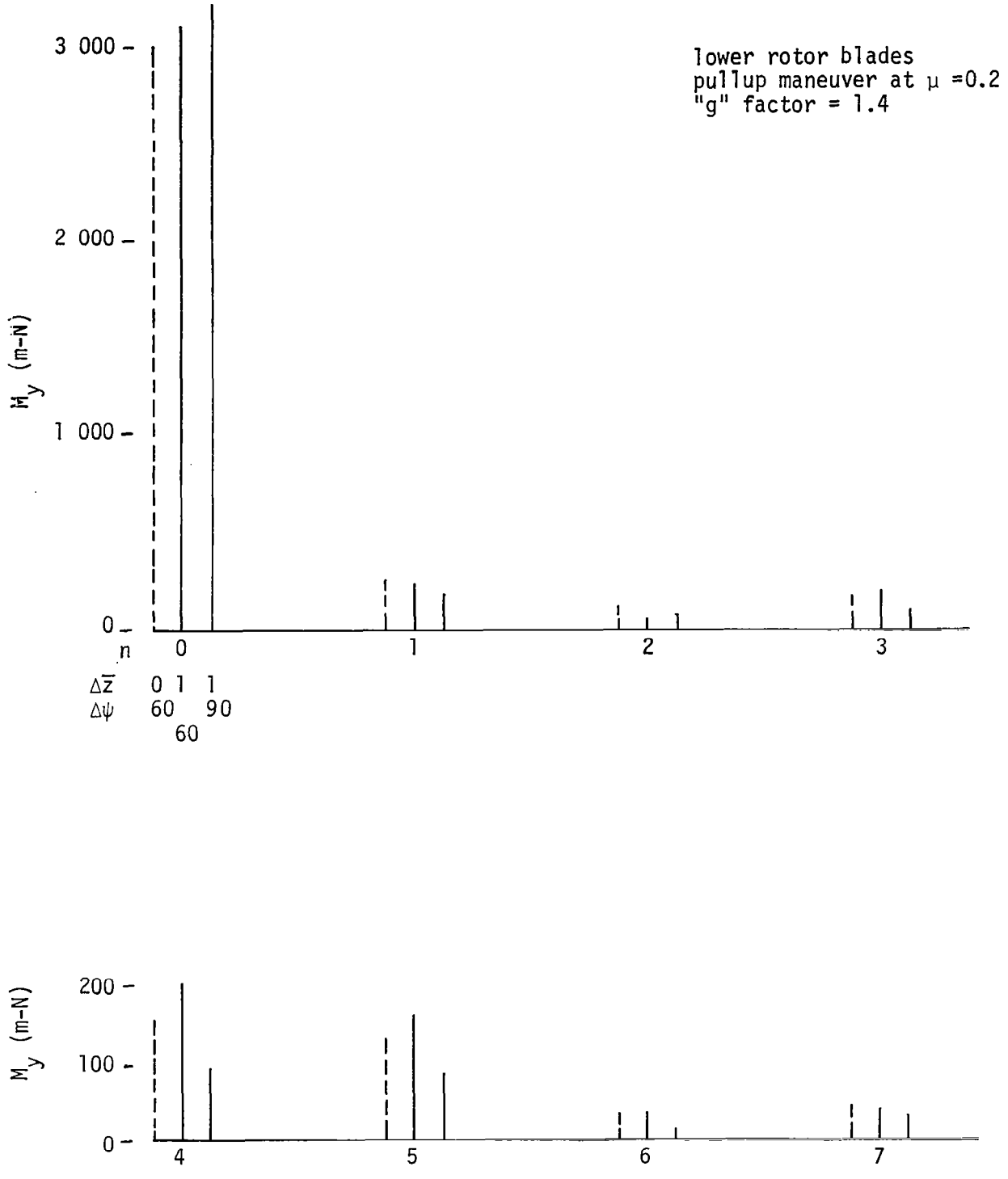

Figure 39. Harmonics of chordwise banding moment at r/R =0.282 for various VGR configurations

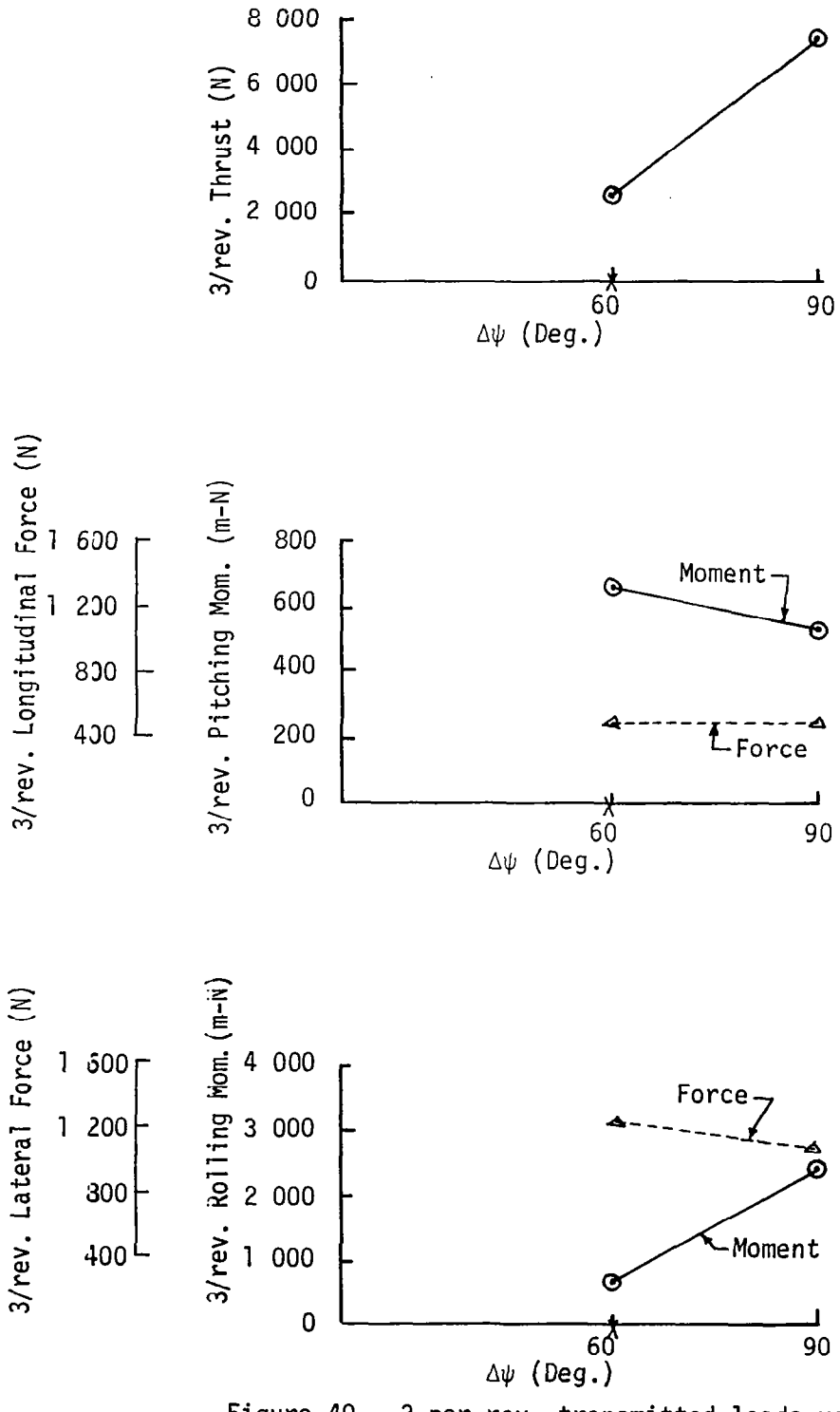

Figure 40. 3 per rev. transmitted loads versus azimuthal spacing, Δψ, for 1.4 "g" pullup maneuvers

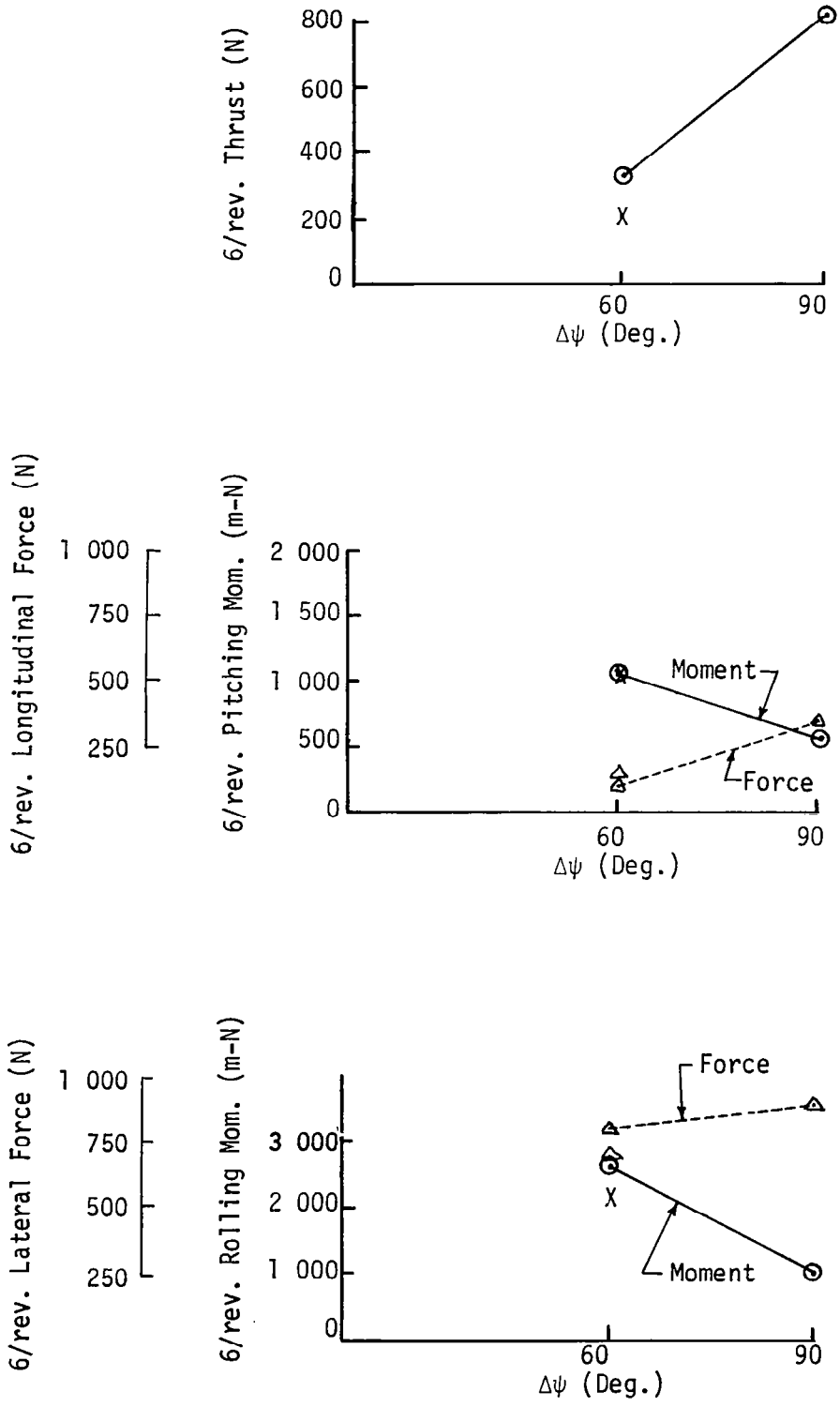

Figure 41. 6 per rev. transmitted loads versus azimuthal spacing, $\Delta\psi$, for 1.4 "g" pullup maneuvers

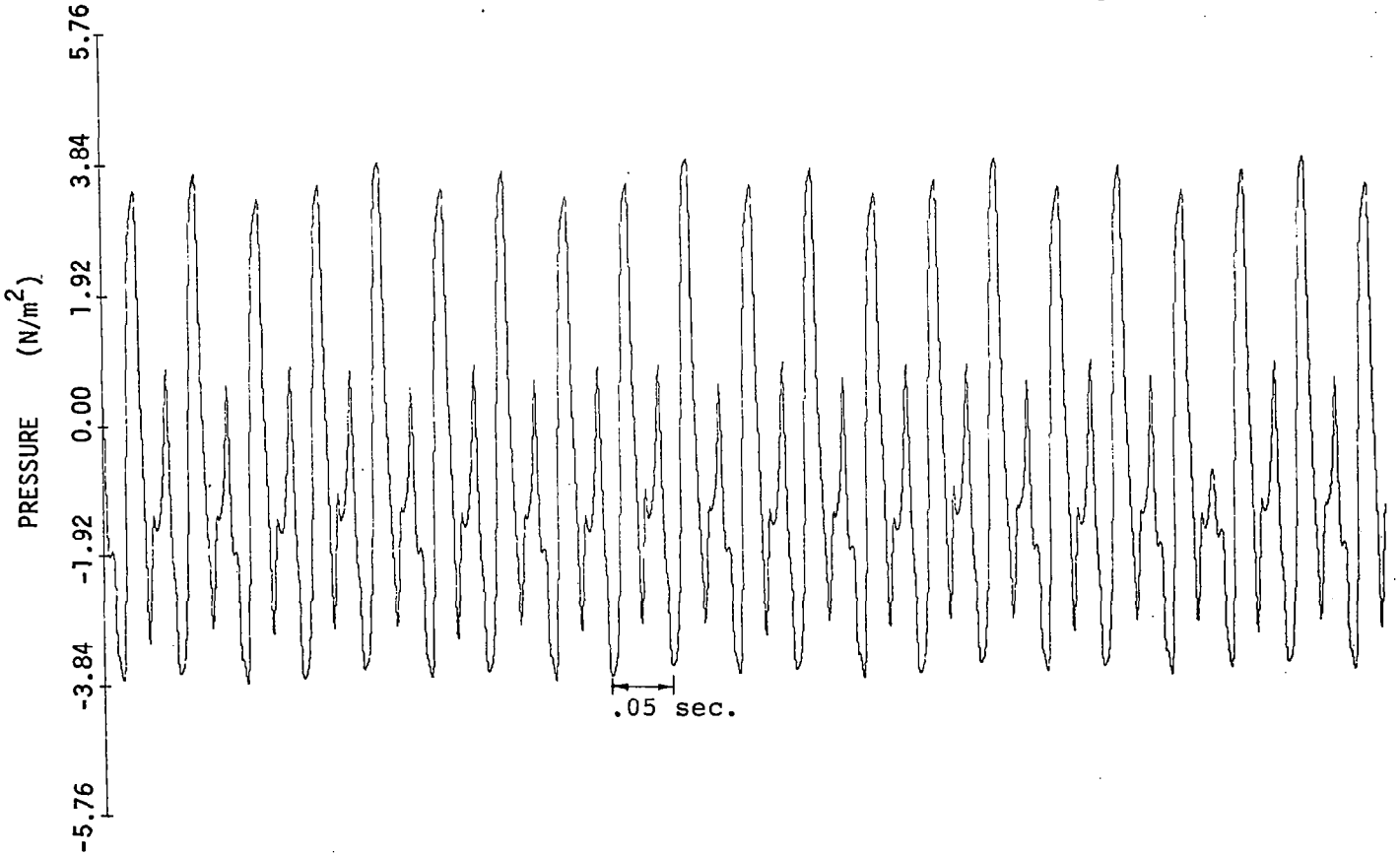

Figure 42. Pressure time history of rotational noise only from six-bladed conventional rotor at μ =0.2

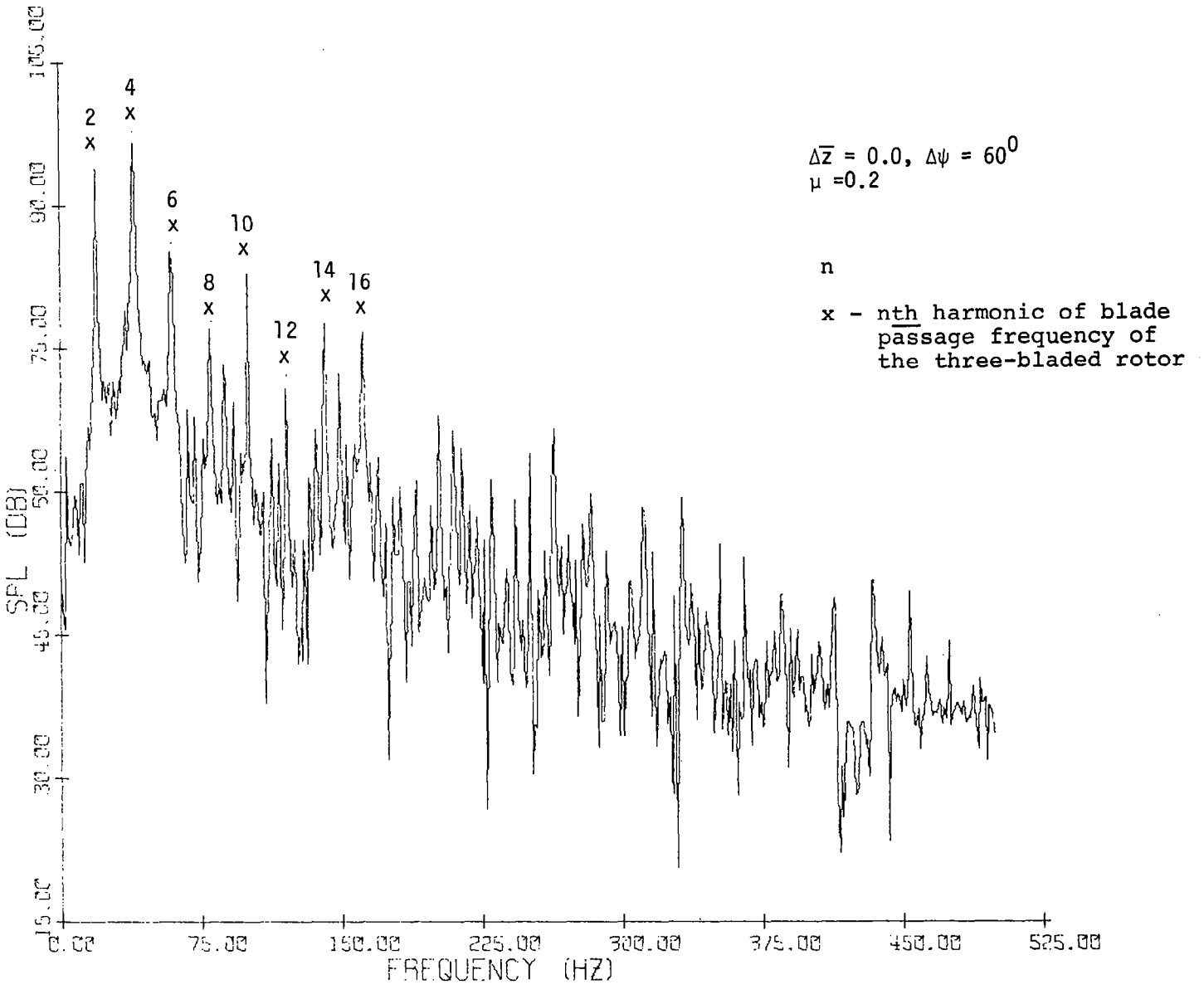

Figure 43. Spectrum of rotational noise only

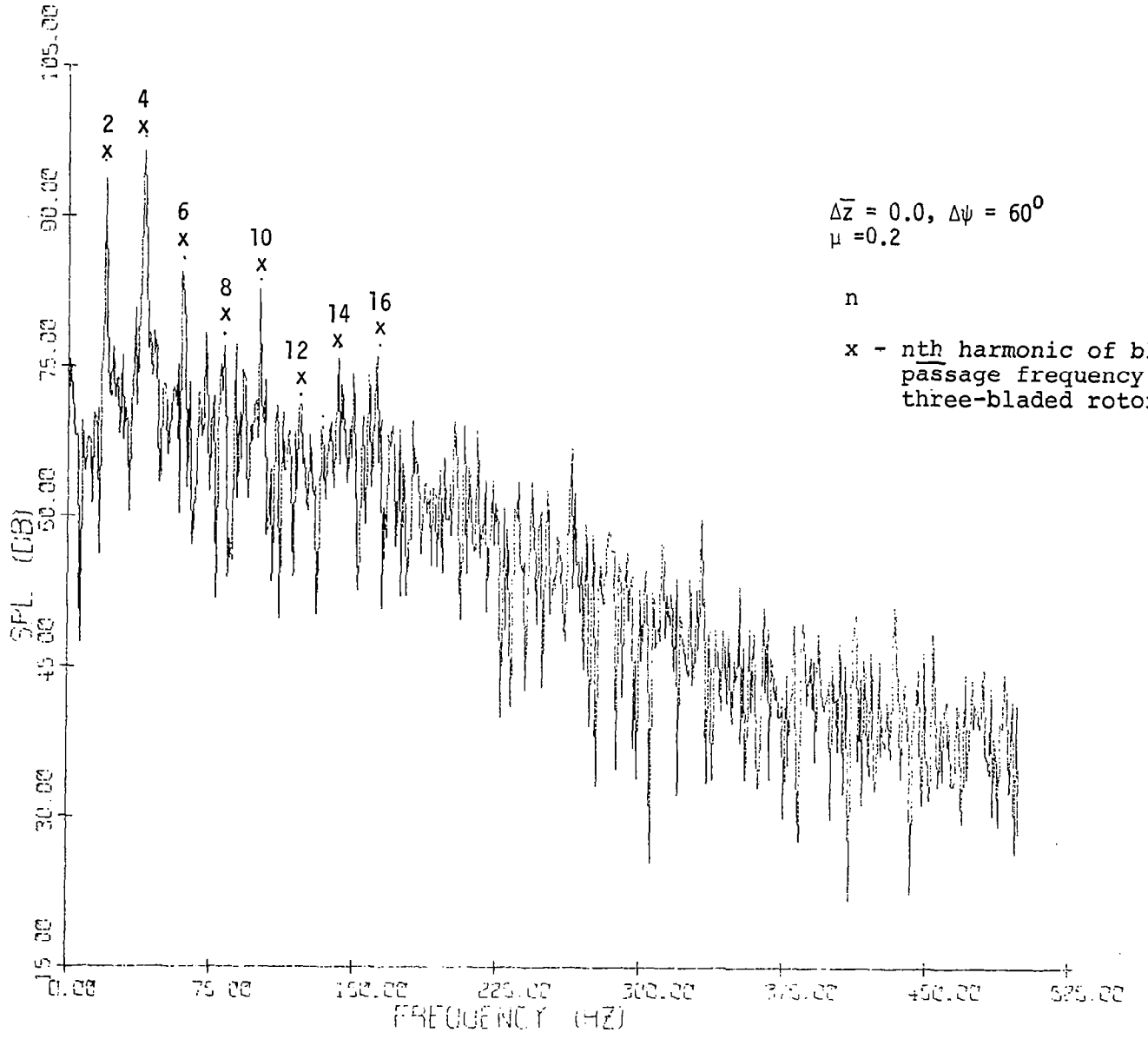

Figure 44. Spectrum of rotational and vortex noise

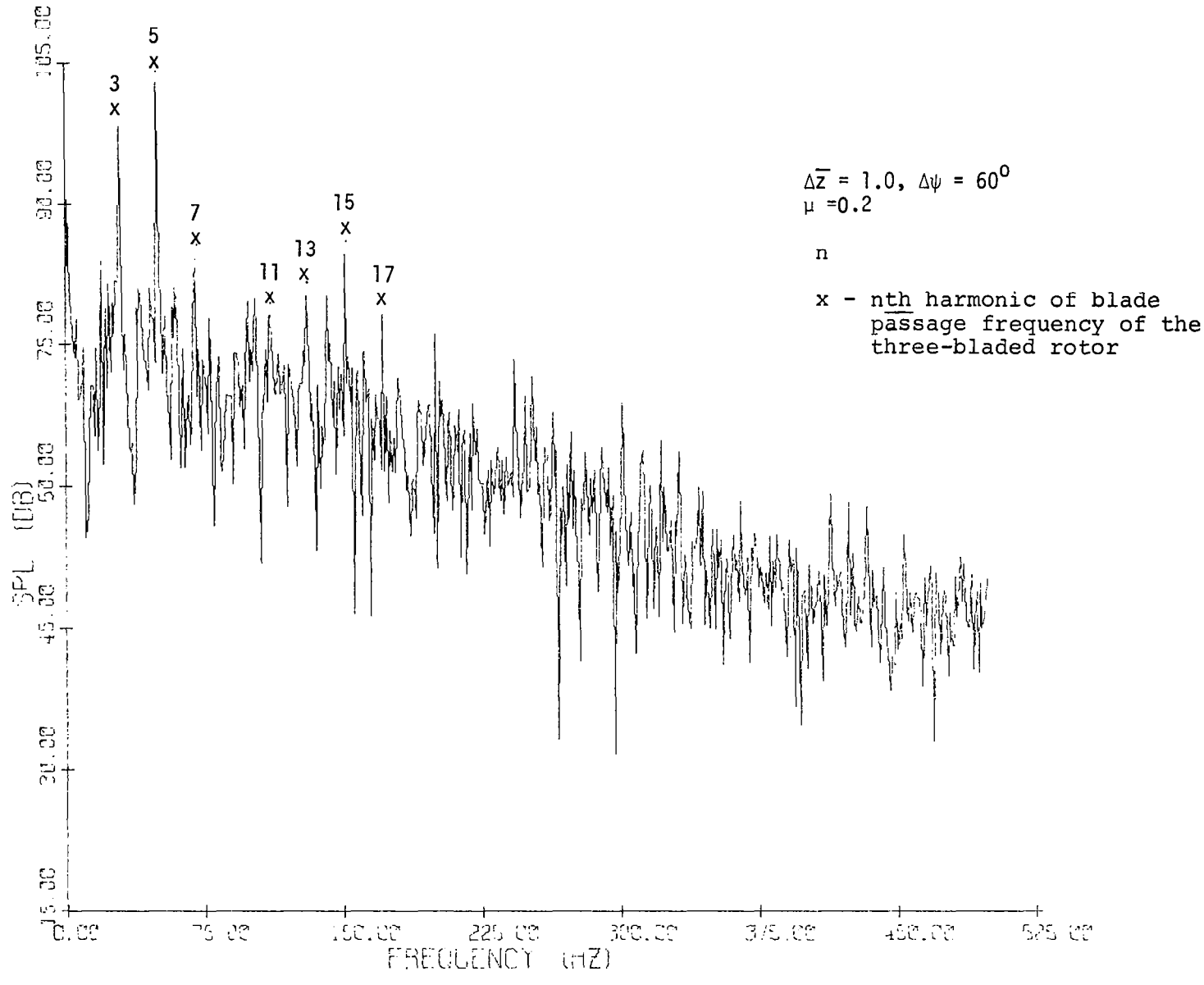

Figure 45. Spectrum of rotational and vortex noise

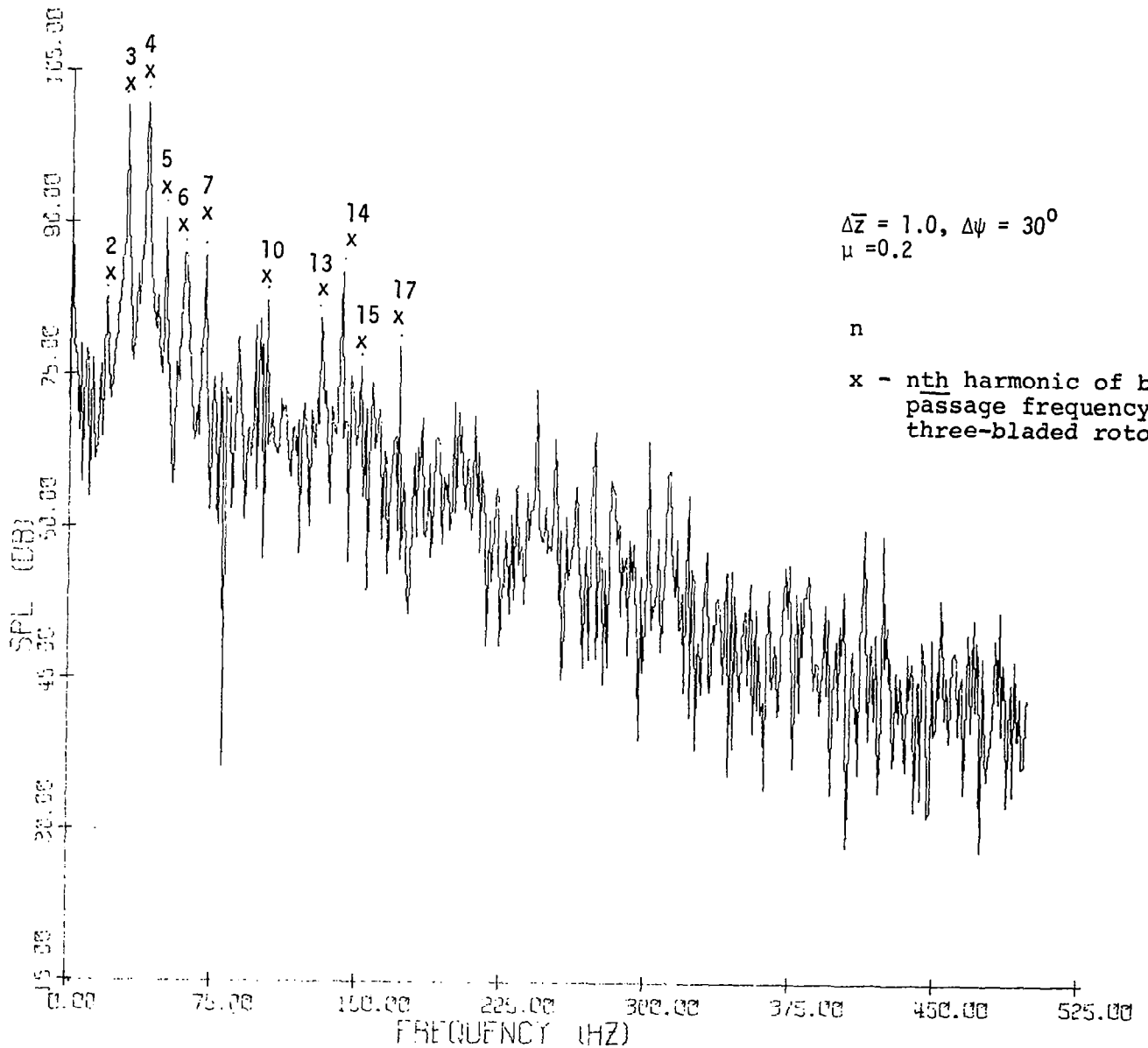

Figure 46. Spectrum of rotational and vortex noise

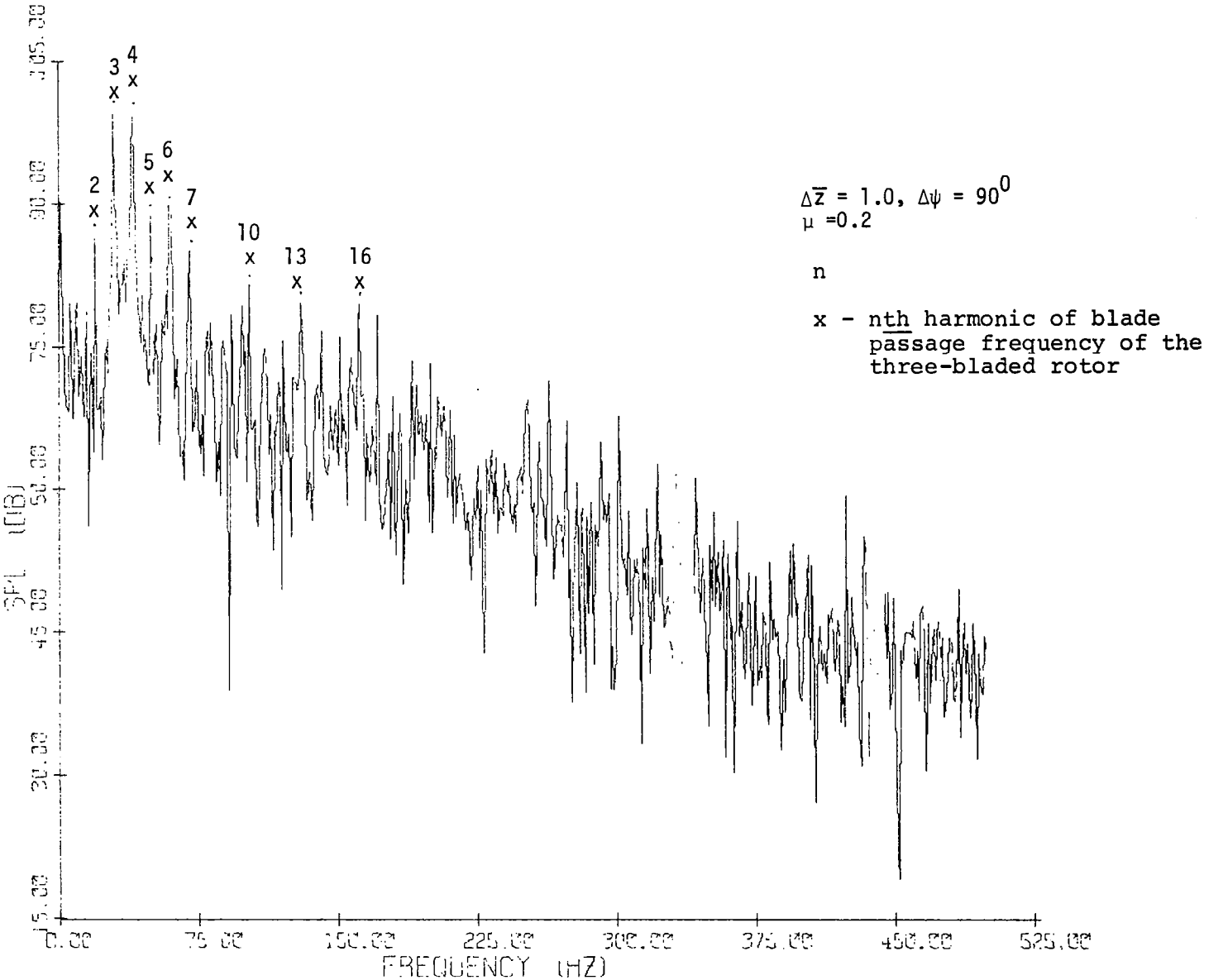

Figure 47. Spectrum of rotational and vortex noise

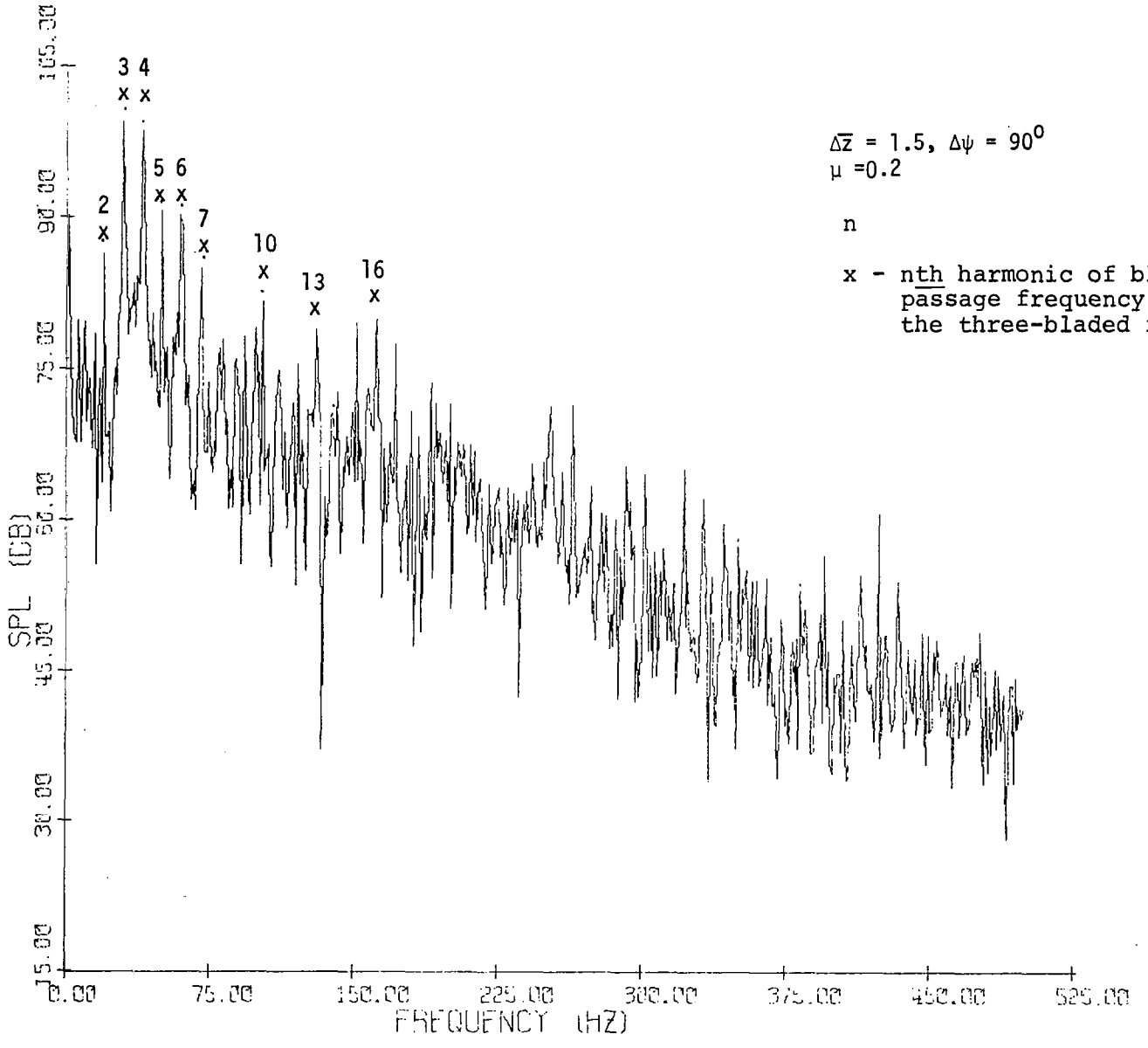

Figure 48. Spectrum of rotational and vortex noise

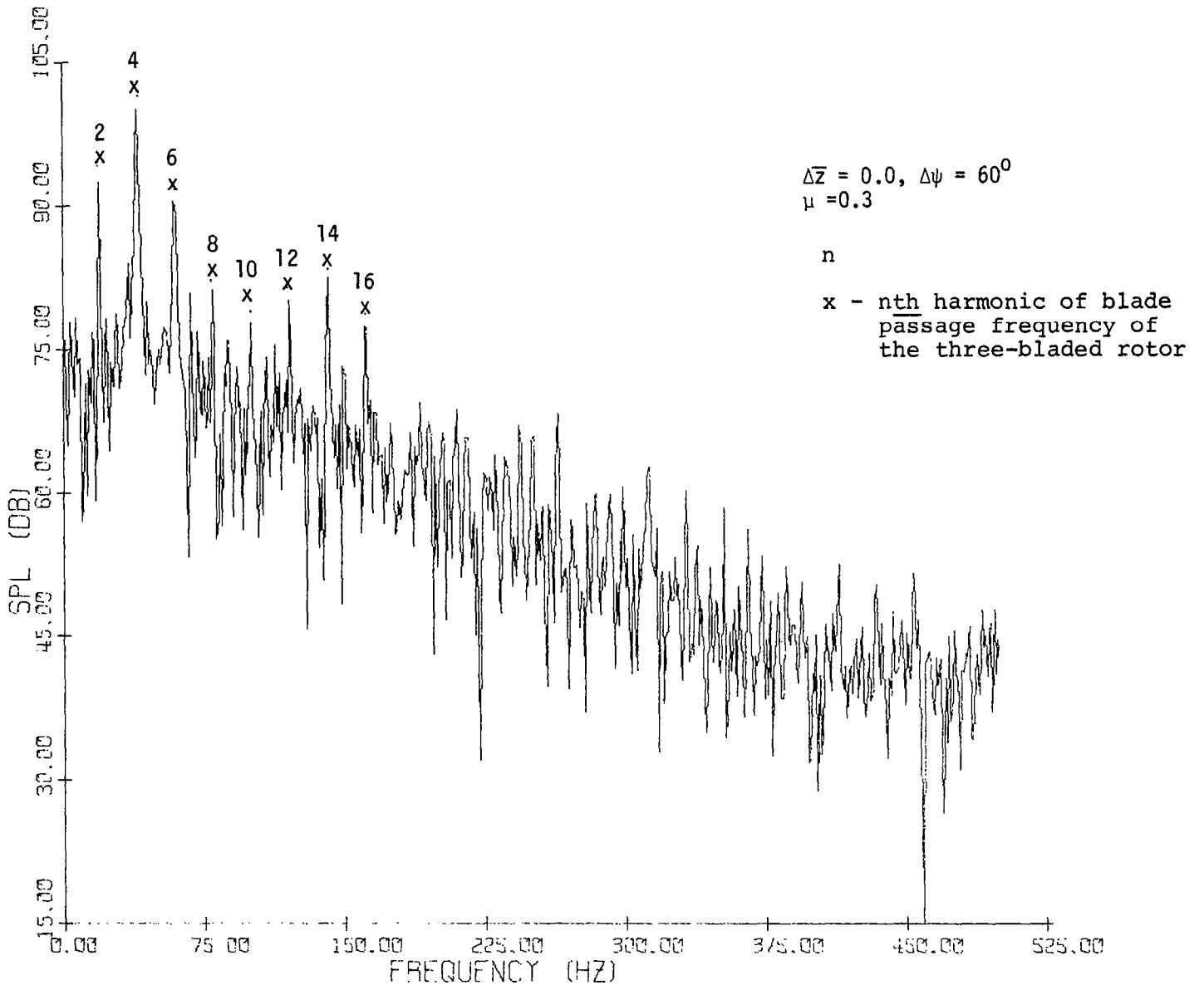

Figure 49. Spectrum of rotational and vortex noise

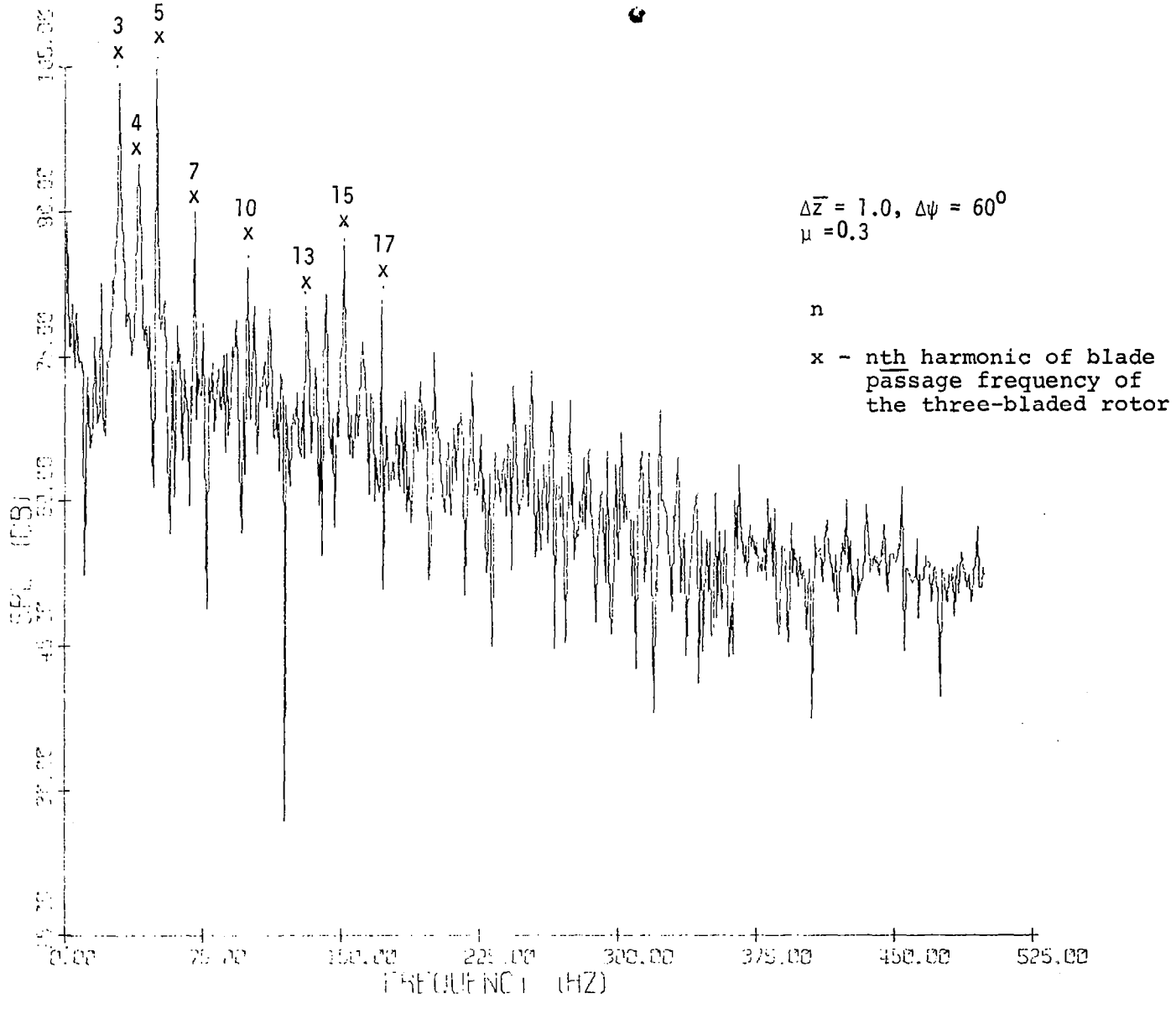

Figure 50. Spectrum of rotational and vortex noise

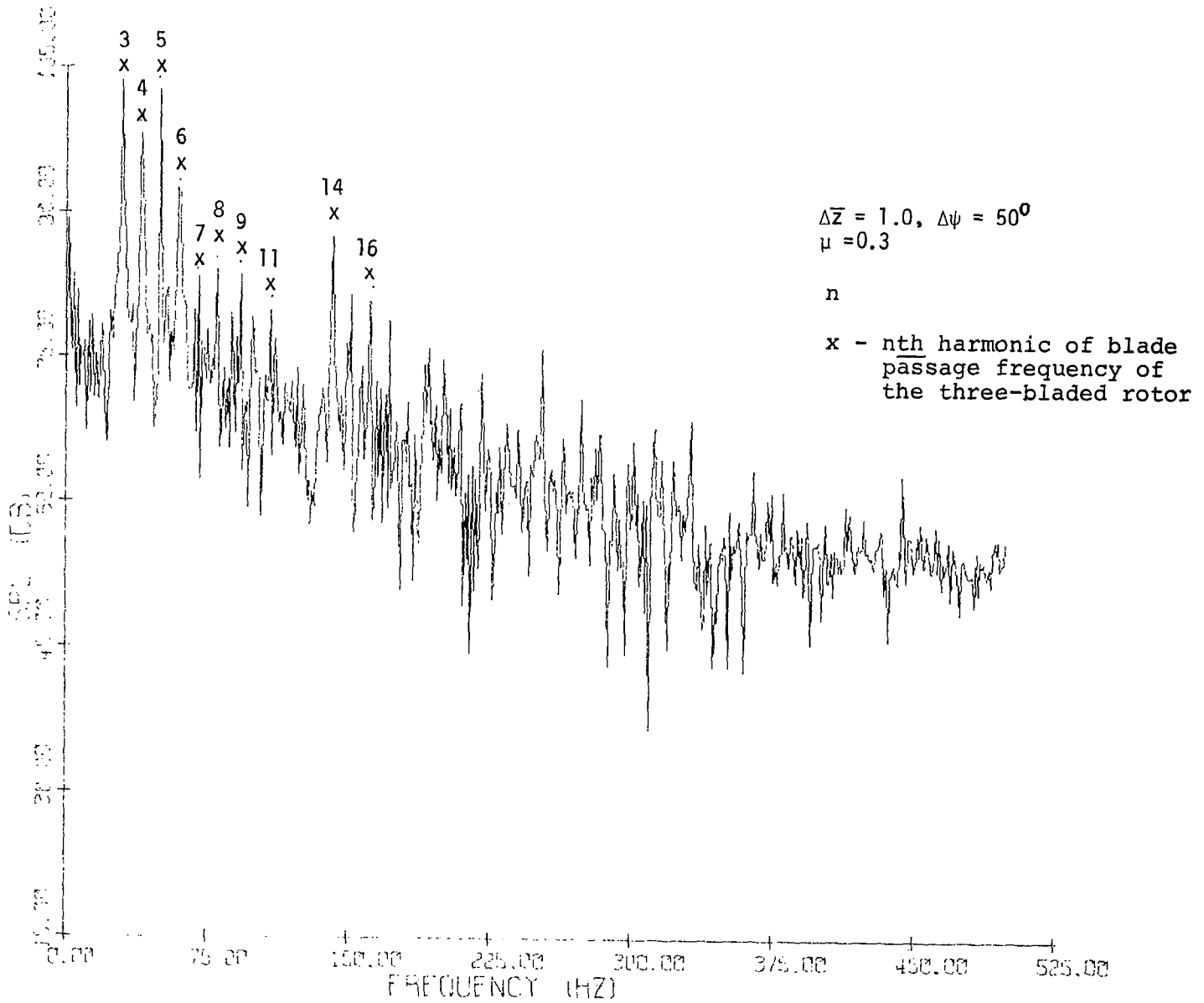

Figure 51. Spectrum of rotational and vortex noise

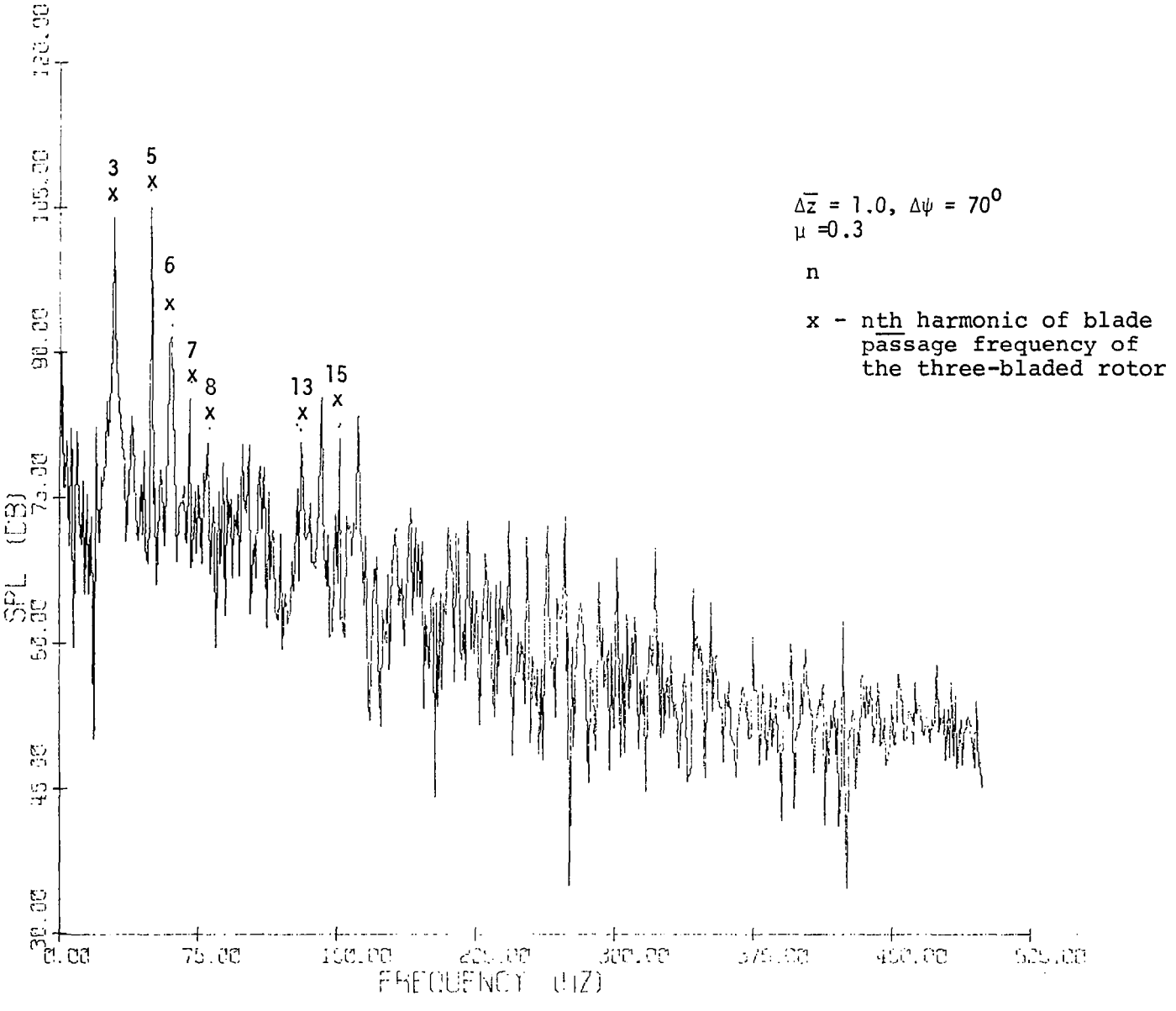

Figure 52. Spectrum of rotational and vortex noise

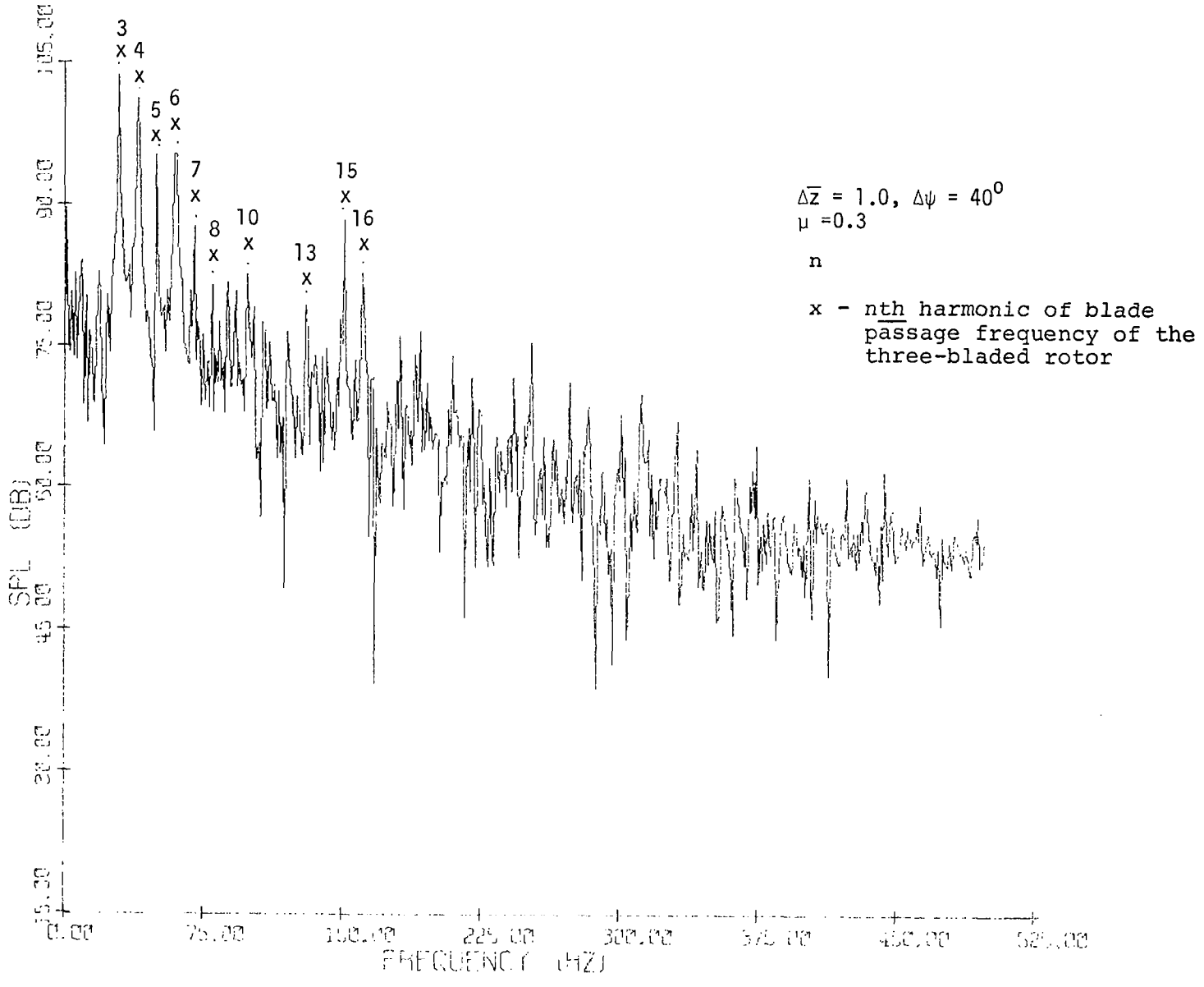

Figure 53. Spectrum of rotational and vortex noise

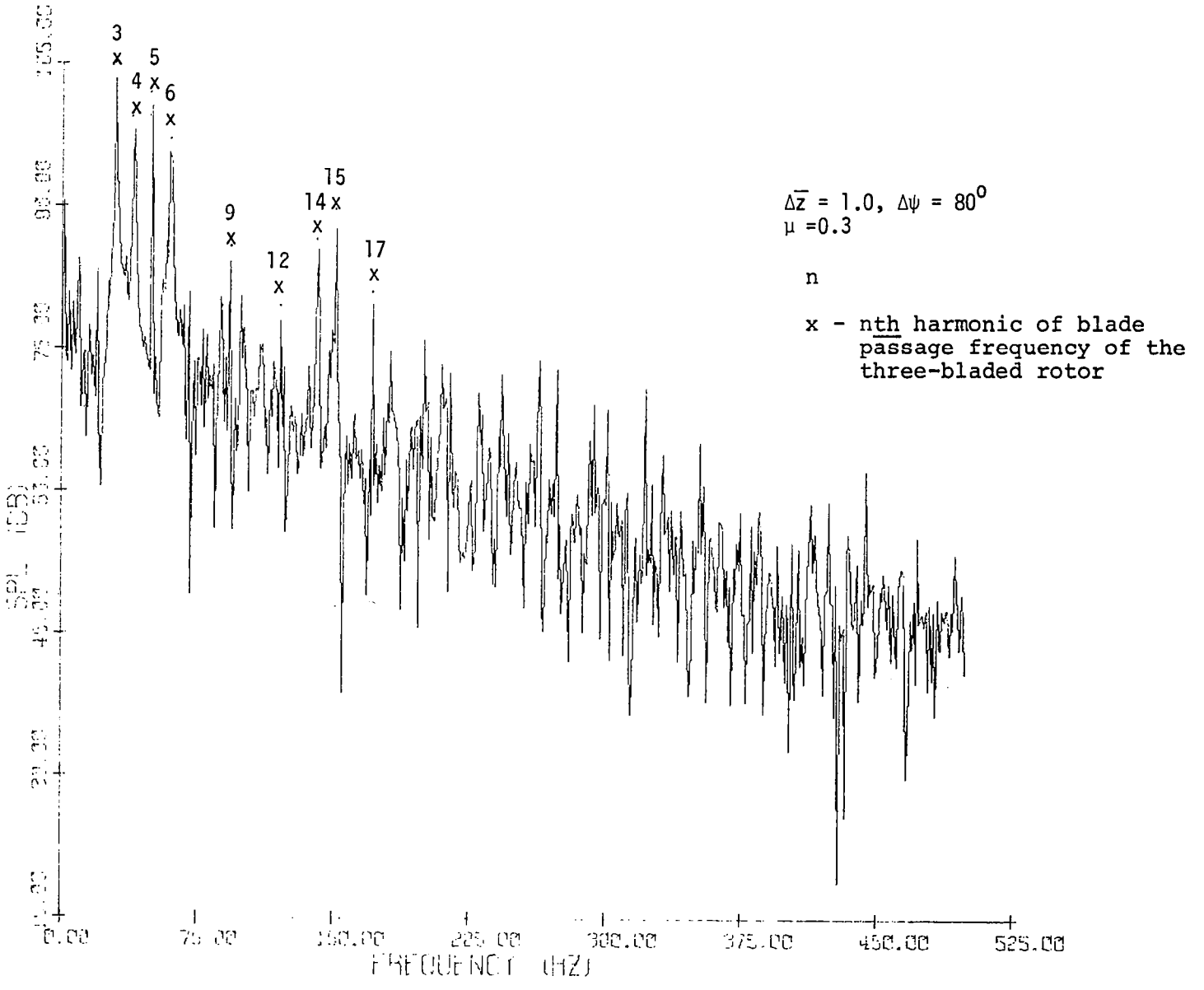

Figure 54. Spectrum of rotational and vortex noise

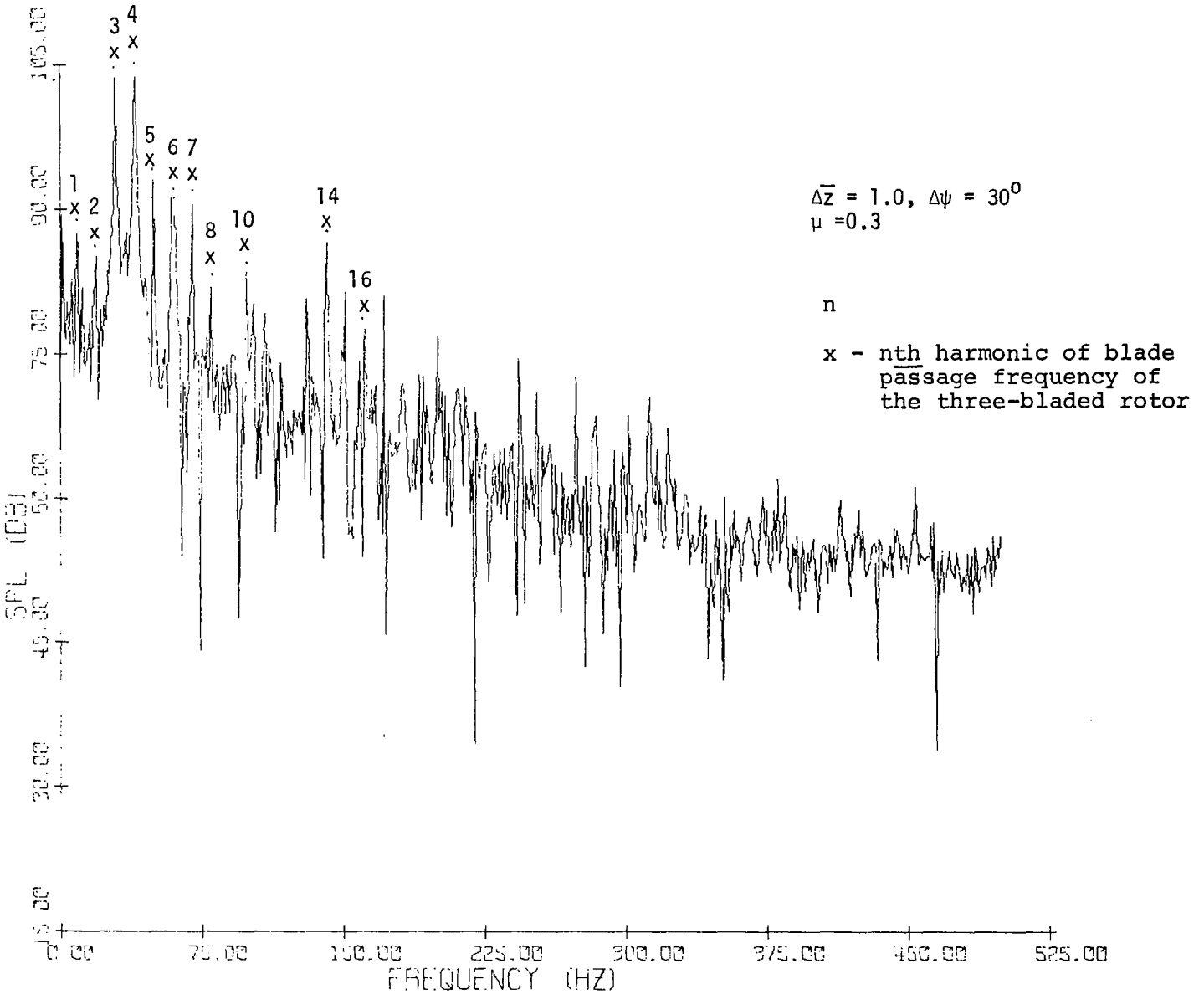

Figure 55. Spectrum of rotational and vortex noise

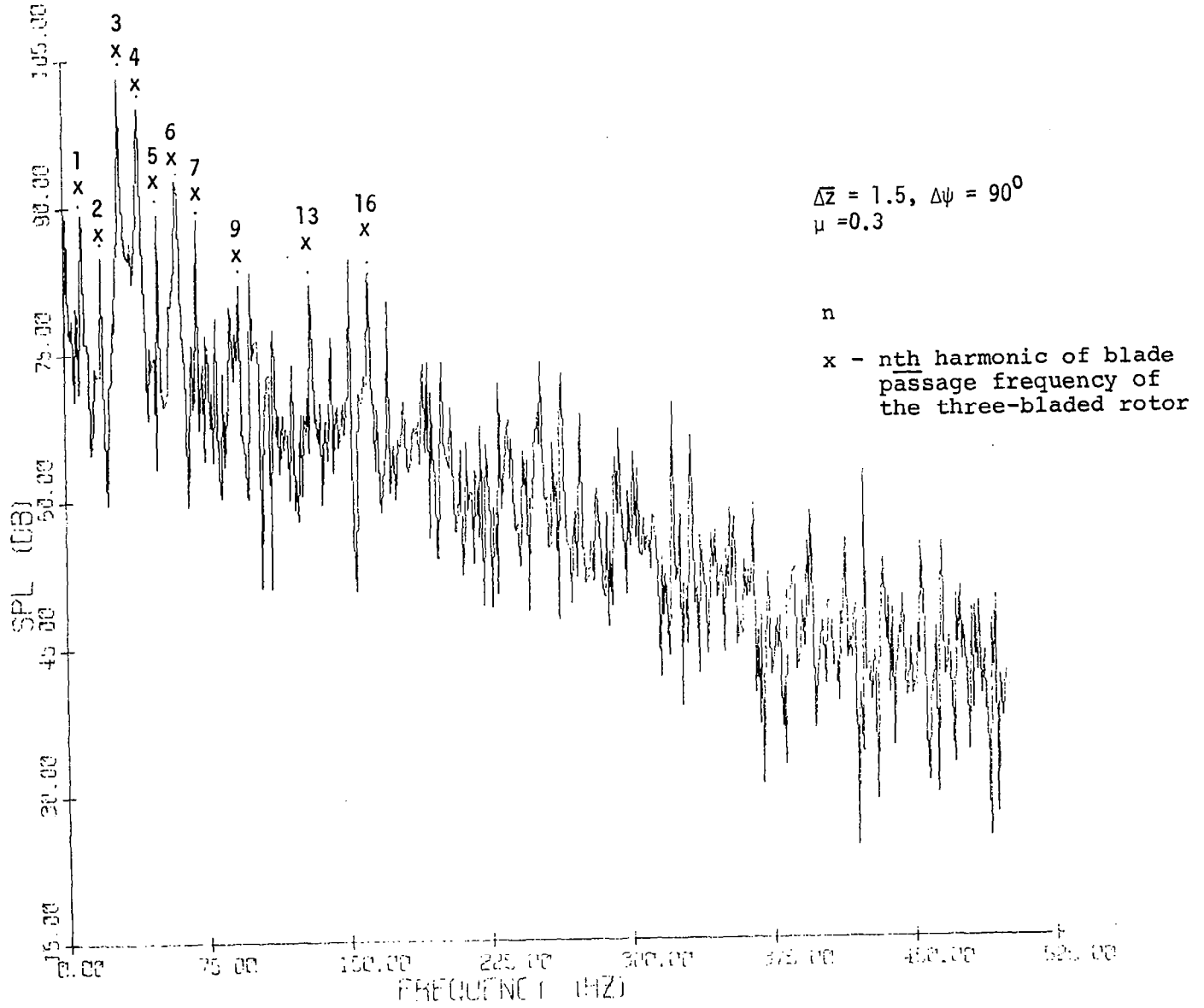

Figure 56. Spectrum of rotational and vortex noise

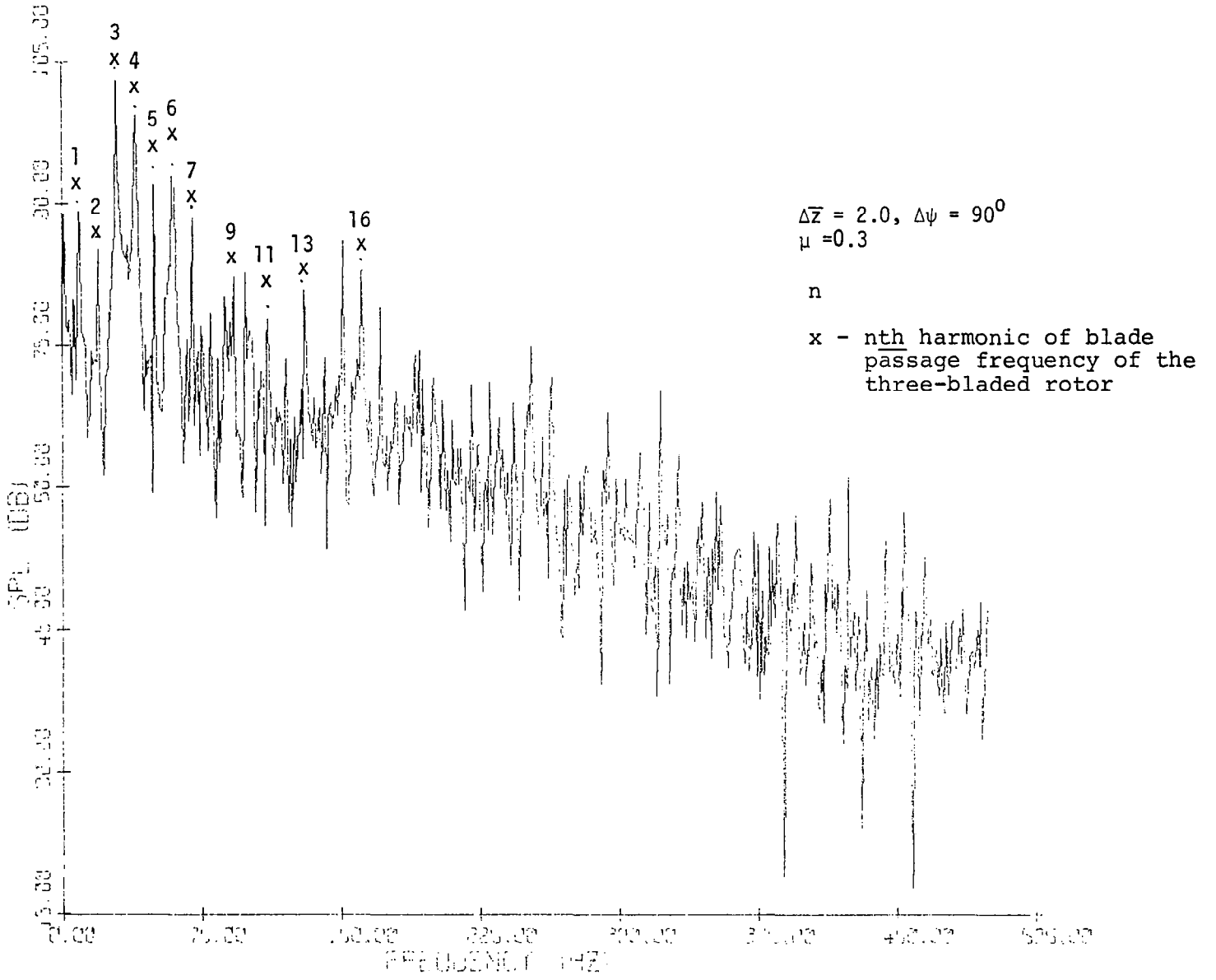

Figure 57. Spectrum of rotational and vortex noise

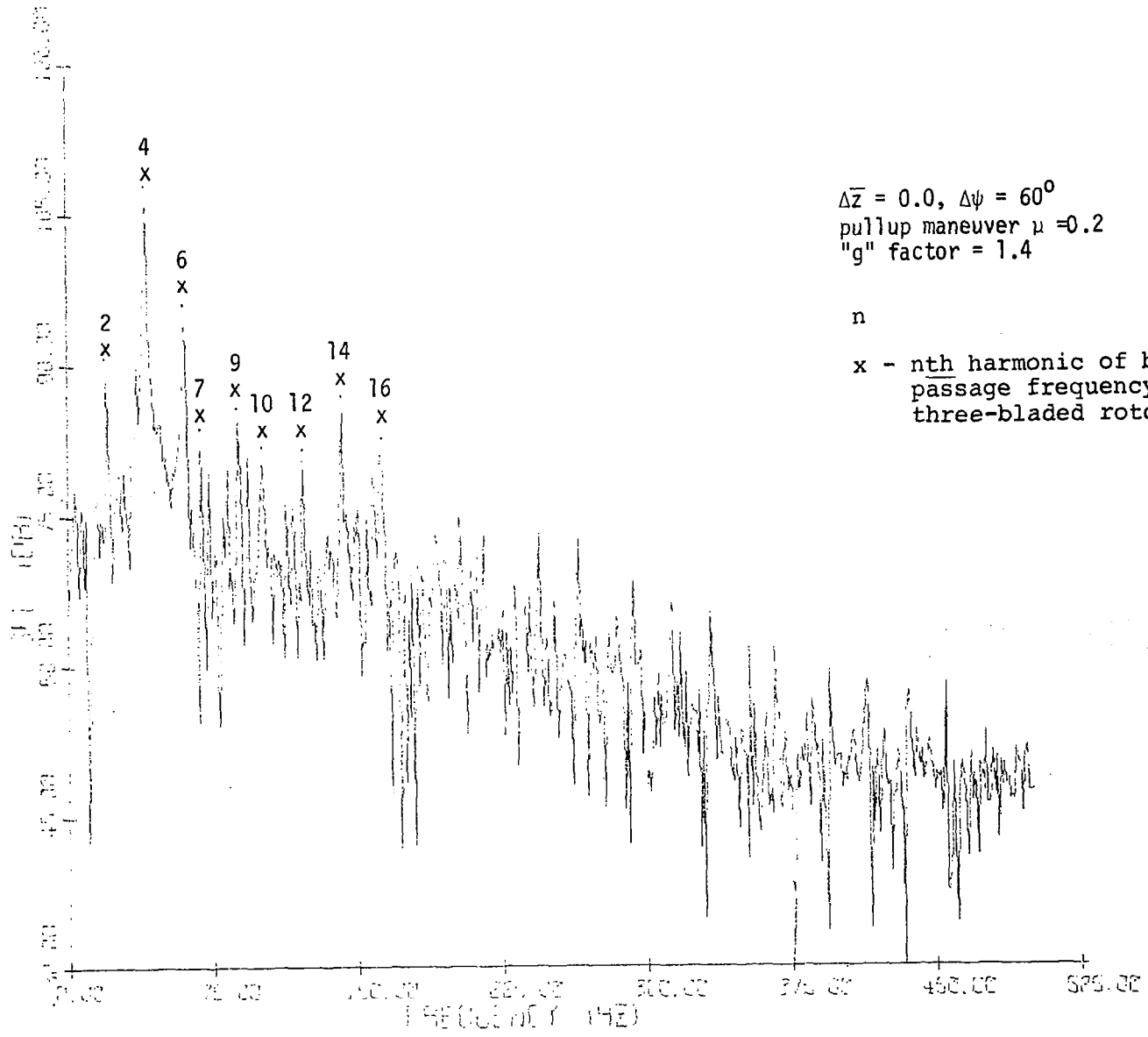

Figure 58. Spectrum of rotational and vortex noise

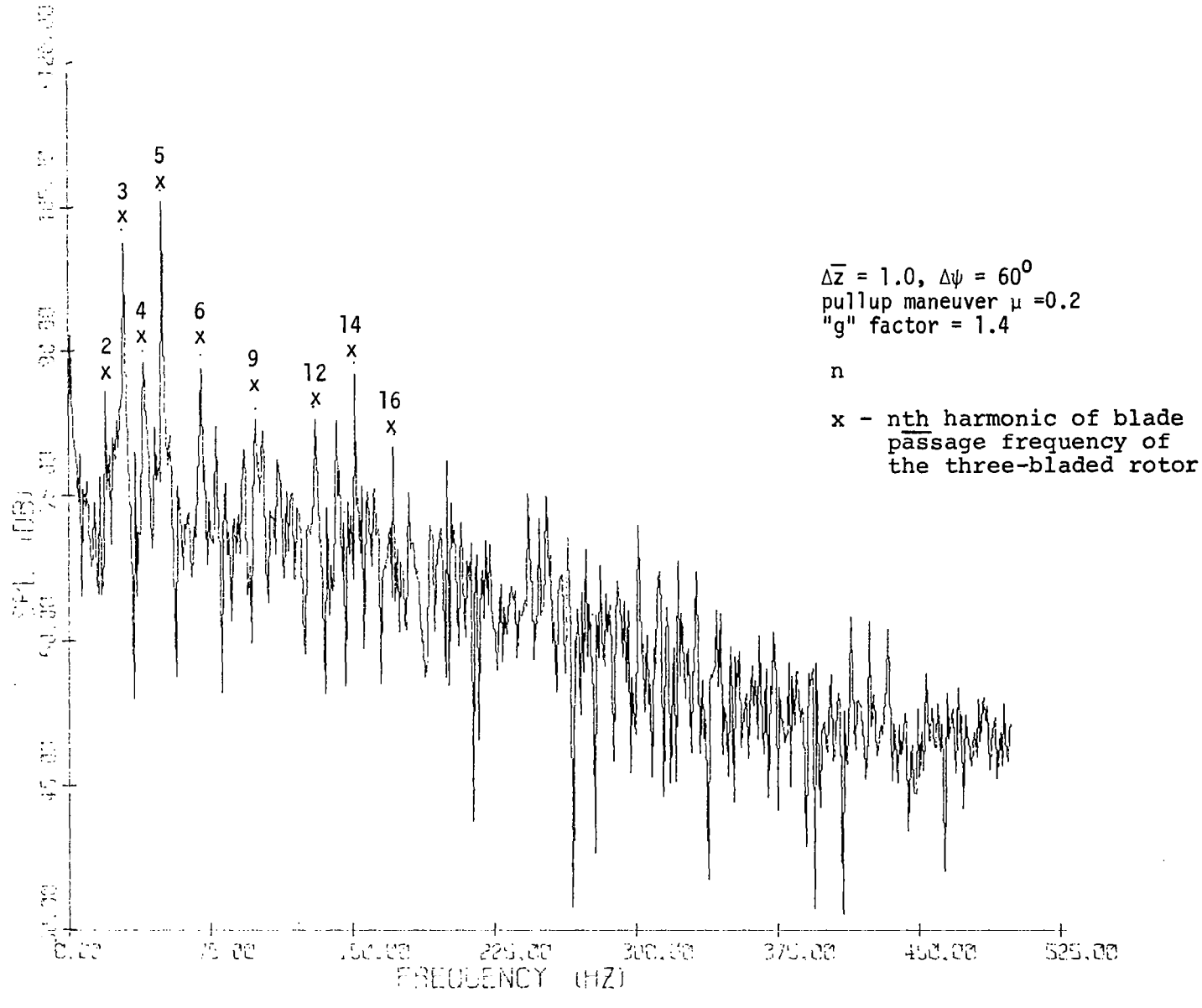

Figure 59. Spectrum of rotational and vortex noise

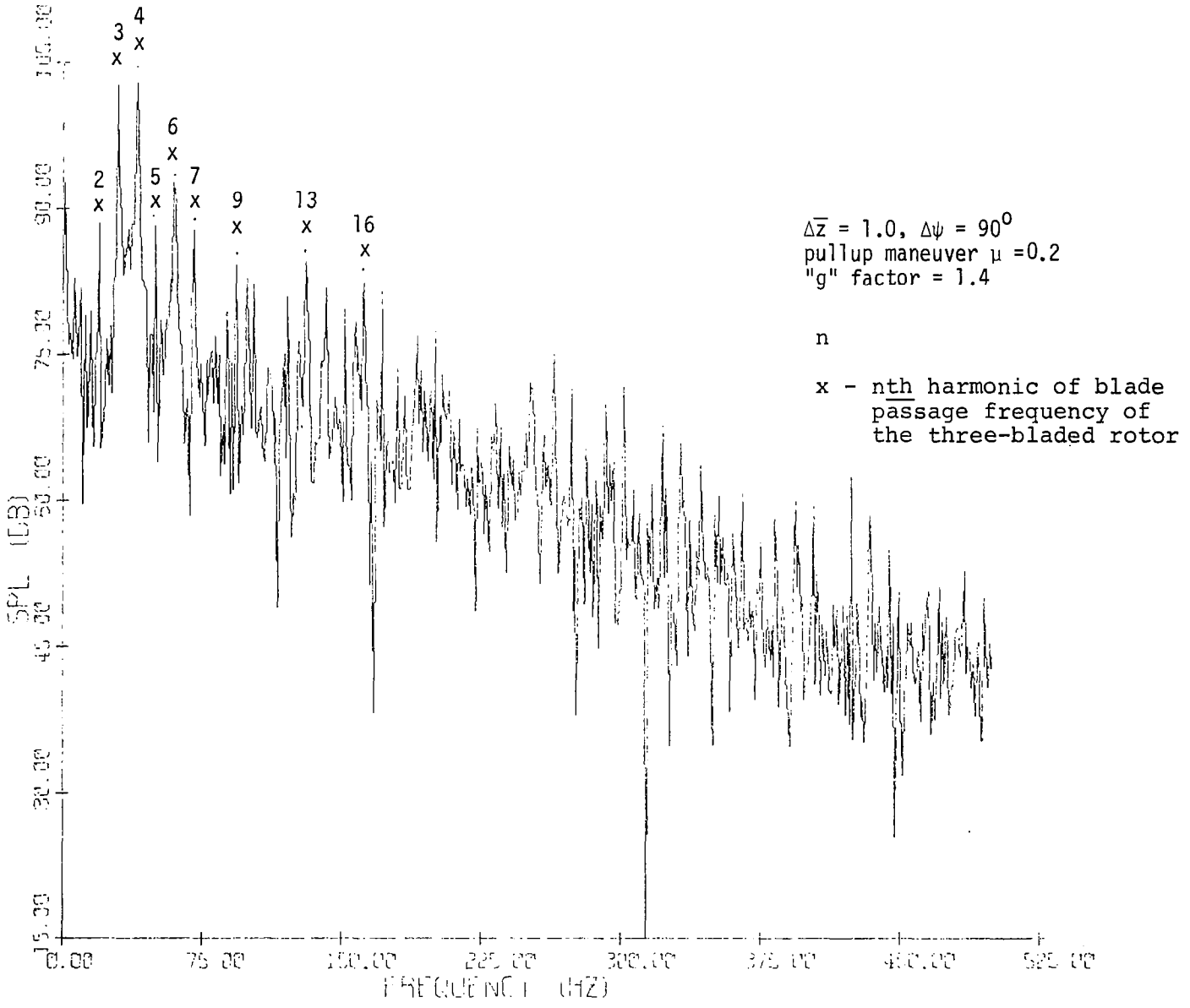

Figure 60. Spectrum of rotational and vortex noise